

REPORT DOCUMENTATION PAGE

Form Approved
OMB No. 0704-0188

Public reporting burden for this collection of information is estimated to average 1 hour per response, including the time for reviewing instructions, searching existing data sources, gathering and maintaining the data needed, and completing and reviewing the collection of information. Send comments regarding this burden estimate or any other aspect of this collection of information, including suggestions for reducing this burden, to Washington Headquarters Services, Directorate for Information Operations and Reports, 1215 Jefferson Davis Highway, Suite 1204, Arlington, VA 22202-4302, and to the Office of Management and Budget, Paperwork Reduction Project (0704-0188), Washington, DC 20503.

1. AGENCY USE ONLY (Leave blank)	2. REPORT DATE	3. REPORT TYPE AND DATES COVERED		
	31 July 1995	FINAL 1 Dec 1992 - 31 May 1995		
4. TITLE AND SUBTITLE		5. FUNDING NUMBERS		
Finite-Element Modeling of the Blockage and Scattering of Lg Wave Propagation		AFOSR Grant PE 61102 F, Proj 2309 AS F49620-93-1-0073		
6. AUTHOR(S)		AFOSR-TR-95		
Dr Yu-Chiung Teng Dr John T Kuo				
7. PERFORMING ORGANIZATION NAME(S) AND ADDRESS(ES)		0675		
Aldridge Laboratory of Applied Geophysics Henry Krumb School of Mines Columbia University New York NY 10027				
9. SPONSORING / MONITORING AGENCY NAME(S) AND ADDRESS(ES)		10. SPONSORING / MONITORING AGENCY REPORT NUMBER		
Air Force Office of Scientific Research Directorate of Math & Geosciences 110 Duncan Ave Bolling AFB DC 20332-8080		Seismology Series: 95-31		
11. SUPPLEMENTARY NOTES				
12a. DISTRIBUTION / AVAILABILITY STATEMENT		12b. DISTRIBUTION CODE		
Approved for Public Release - Distribution Unlimited				
13. ABSTRACT (Maximum 200 words)				
<p>The objective was to investigate the blockage and scattering of Lg wave propagation due to lateral crustal heterogeneities; the particular case comparing paths across the Barents Sea, across the Baltic shield from Novaya Zemlya, and across the Baltic shield from the Kola Peninsula. The emphasis was to quantify the presence of a large basin in the propagation path. Geological structure models were constructed and endowed with specific geophysical characteristics, e.g. uncompensated isostatically; island margin with symmetrical depression. The Sn, Lg, and scattered waves are not dependent on frequency for the three center frequencies selected. For a given center frequency the Lg propagation is dependent on basin width and the velocity of the sediments causes significant influence. With reasonable Q for the sediments of the basin, the blockage is very much accentuated. Comparison with synthetics and the imposed models with three direct comparisons of finite-element results and the observational data available, the blockage of Lg is found to be caused by the low-velocity sediments in the Barents Sea. All other paths studied did not show an influence imposed by geologic structure.</p>				
14. SUBJECT TERMS		15. NUMBER OF PAGES		
Lg Waves Sediment Blockage Regional Wave Propagation		99		
16. PRICE CODE				
17. SECURITY CLASSIFICATION OF REPORT		18. SECURITY CLASSIFICATION OF THIS PAGE	19. SECURITY CLASSIFICATION OF ABSTRACT	20. LIMITATION OF ABSTRACT
UNCLASSIFIED		UNCLASSIFIED	UNCLASSIFIED	UNCLASSIFIED

19951018062

FINAL REPORT
TO
THE AIR FORCE OFFICE OF SCIENTIFIC RESEARCH

CONTRACT NO: F49620-93-0073
PROJECT MONITOR: Dr. Stanley Dickinson

**FINITE-ELEMENT MODELING OF THE BLOCKAGE AND
SCATTERING OF Lg WAVE PROPAGATION**

Yu-Chiung Teng and John T. Kuo

**Aldridge Laboratory of Applied Geophysics
Henry Krumb School of Mines
Columbia University
New York, New York 10027**

Accesion For	
NTIS	CRA&I
DTIC	TAB
Unannounced	
Justification _____	
By _____	
Distribution / _____	
Availability Codes	
Dist	Avail and / or Special
A-1	

July, 1995

**FINITE-ELEMENT MODELING OF
THE BLOCKAGE AND SCATTERING
OF Lg WAVE PROPAGATION**

Columbia University

July, 1995

TABLE OF CONTENTS

Abstract	1
Introduction	5
A Fast Computation Algorithm Of The Finite Element Method For The Anti-Plane Strain Approximations.....	10
Geological Structural Models	16
Model for Novaya Zemlya to ARCESS	16
Kola Peninsula PNE to NORSAR	20
Model for Novaya Zemlya to NORSAR	23
Nuclear Test Source Simulation	24
Finite-Element Modeling Various Effects On Lg	26
Comparisons Of Finite-Element Modeling Results With Real (Observational) Data	73
Finite-element Modeling of the December 4, 1988 Novaya Zemlya Explosion and Compared with the ARCESS Data	77
Finite-element Modeling of the September 4, 1972 Kola Peninsula Explosion and Compared with the NORSAR Data	80
Finite-element modeling of the October 25, 1984 Novaya Zemlya Explosion and Compared with the NORSAR Data.....	83
Conclusions	89
References	92

Abstract

This report constitutes the final report to the Air Force Office of Scientific Research under the Contract F49620-93-1-0073 which commenced on December 1, 1993, for the research project on the Blockage and Scattering of Lg Waves.

The objective of the project is to investigate by means of finite-element modeling of the problem of blockage and scattering of Lg wave propagation due to lateral crustal heterogeneities, particularly from presumed explosions at test sites of Novaya Zemlya across the Barents Sea to ARCESS, and across the Baltic shield to NORSAR, and from the Kola Peninsula explosion across the Baltic shield to NORSAR. We specifically address the anti-strain problem of SH waves related to the Sn and Lg waves so that there would be no Pn, SVn, SV type of Lg waves, and their conversions. This research project is intended to provide a more quantitative understanding of the blockage and scattering of the Lg wave propagation due to the presence of a basin.

Three nuclear explosions were particularly finite-element modeled concerning the blockage and scattering of the Lg wave propagation due to the presence of the basin of the Barents Sea in comparison with the Lg wave propagation through the Baltic continental shield without encountering the obstacle of the basin of the Barents Sea. These three explosions are: (1) the December 4, 1988 explosion from Novaya Zemlya across the Barents Sea to ARCESS with an epicentral distance of 1,100 km, (2) the September 4, 1972 explosion from Kola Peninsula through the Baltic continental shield to NORSAR with an epicentral distance of 1,310 km., and (3) the October 25, 1984 explosion from Novaya Zemlya across the Barents Sea through the Baltic

continental shield to NORSAR with an epicentral distance of 2,300 km.

Geological structure models for the great-circle paths of the Lg wave propagation of the above three presumed nuclear explosions were constructed and designated as (1) Island Margin Model, (2) Model I, (3) Model II, (4) Model III, and (5) Model IV. Island Margin Model is characterized by a sloping interface of the crust and the upper mantle with a dimension of 450 km x 60 km. Model I and Model II extend from the island margin of Novaya Zemlya through the Barents Sea to ARCESS. The island margin portion of the great-circle path is common to both these two models. The Barents Sea portion of these two models is modeled as an idealized symmetrically shaped sedimentary basin, which is placed in the upper crust and located at the center. Under the basin, Model I is assumed to be isostatically uncompensated with a horizontal interface between the lower crust and the upper mantle. Model II is assumed to be isostatically compensated so that the interface between the lower crust and the upper mantle has an anti-root at the Moho. The Baltic shield alone is designated as Model III. Model IV includes three segments, namely, the island margin, the Barents Sea and the Baltic shield. Model III is now connected to Model I or Model II to form Model IV.

The nuclear source for simplicity is simulated by an impulsive explosion source of the first derivative of Gaussian type of forcing function. This primary explosive source is placed on the leeward side of the island. Seismic waves so generated by the impulsive source in Island Margin Model were then used as the input waves for Model I and Model II to provide the continuation of the Lg wave propagation from the explosive source to the receiving station.

Three center-frequencies of the source, namely, 0.167, 0.334, and 0.667 Hz were used to investigate the effect of the center-frequency of the source on the Lg wave

propagation. In order to study the effects of basin width and velocity of sediments on the Lg wave propagation, two basin widths, 150 km and 250 km, were used, moreover, three different sediment S-wave velocities, 2.20, 2.70, and 3.51 km/sec were used for the basin for each basin width. An average S-wave velocity of the granitic and basaltic crust 3.51 km/sec was kept throughout all modelings. The effect of S-wave attenuation in terms of Q_s on the Lg wave propagation is significant. A series of Q_s ranging from ∞ , 150, 100, and 50 have been used in the evaluation of the blockage of the Lg wave propagation.

For the center-frequencies 0.167, 0.334 and 0.667 Hz of the source, the effect of frequency content on Lg is only minor. The arrivals both Sn and Lg are on time except the arrivals of Sn are more emergent for the center-frequency of 0.167 Hz. The amplitudes of Sn, Lg and scattered waves for these three frequencies are nearly independent of frequency. As the transmission path of Sn is principally through the upper mantle, the Sn arrival is virtually transparent of the presence of the basin.

The Lg waves are well developed in the absence of the Barents Sea. For a given center-frequency of the source, the Lg wave propagation is dependent on the dimension of basin width. The amplitude of the Lg wave decays more rapidly for a large basin width than for a small basin width. Moreover, the presence of a basin causes time delay of the Lg wave propagation.

The velocity of sediments in the basin plays a significant role in the propagation and blockage of the Lg waves. The velocity contrast between the sediments in the basin and the surrounding crust influences the development and appearance of the Lg waves. A higher value of velocity contrast causes a lengthening of the Lg wave train.

Among all the effects, one of the most important factors is the effect of attenuation.

With reasonable Qs for the sediments in the basin, the blockage of the Lg wave is very much accentuated. Therefore, estimation of the quality factors not only for the sediments in the basin but also for the surrounding crust becomes important.

Comparisons of the finite-element modeling results of the December 4, 1988 Novaya Zemlya explosion to ARCESS and of the September 4, 1972 Kola Peninsula explosion to NORSAR with the real data of the seismic traces FRAO and N01A0(a), respectively show good agreement. The Sn waves are nearly the same for both the explosions. The wave train of Lg is completely absent for the former Novaya Zemlya explosion and is perfectly developed for the latter Kola Peninsula explosion.

Comparison of the finite-element simulated results of the October 25, 1984 Novaya Zemlya explosion with the NORSAR trace N01A0(b) shows that the time of the arrival of Sn at the NORSAR station agrees with the finite-element modeling calculation perfectly. The arrival of early Lg with small amplitude, which was interpreted by Baumgardt as a converted Lg at the continental margin of the Baltic shield, also agrees the finite-element simulated trace. The Lg waves as they are propagated across the Barents Sea are suffered a great deal of blockage by the low-velocity sediments in the basin. Although Lg to Sn conversion and Lg scattering might also have taken place at the Baltic shield continental margin, such conversion and scattering did not cause any major changes in the already small amplitude Lg waves.

On the basis of finite-element modeling and the above three direct comparisons between the finite-element modeling results and the observational data, the blockage of Lg for the propagation paths from Novaya Zemlya to ARCESS and to NORSAR is caused by the presence of the low-velocity sediments in the Barents Sea.

Introduction

The monitoring of underground nuclear tests, unlike that of atmosphere and under-water nuclear tests, can be detected with relatively high degree of confidence. It remains a critical part of the global verification system.

Seismology provides a technical means for monitoring underground nuclear testing on the basis of investigating seismograms and knowing the characteristic general properties of the propagation paths of teleseismic body and surface waves and of regional waves. Teleseismic body and surface waves are recorded to a distance over 2,000 km. Regional waves include Pn, Pg, Sn, and Lg, which are recorded to a distance less than 2,000 km. Seismologists are now able not only to calculate the distance to the seismic event and to deduce the type of wave motion, but also to make yield estimation and event identification based on Lg amplitudes.

The Lg waves have been in continuous attention for nearly one half of a century. The problems of basic understanding of generation, propagation, blockage, and scattering remain highly challenged. In the sequel, we would selectively review a few contributions to the progress of the investigation of Lg waves, particularly pertaining to the blockage and scattering of Lg waves.

The Lg wave was first identified by Press and Ewing (1952). Based on their studies of seismograms recorded in North America, they defined Lg to have periods of 0.5 to 6 seconds, phase velocities between 2.0 and 3.5 km/sec, and an inverse dispersion at distances greater than 20°. They noticed that Lg arrivals are purely continental paths and are gradually disappeared as the oceanic portion of the path increases in

length beyond 100 km. The arrivals are observed on all three components but are larger on the horizontals.

Knopoff et al. (1975) and Panza and Calcagnile (1975) found that a low velocity channel is not necessary for the existence of Lg waves. Bouchon (1982) used an alternative method to evaluate the Green's functions for elastic layered media, and computed complete synthetic seismograms at short distances (150-350 km) to model an earthquake in France. He concluded that the Lg arrivals are composed of multiply reflected post-critical SH and SV rays. Both the lateral crustal heterogeneities and the irregularities in the shape of the two major reflectors (the free surface and the Moho discontinuity) should most affect the Lg wave propagation. Cara et al. (1981) used an array method devised by Cara and Minster (1981) to analyze data recorded in northwestern Sierra Nevada and in southern California. They concluded that representation of Lg as a single multi-mode wave train could only explain observations in the initial portions of the wave train with group velocity greater than 3.2 km/sec, while the later portions of the Lg waveform are strongly affected by reflections and diffractions from any discontinuities in structure. Kennett (1986) used a ray diagram approach to explain qualitatively the blockage of Lg. Regan and Harkrider (1989) used a hybrid of propagator matrix and finite-element methods to study the effects of continental margin on SH waves.

The efficiency of Lg wave propagation highly depends on the structure and lithology of geological provinces along its propagation path. Ruzaikin et al. (1977) attributed the inefficient propagation of Lg in the Tibetan Plateau to the variation of crustal thickness, where an unusual thickness of crust is present. Kennett et al. (1985) suggested that the Lg propagation across the Norwegian Sea might be suffered from a blockage of regional crustal thickening beneath a graben structure of a basin.

Baumgardt (1985, 1990a), along the same vein, attributed to the partial blockage of Lg propagation in Eurasia by the presence of the Ural Mountains from Semipalatinsk test site in eastern Kazakh to ARCESS. Piwinskii (1981) suggested that the missing granitic layer may cause the blockage of Lg waves. Chan and Mitchell (1985), and Mitchell and Hwang (1987) suggested that the reduction of Lg amplitude might be caused by the attenuation of the thick low-Q sediments as the Lg waves travel crossing the Barents Sea.

Recently, Baumgardt (1990a, 1990b, 1991) used the incoherent beam method (Baumgardt, 1985) and ray tracing to investigate the Lg wave recorded at the regional arrays NORESS and ARCESS, and Graefenburg from presumed nuclear explosions on the northwestern Russian platform and at test sites of Novaya Zemlya. Baumgardt found that the Lg waves are almost completely missing at ARCESS and very poorly recorded at NORESS, while "the Lg energy of some kind appears to get through to the Graefenburg array at about the time expected for on-time Lg." It is apparent that variations of Lg amplitudes are closely associated with the problem of blockage and scattering of Lg waves along its propagation path. Most recently, Cao and Muirhead (1993) used the finite difference method to simulate Lg propagation in a laterally varying continental path and concluded that the existence of a water column and topographic variations of sea bottom and Moho could be important factors for the severe Lg attenuation along a continental path.

Upon Nuttli (1973) proposed a formula to relate amplitude and distance of Lg waves as a high mode wave traveling with minimum group velocity, and in turn, to define a magnitude scale (Mb) for source strength at short periods, attention has been further focused toward variations of Lg amplitude in event identification and yield estimation.

Nevertheless, there is still a great deal of uncertainties in basic understanding of the generation and propagation of Lg waves in a laterally heterogeneous crust that is relevant to yield estimation and event identification for nuclear test detection. One of the problems of Lg propagation in the earth crust has been the blockage and scattering along its propagation path, and the mechanisms affecting its propagation.

The 1989 announced intention of the former Soviets to shift their underground nuclear testing activities from the test site near Semipalatinskin, western Kazakh to the Arctic island of Novaya Zemlya, made the study of regional Lg propagation from Novaya Zemlya to the Scandinavian arrays relevant.

This research is motivated by the works of a number of investigators, who suggested that the blockage of Lg wave propagation in the continents primarily due to lateral crustal heterogeneities, and particularly by a series of papers by Baumgardt (1985, 1987, 1990a, 1990b, and 1991), addressing the problem of the blockage and scattering of the Lg wave propagation from the Russian test sites to the Scandinavian arrays due to the presence of the Barents Sea Basin. A more quantitative understanding of the blockage and scattering of Lg propagation and their mechanisms from Novaya Zemlya to the regional arrays may enhance the use of Lg amplitude discrimination as event identification and yield estimation elsewhere.

In his F-K analyses of Lg azimuths, Baumgardt (1990a) showed that for the first arrival Lg, the Lg propagation is nearly along a great-circle path from source to receiver, although the late-arrivals of Lg can be multipathed. In this research, we have focused our attention on the study of early Lg arrivals, i.e., the great-circle path Lg arrivals, and on solving the problem of anti-plane strain by means of finite-element modeling of SH wave propagation in geologically realistic structural models. These models include the island margin margin model, i.e., Novaya Zemlya, the Barents

Sea, a deep sedimentary basin, and the Baltic continental shield. Although our initial models are still somewhat simplified, they are essential to gain basic understanding of the blockage and scattering of Lg propagation across the laterally heterogeneous crust geological province by province.

A Fast Computation Algorithm Of The Finite Element Method For The Anti-Plane Strain Approximations

For the case of anti-plane strain in a Cartesian system of coordinates x , y and z , the displacement components u_x and u_y vanish everywhere, and $u_z = w(x, y, t)$ is independent of the coordinate z . The non-vanishing stresses are

$$\tau_{xz} = \mu \frac{\partial w}{\partial x}, \quad \tau_{yz} = \mu \frac{\partial w}{\partial y}. \quad (1)$$

The governing equation has the form of wave equation:

$$\frac{\partial^2 w}{\partial x^2} + \frac{\partial^2 w}{\partial y^2} = \frac{1}{c^2} \frac{\partial^2 w}{\partial t^2} + S, \quad c^2 = \mu/\rho, \quad (2)$$

where c is the velocity of the shear wave, μ is the rigidity, ρ is the mass density, and S is the applied source function.

In finite element algorithm, the functional formulation corresponding to equation (2), and the boundary conditions, can be written as

$$X = \int \left\{ \frac{\mu}{2} \left[\left(\frac{\partial w}{\partial x} \right)^2 + \left(\frac{\partial w}{\partial y} \right)^2 \right] + \left(S + \rho \frac{\partial^2 w}{\partial t^2} \right) \right\} dx dy. \quad (3)$$

For wave attenuation, we may introduce a damping term in equation (3) so that

$$S + \rho \frac{\partial^2 w}{\partial t^2}$$

is replaced by

$$S + \mu' \frac{\partial w}{\partial t} + \rho \frac{\partial^2 w}{\partial t^2},$$

where μ' is related to μ , the shear modulus, and is to be empirically determined.

Equation (3) must be minimized with respect to the displacement w . (See any finite element text book, for example, Zienkiewicz (1977) for details.)

The simplest two-dimensional finite element in space is defined by nodal points i, j, k , and straight line boundaries as shown in Figure 1-(a). Each nodal point has one degree of freedom. The functions of the displacement field $w(x, y, t)$ at any point within the triangle element is approximated by the linear polynomials

$$w = g_1 + g_2 x + g_3 y. \quad (4)$$

The three coefficients $g_m (m = 1, 2, 3)$ can be evaluated by solving one set of simultaneous linear equations. These simultaneous equations can be obtained by equating the values of the displacements at the triangle nodes i, j , and k . Then, the coefficients g_m can be solved in terms of the nodal coordinates. Once these coefficients are determined, we can write the displacement at an arbitrary point within the triangle element as

$$\{w\} = [N] \{w\}^e = [N_i, N_j, N_k] \{w_i, w_j, w_k\}^T, \quad (5)$$

where w^e is a column vector with three nodal displacements of the triangle element, and N_i, N_j, N_k , or $[N]$ are the shape functions, which are expressed in terms of the nodal coordinates, and have the form (Zienkiewicz, 1977):

$$N_m = (a_m + b_m x + c_m y)/2\Delta, \quad m = i, j, k, \quad (6)$$

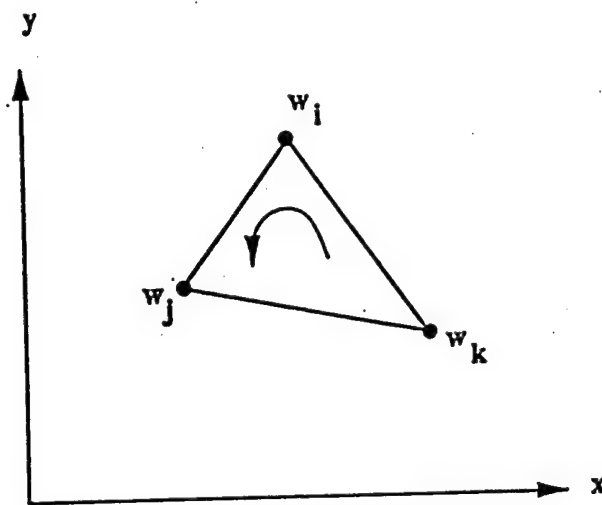


Figure 1-(a). A Single Triangle Element

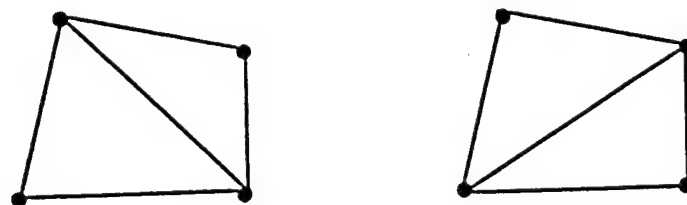


Figure 1-(b). Two Distinct Ways of a Quadrilateral Element and Its Subdivision into Two Triangles

where Δ is the area of triangle ijk :

$$\Delta = \frac{1}{2} \{(x_j y_k - y_j x_k) + (x_k y_i - y_k x_i) + (x_i y_j - y_i x_j)\}, \quad (7)$$

$$\begin{aligned} a_i &= x_j y_k - y_j x_k, \\ b_i &= y_j - y_k, \\ c_i &= x_k - x_j. \end{aligned} \quad (8)$$

The other coefficients can be obtained by cyclic permutation of subscripts in the order i, j , and k .

Taking the minimization of the functional (3) with respect to the displacement field, we have

$$\frac{\partial \chi}{\partial \{w\}} = 0. \quad (9)$$

The final system of equation is

$$[M] \{\ddot{w}\} + [C] \{\dot{w}\} + [K] \{w\} + [S] = 0, \quad (10)$$

where

$$\dot{M}_{ij} = \sum m_{ij}^e, \quad (\text{mass}) \quad (11)$$

$$C_{ij} = \sum c_{ij}^e, \quad (\text{damping}) \quad (12)$$

$$K_{ij} = \sum k_{ij}^e, \quad (\text{stiffness}) \quad (13)$$

$$m_{ij}^e = \int N_i \rho N_j dx dy, \quad (14)$$

$$c_{ij}^e = \int \mu' \left[\frac{\partial N_i}{\partial x} \frac{\partial N_j}{\partial x} + \frac{\partial N_i}{\partial y} \frac{\partial N_j}{\partial y} \right] dx dy. \quad (15)$$

$$k_{ij}^e = \int \mu \left[\frac{\partial N_i}{\partial x} \frac{\partial N_j}{\partial x} + \frac{\partial N_i}{\partial y} \frac{\partial N_j}{\partial y} \right] dx dy. \quad (16)$$

The total displacement field within each element can be obtained as

$$w = (b_i w_i + b_j w_j + b_k w_k) / 2\Delta, \quad (17)$$

In the finite-element modeling, we adopt a four-node quadrilateral element as the basic element in the global numbering system. The quadrilateral element is comprised by two constant strain triangles (2CST). The two distinct ways of a quadrilateral element and its subdivision into two triangles are shown as in Figure 1-(b). The stiffness and mass of each quadrilateral element are obtained by averaging the results of the two types of subdivisions in order to reduce the skew effect.

In equation (10), the global stiffness matrix is a $N \times N$ square matrix, where N is the total number of nodal equations. In order to prevent the stringent requirement of the computer in-core storage of the global stiffness matrix for a large sized model involving long computational time, we adopt a nodal-point-oriented approach (Teng, 1981). The zero matrix elements in the global stiffness matrix are discarded to achieve a fast computational algorithm (Teng, 1989).

In adopting the nodal-point-oriented method and taking advantage of the use of uniform grid of finite elements, we reduce this large $N \times N$ square matrix for global stiffness in 2D for a one-degree-of-freedom problem to a row vector with only 9 members disregarding no matter how large the size of the finite-element model may be as follows:

$$\{K\} = \{K_1, K_2, K_3, \dots, K_9\}. \quad (18)$$

For time integration, we use an explicit central difference scheme:

$$\{w(t + \Delta t)\} = \{\dot{w}(t)\} + \{w(t)\} \Delta t, \quad (19)$$

$$\{\dot{w}(t + \Delta t)\} = \{\dot{w}(t)\} - [K][M]^{-1} \{w(t + \Delta t)\} \Delta t. \quad (20)$$

Geological Structural Models

Gramberg (1988) and Clarke and Rachlin (1990) provided fairly comprehensive geological maps of the Barents Sea and its vicinities, including Novaya Zemlya, the Kola Peninsula, Cheshkaya Bay, just above the Arctic Circle, as shown in Figure 2-(a). Presumably, on the basis of the geological information given, Baumgardt (1990b) has constructed a NW-SE geological cross section through A-B (Figure 2-(b)), showing (1) the absence of granitic layer under the southern Barents Sea Basin, contrary to the presence of a granitic layer under the Pechora Plate and the Central Barents Rise, (2) the thick accumulation of terrigenous sediments under the Barents Sea Basin, and the thin terrigenous sediments over the Plate and the Rise, (3) the variable thicknesses of basaltic layer present under the Plate, the Basin and the Rise, and (4) the bending of the Moho due to the loading of the thick accumulation of sediments in the Basin, and the irregularities of the depth of the Moho, ranging from about 30 km to 37 km under the Basin, 40 km under the Rise, and nearly 50 km under the Plate.

1 Model for Novaya Zemlya to ARCESS:

Similar geological cross sections along the great-circle path from Novaya Zemlya to ARCESS, can be approximated constructed. From Novaya Zemlya to the Scandinavian arrays, NORSAR, the great-circle path of Lg essentially traverse major geological provinces, (1) the island margin with variable crust thicknesses (from Novaya Zemlya to the Barents Sea), (2) the basin with variable width, depth and sediments (the Barents Sea Basin), (3) the shield margin (from the Barents Sea to the Baltic shield),

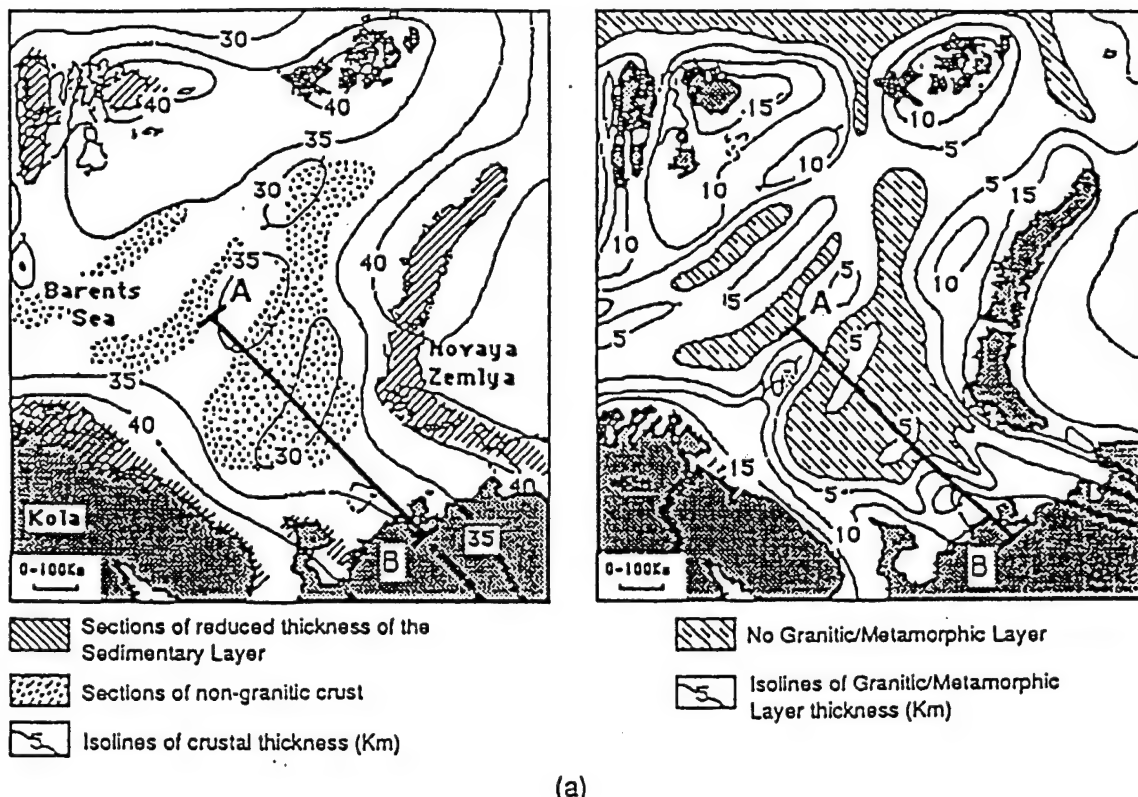
and finally (4) the Baltic shield.

The Barents Sea Basin can be characterized by variations of crustal thickness with sediments accumulation as much as 15 km, and by missing of a granitic layer. This structure is based on low magnetic anomalies caused by the missing of granitic layer and on high in gravity anomalies caused by the elevated Moho. As reported, the granitic layer in the adjacent province is characterized by P-wave velocities on the order of 6.0 to 6.5 km/sec, and S-wave velocities 3.46 to 3.75 km/sec (Clarke and Rachlin, 1990).

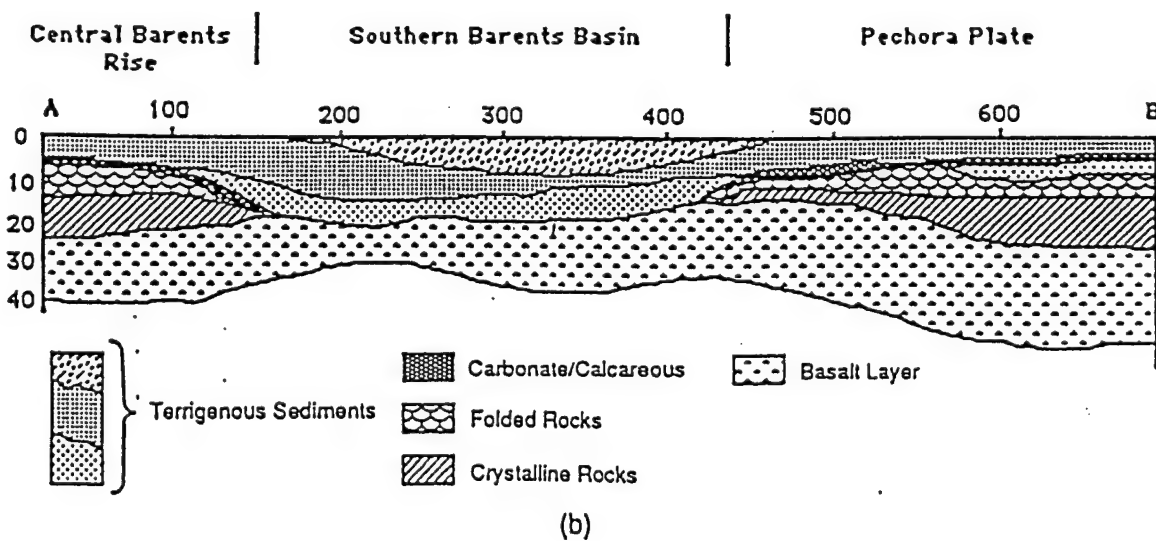
The sediments in the Barents Sea Basin assume P-wave velocities from 3.9 to 5.5 km/sec, and, correspondingly, S-wave velocities 2.2 to 3.17 km/sec (Baumgardt, 1990a, 1991). The basaltic layer assumes P-wave velocities from 6.5 to 6.8 km/sec and S-wave velocities from 3.47 to 3.63 km/sec. The upper mantle is assumed to be normal with P-wave velocities ranging from 8.1 to 8.2 km/sec, and S-wave velocities of 4.6 to 4.7 km/sec.

The density of the sediments are taken to be 2.3 to 2.5 gm/cm³; that of granitic layer 2.67; that of basaltic layer 3.0 in the crust; and that of ultrabasic rocks in the upper mantle 3.27.

Two basic models, which are referred to as "Model I" and "Model II," as shown in Figure 3 were constructed to simulate the geological structures along the path from the former USSR nuclear test sites at Novaya Zemlya through the Barents Sea to ARCESS. The island margin portion of the path alone, which is common to both these two basic models, is referred to as "Island Margin Model."



(a)



(b)

Figure 2. (a) Geologic Maps of Barents Sea Basin (After Gramberg, 1988).
 (b) NW-SE Cross Section (AB) Across the Basin (After Baumgardt, 1990b).

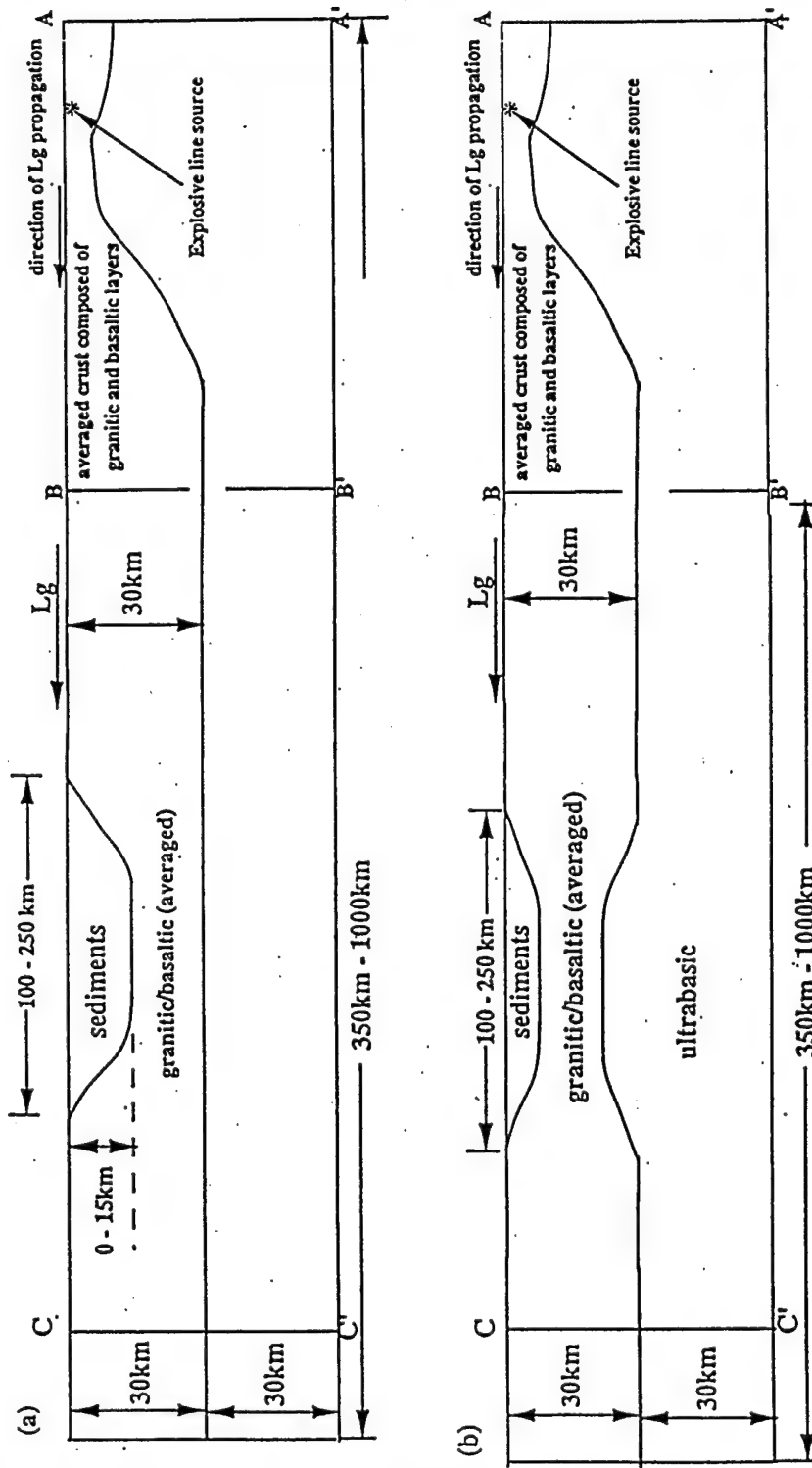


Figure 3. (a) Model I simulating the geological structure along the path from the former USSR nuclear test sites Novya Zemlya to the Barents Sea, which is represented by a sedimentary basin.

(b) Model II simulating the geological structure along the path from the former USSR nuclear test sites Novya Zemlya to the Barents Sea, which is represented by a sedimentary basin as in Figure 2-(a); in addition, the Moho is assumed to have been uplifted with an identical anti-shape of the sedimentary basin.

1.1 Island Margin Model:

Island Margin model is characterized by a sloping interface of the crust and the upper mantle. The model assumes a dimension of 450 km x 60 km. A simulated source is located on the leeward side of the island of the model (Figure 4-(a)).

The right-side artificially terminated boundary is placed on the other side of the island at AA'; the left-side artificially terminated boundary is placed about 100 km from BB'.

1.2 Model I and Model II:

Model I and Model II extend from the island margin of Novaya Zemlya through the Barents Sea to ARCESS. As the island margin portion of the path is common to both these two models, the Barents Sea portion of these two basic models is modeled as an idealized symmetrically shaped sedimentary basin, which is placed in the upper crust and located at the center.

Under the basin, Model I is assumed to be isostatically uncompensated so that the interface between the lower crust and the upper mantle is horizontal, and Model II is assumed to be isostatically compensated and the interface is intruded by an uplifted Moho with an identical anti-shape of the sedimentary basin.

The S-wave velocities of the granitic/basaltic (averaged) layer and the upper mantle are taken to be 3.51 km/sec and 4.7 km/sec, respectively.

The widths of the sedimentary basin Model I and II include 150 km and 250 km.

2 Kola Peninsula PNE to NORSAR:

The great-circle path from Kola Peninsula PNE to NORSAR virtually lies in the geological province of the Baltic shield. Geological structures in the shield areas

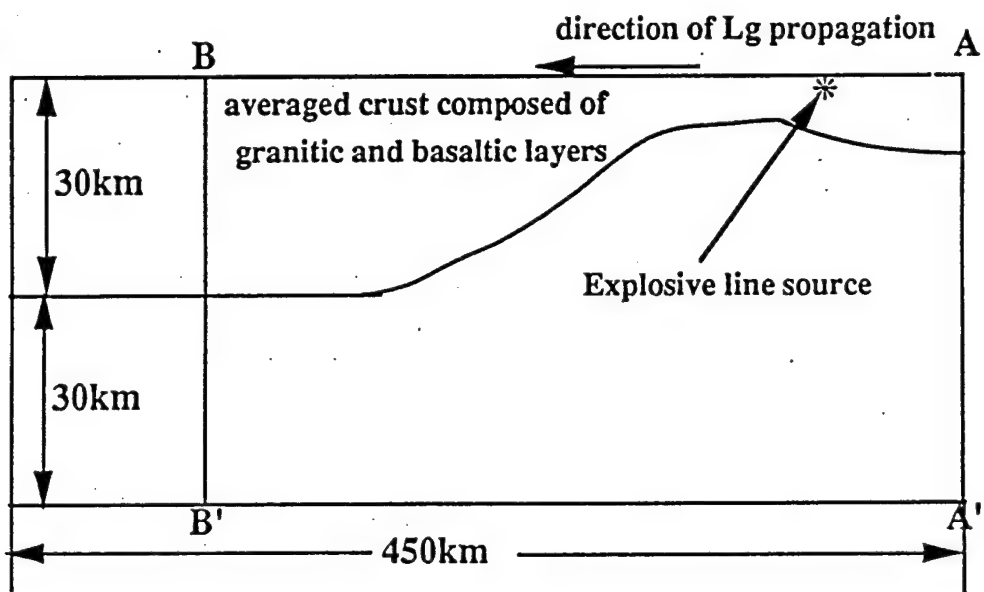


Figure 4-(a). The Island Margin Model

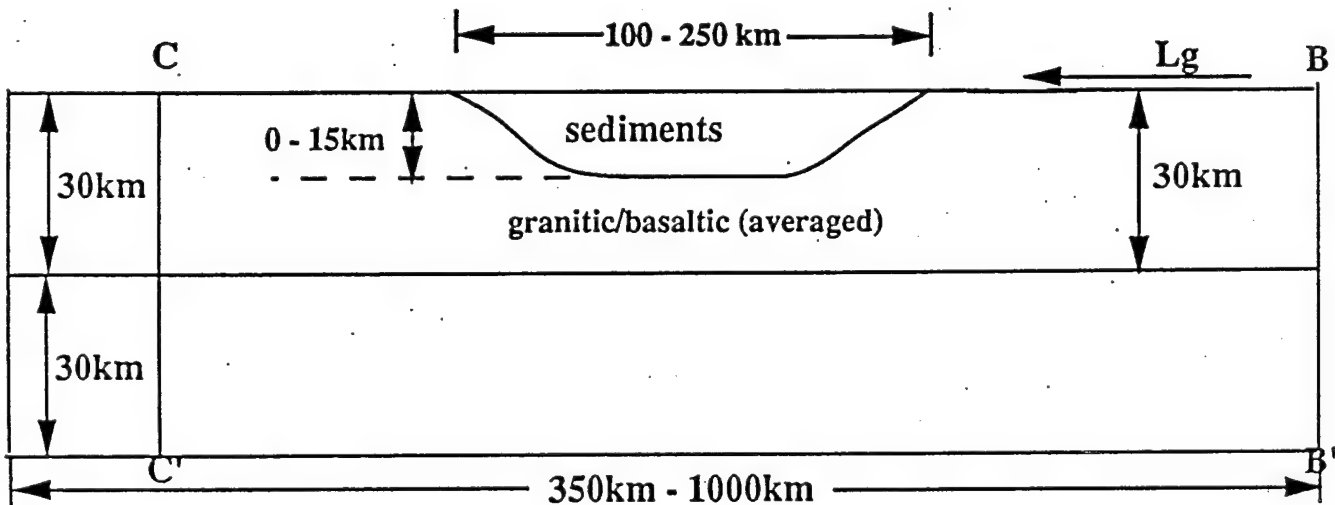


Figure 4-(b). The Basin Model

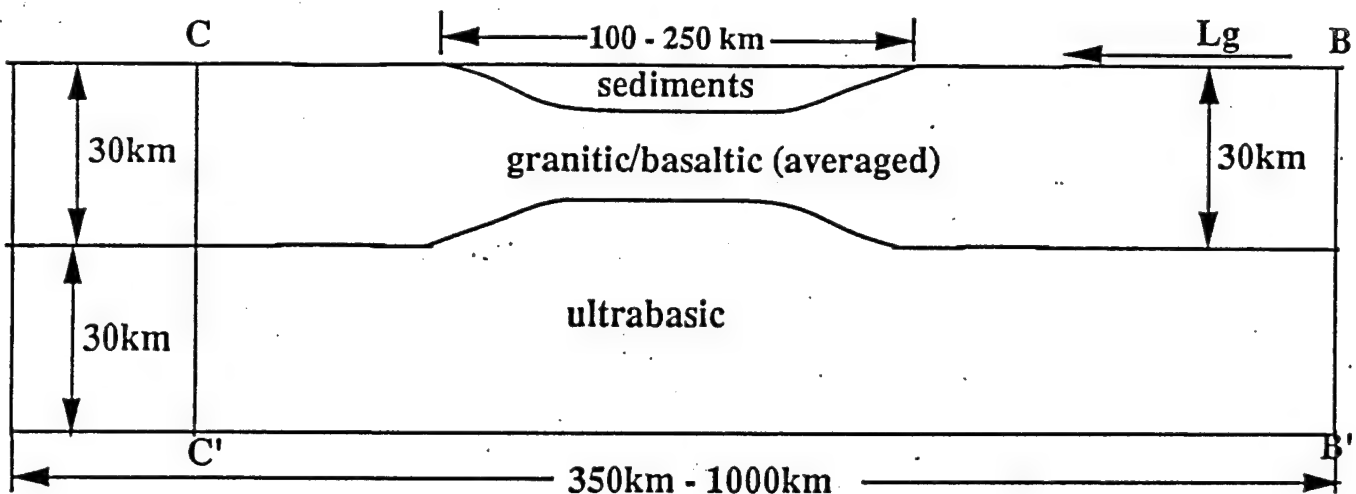


Figure 4-(c). The Basin and Crust-Pinch Model

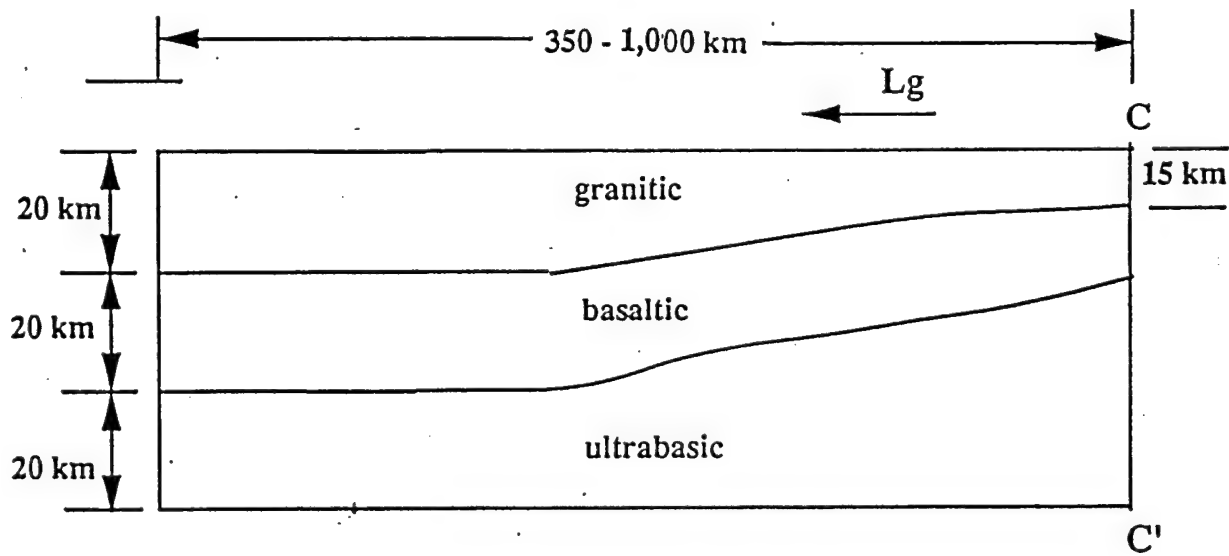


Figure 4-(d). The Baltic Shield Margin Model.

for example, the Canadian Shield and the Baltic shield are fairly well known. The shield crust basically consists of granitic and basaltic layers with relatively higher P- and S-wave velocities and densities as compared with those in a normal crust. The velocities for the upper mantle ultrabasic rocks are assumed to be those in normal geological provinces. A geological structure for the great path from Kola Peninsula PNE to NORSAR would involve the Baltic shield margin and the shield itself. It may be appropriate to model this great-circle path, designated as Model III as shown in Figure 4-(d), in which the Baltic shield margin has a thin layer of lower S-wave velocity over a thinner crust, and the crust of 30 km, then gradually increases to about 40 km toward NORSAR.

3 Model for Novaya Zemlya to NORSAR:

The model for the great-circle path for the former USSR test sites from Novaya Zemlya to NORSAR includes the island margin, the Barents Sea, the Baltic shield margin and the Baltic shield. Therefore, the model is the combination of the models for all these provinces, namely, Model I and Model III, which we refer to as Model IV as shown in Figure 4-(d). The physical parameters and the geometrical configuration of Model IV, some of which are given above, will be discussed in more details in the later section on comparisons of the finite element modeling results with observational data.

Nuclear Test Source Simulation

The nuclear test source for simplicity may be simulated by an impulsive explosion source of the first derivative of Gaussian type forcing functions. This primary source is placed on the leeward side of Island Margin Model of Novaya Zemlya.

In view of the predominant frequency of Lg waves and the availability of our computer power, a compromise of the frequency content of the source was made. Three center- frequencies of the simulated nuclear source included 0.167 Hz, 0.334 Hz, and 0.667 Hz, corresponding to periods 6 sec, 3 sec, and 1.5 sec, respectively to investigate the effect of the source frequency contents on the Lg wave propagation.

Since our finite-element method is an explicit one, it requires at least 10-12 grid points per wavelength in each spatial dimension of discretization in order to avoid grid dispersion and grid anisotropy, and time step to satisfy the CRL conditions in order to achieve accurate results. Therefore, we consider the lowest S-wave velocity of 2.20 km/sec and the highest velocity of 4.70 km/sec, and, for example, the maximum dimension of the constructed finite-element model for Novaya Zemlya to ARCESS of 1,450 km x 60 km, and one degree of freedom. In this case of the finite-element method requires a total of solving $5,273 \times 219$, $2,637 \times 110$, and $1,319 \times 55$ equations for the cases of 0.667 Hz, 0.334 hz, and 0.167 Hz, respectively. The spatial dimension of the element would be less than 1,098 m, 549 m, and 275 m, and the time steps 0.039 sec, 0.078 sec, and 0.156 sec, respectively.

Seismic waves so generated by the impulsive source in Island Margin Model received at the cross section BB' are then used as the input waves at BB' for Model I

and Model II to provide the continuity of the Lg wave propagation from an impulsive source on Island Margin Model to the basin portion of the model of Novaya Zemlya to ARCESS in question (Figure 4-(b) or Figure 4-(c).) The input waves from the cross section CC' provides the continuity of the impulsive source for Model IV, for the great-circle path from Novaya Zemlya across the Barents Sea, through the Baltic shield to NORSAR.

Finite-Element Modeling Various Effects On Lg

1 Island Margin Model:

First we have investigated how the Lg wave is propagated through the island margin of Island Margin Model, the configuration of which is shown in Figure 4-(a). The sloping interface at the island margin is about 14° . In the crust, the S-wave velocity as mentioned previously, was taken to be an average velocity of granitic and basaltic layers 3.51 km/sec; and that of the upper mantle 4.7 km/sec.

Figures 5-(a), 5-(b), 5-(c) are the finite-element synthetic seismograms observed at the epicentral distance from 10 to 250 km for an impulsive source of 0.167 Hz, 0.334 Hz, and 0.667 Hz, respectively. Since we have only solved the anti-plane strain problem of SH waves, as expected, we only observed the arrivals of the Sn and Lg waves. If we would have solved the problems of plane strain, we would have observed a relatively sharp Pn onset, an emergent arrival corresponding to Sn onset disregarding anisotropy, converted waves and the strong Lg arrivals.

The arrival of Sn for an impulsive source with a center frequency of 0.167 Hz as shown in Figure 5-(a) has a comparatively longer duration than that with the center frequencies of 0.334 and 0.667 Hz in the epicentral distances from 410 to 650 km as investigated. The Lg wave begins with the direct arrival of SH, which is often included in the energy envelop of the Lg waves.

In order to illustrate the crustal wave guide phenomenon for the energy penetration

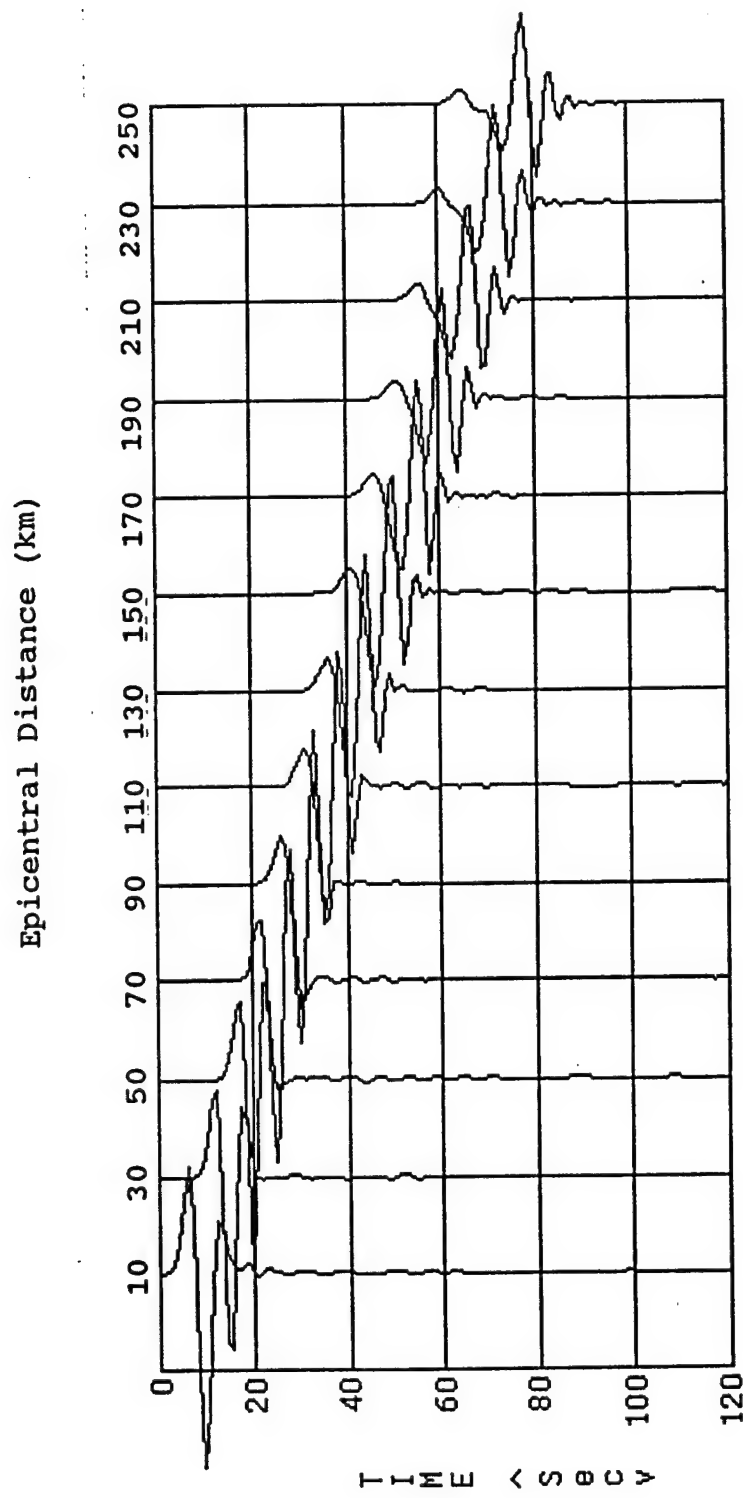


Figure 5-(a). The finite-element synthetic seismogram of Lg waves by an impulsive line source with center frequency of 0.167 Hz as observed at distances of 10 km to 250 km from the source of the Island Margin Model

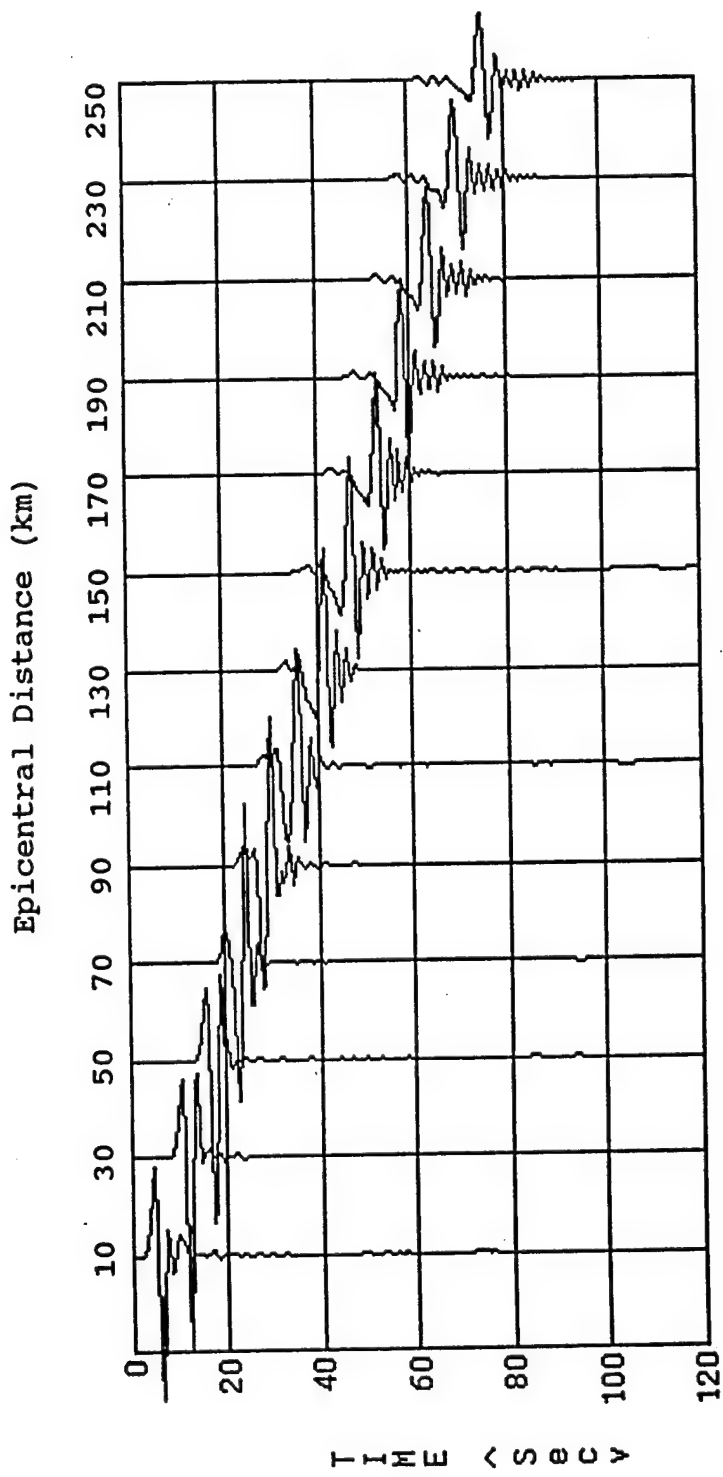


Figure 5-(b). The finite-element synthetic seismogram of Lg waves by an impulsive line source with center frequency of 0.334 Hz as observed at distances of 10 km to 250 km from the source of the Island Margin Model

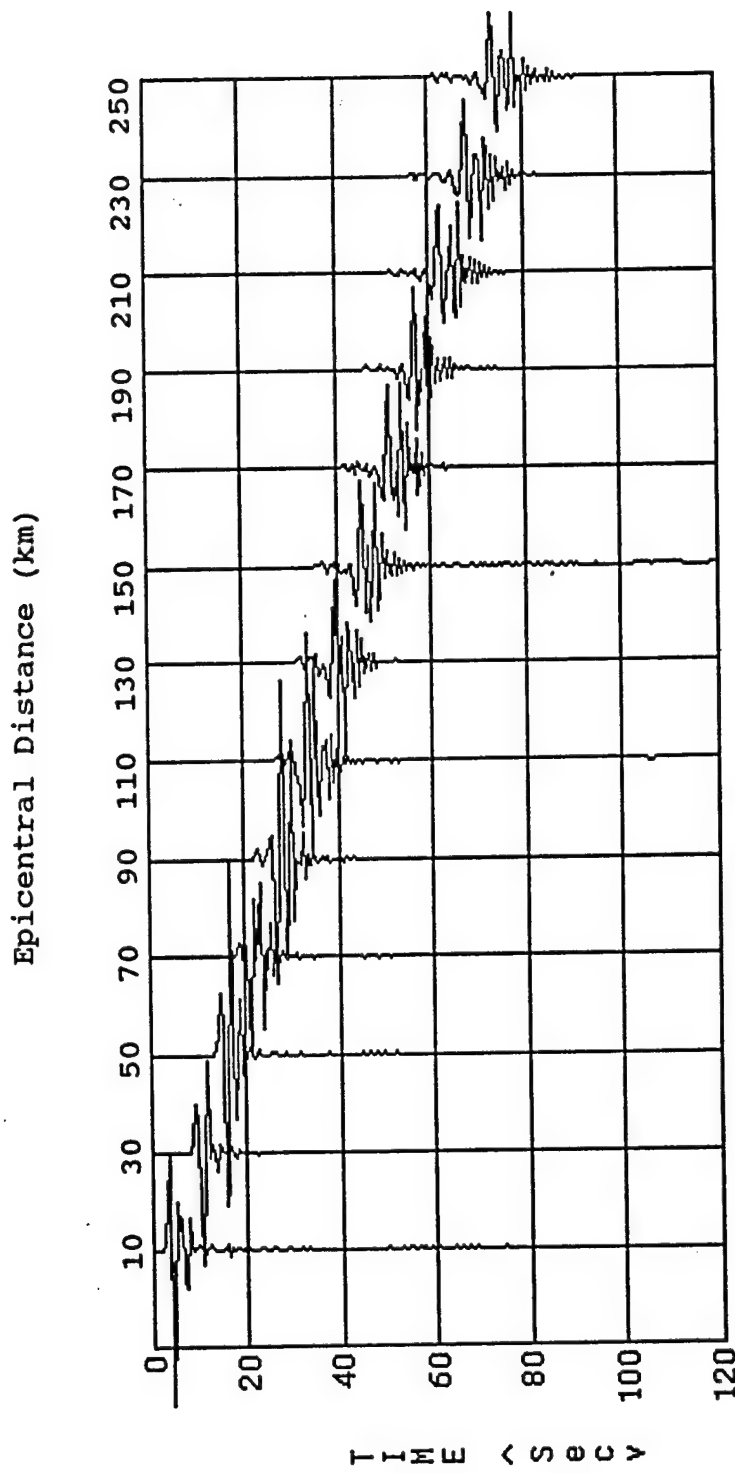


Figure 5-(c). The finite-element synthetic seismogram of Ig waves by an impulsive line source with center frequency of 0.667 Hz as observed at distances of 10 km to 250 km from the source of the Island Margin Model

of the Sn and Lg waves and to provide the Lg generating source for subsequent continuation to large lateral dimension models, we have also calculated the finite-element synthetic seismograms at the cross section of BB' as a function of depth from the crust through the upper mantle. The epicentral distance to the cross section BB' is 400 km. Figures 6-(a), 6-(b) and 6-(c) are the seismic responses at the cross section BB' with an impulsive source corresponding to the center frequencies 0.167, 0.334, and 0.667 Hz, respectively. As the interface of the crust and the upper mantle at BB' for Island Margin Model is placed at a depth of 30 km, all the SH-wave energy is virtually trapped in the crust to make it a perfect wave guide for the Lg wave generation and propagation. However, for the center frequencies of 0.167 and 0.334 Hz, there are significant energy leakaged from the crust into the upper mantle. For the center frequency of the source of 0.667 Hz (Figure 6-(c)), the energy of Lg is all confined to the crust. For a lower center frequency 0.167 Hz such as shown in Figure 6-(a), the energy of Lg in the subsurface is transmitted through the upper mantle as deep as a half of the crustal thickness to a depth of 45 km; that in Figure 6-(b) with a center frequency of 0.334 Hz, the energy of Lg is transmitted through the upper mantle to a depth of about 38 km, or a quarter of the crustal thickness. Therefore, a crustal wave guide of Lg waves for a transitional region of variable thickness of the crust such as for the island margin model is of frequency dependence.

In Figures 6-(a),(b), and (c), there are interesting events, which are generally not observed on the surface. These arrivals in the upper mantle are ahead of the arrival of Sn in the crust as a multiply reflected S wave in the margin and then refracted and transmitted into the upper mantle. We refer these arrivals as S_{clR} , where 'cl' stands for the reflected wave in the crust, and 'R' stands for refracted and transmitted through the upper mantle. The amplitude of S_{clR} increases as a function of depth as shown in

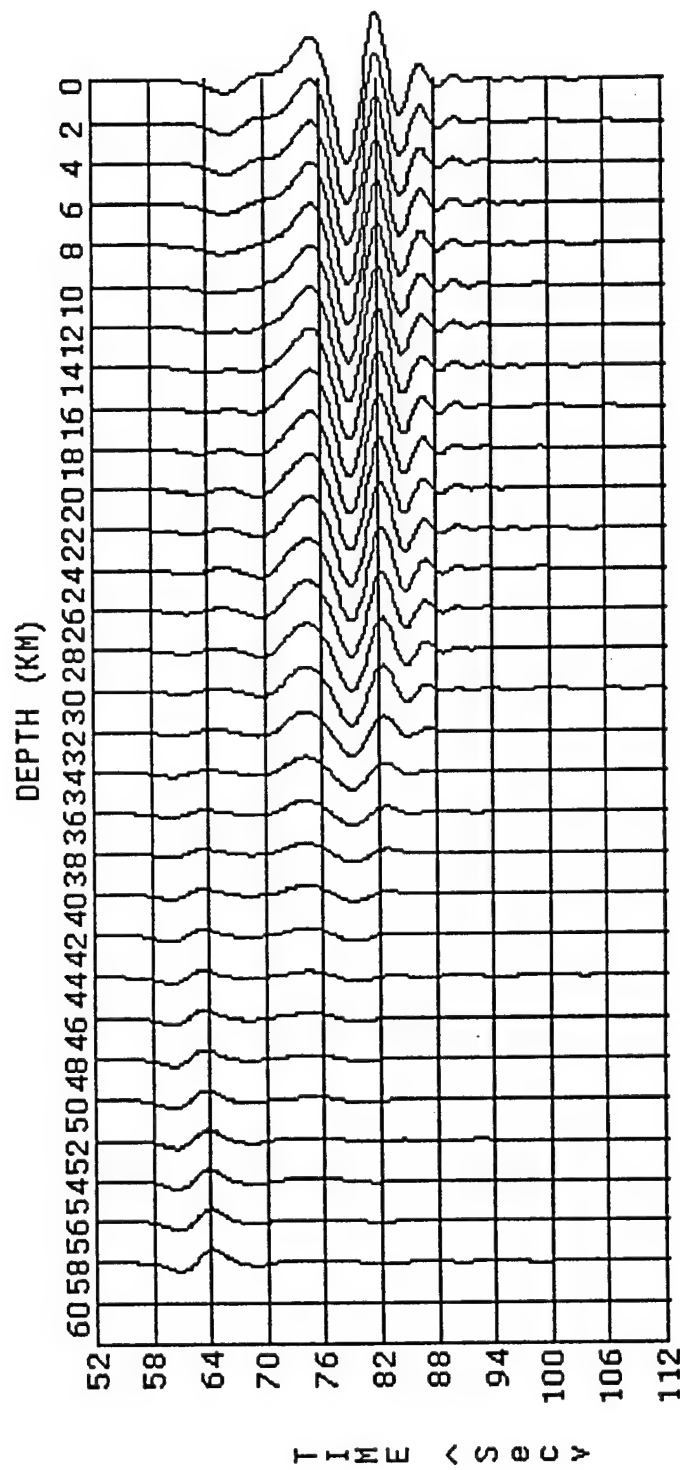


Figure 6-(a). The seismic responses of Lg waves by an impulsive source with center frequency of 0.167 Hz as observed along the vertical section BB' of the Island Margin Model, which are used to excite the Basin Model.

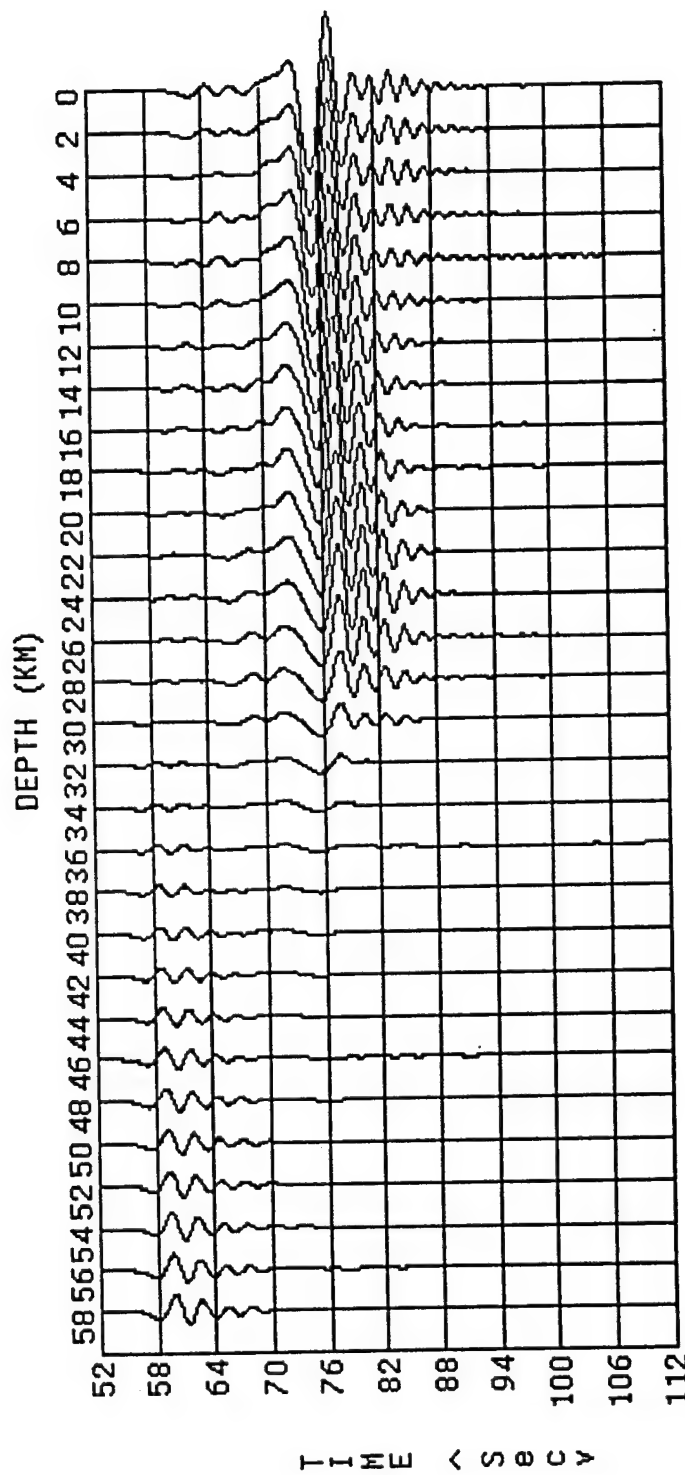


Figure 6-(b). The seismic responses of Lg waves by an impulsive source with center frequency of 0.334 Hz as observed along the vertical section BB' of the Island Margin Model, which are used to excite the Basin Model.

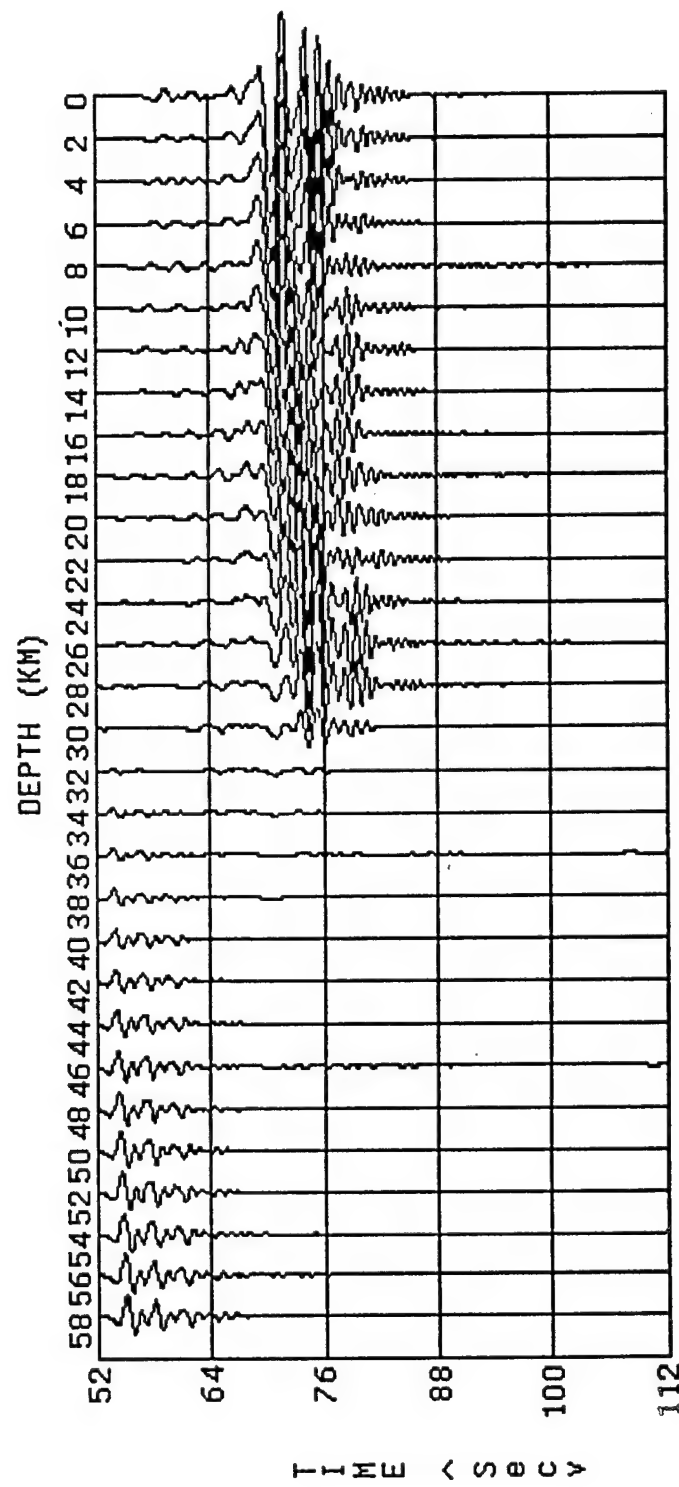


Figure 6-(c). The seismic responses of Lg waves by an impulsive source with center frequency of 0.667 Hz as observed along the vertical section BB' of the Island Margin Model, which are used to excite the Basin Model.

Figures 6-(a), (b), and (c). The average envelops of the Lg waves are broader for the source with lower center-frequencies of the impulsive source.

One of the significant findings for Island Margin Model is that shear wave reverberation in the averaged granitic/basaltic layer is clearly shown to produce an expected group velocity for the Lg wave of approximately 3.5 km/sec, and that for the Sn wave of 4.4 km/sec.

2 Model I and Model II:

We have studied the following effects on the Lg wave propagation for Model I and Model II.

1. Frequency content of a simulated explosive source, including its center frequencies, 0.167, 0.334, and 0.667 Hz.
2. Basin width and velocity of a sedimentary basin in Model I and Model II, which connect to Island Margin Model at the cross-section junction of continuity BB'. Two basin widths, 150 km and 250 km, and three different sediment S-wave velocities, viz., 2.20, 2.70, and 3.51 km/sec, were used for the basin for each width of the basin.

The crust was assumed to have an average S-wave velocity of the granitic and basaltic layers, namely, 3.51 km/sec. When the sediment velocity becomes 3.51 km/sec, there would be no presence of the basin. The upper mantle assumes a S-wave velocity of 4.70 km/sec.

2.1 Without Sedimentary Basin:

We begin with Model I and Model II without the presence of a sedimentary basin, i.e., the sedimentary basin is replaced by the material of the crust. In the present case, we simply used an average S-wave of 3.51 km/sec velocity for the entire crust.

Without the presence of a sedimentary basin, there would be no uplifted Moho in Model II so that geologically it makes sense, as most of the crusts on the earth are isostatically balanced particularly in a shield area. Therefore, Model I is exactly identical to Model II. In the sequel, we use either Model I or Model II that means the interface of the lower crust and the upper mantle is horizontal.

Figures 7-(a), 7-(b), and 7-(c) give the finite-element synthetic seismograms for two identical models, Model I and Model II, in which the sedimentary basin is replaced by the crustal material, with an impulsive source with the center-frequencies of 0.167, 0.334, and 0.667 Hz, respectively. In the present case, Model I and Model II are simply a layer of crust with a thickness of 30 km over the upper mantle of 30 km. The source is located on the leeward side of Island Margin Model. The continuation part of Island Margin Model of Model I or Model II was excited by the waves arrived at the cross section BB' as the result of an impulsive source located in Island Margin Model. The range of these figures is referred to with reference to the cross section BB' of Model I or Model II. A distance of 400 km must be added to the range in order to obtain the epicentral distance in Model I or Model II.

The essential features of Sn and Lg and the scattered Sn and Lg for an impulsive source with the center frequencies 0.167 Hz, 0.334, and 0.667 Hz are precisely similar. The emergent arrivals corresponding to the Sn onset are clearly observed. It follows with distinct strong arrivals of Lg waves.

3 Model I:

3.1 Effects of Sediment Velocity:

Figures 8-(a) and 8-(b) are the finite-element synthetic seismograms obtained from Model I with a basin width of 150 km and two different sediment velocities, 2.7 km/sec

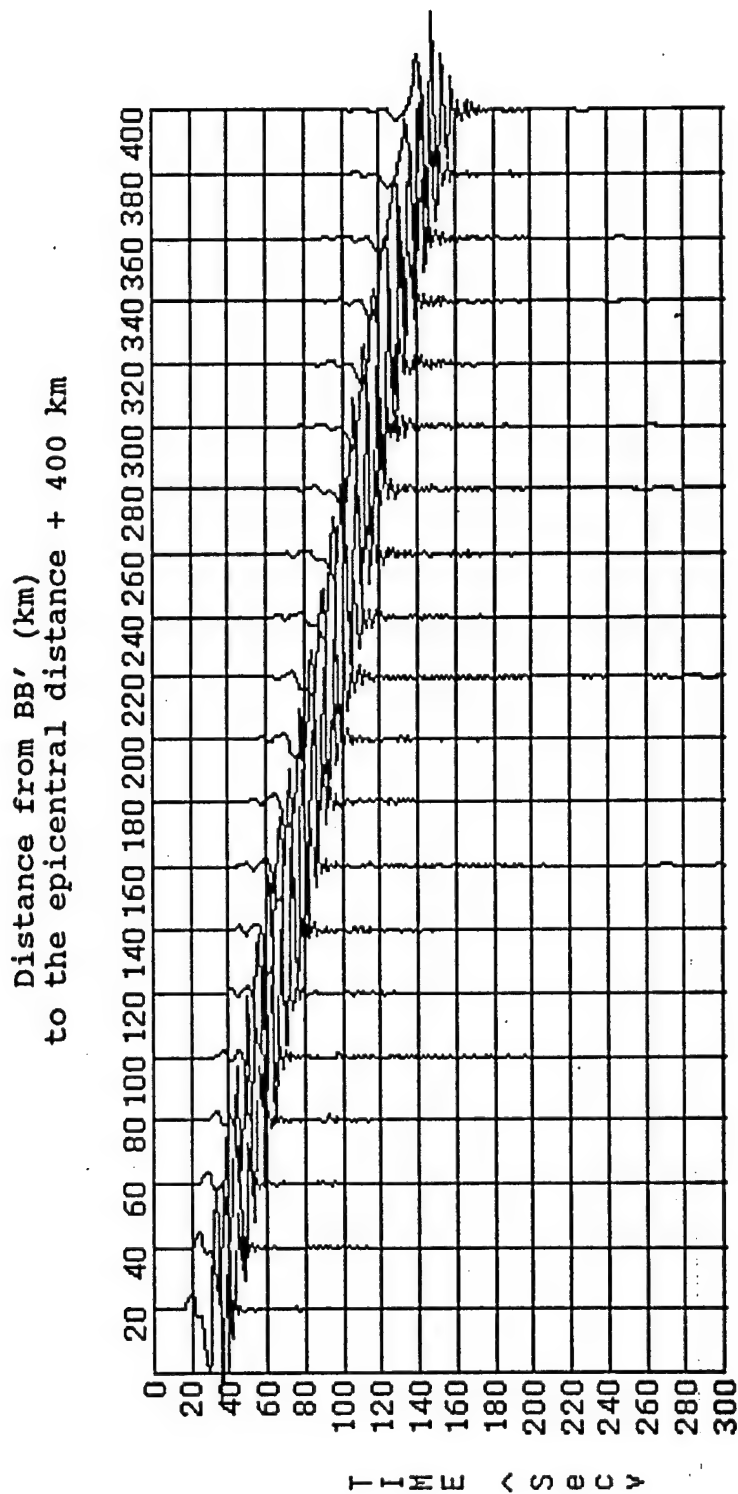


Figure 7-(a). The finite-element synthetic seismogram for the Basin Model of Figure 4-(b), (basin width = 250 km, basin depth = 15 km), with the basin velocity of 3.51 km/sec, as observed at distances of 20 km to 400 km by a source with a center frequency 0.167 Hz. (the basin is replaced by averaged granitic/basaltic material, i.e., no basin.)

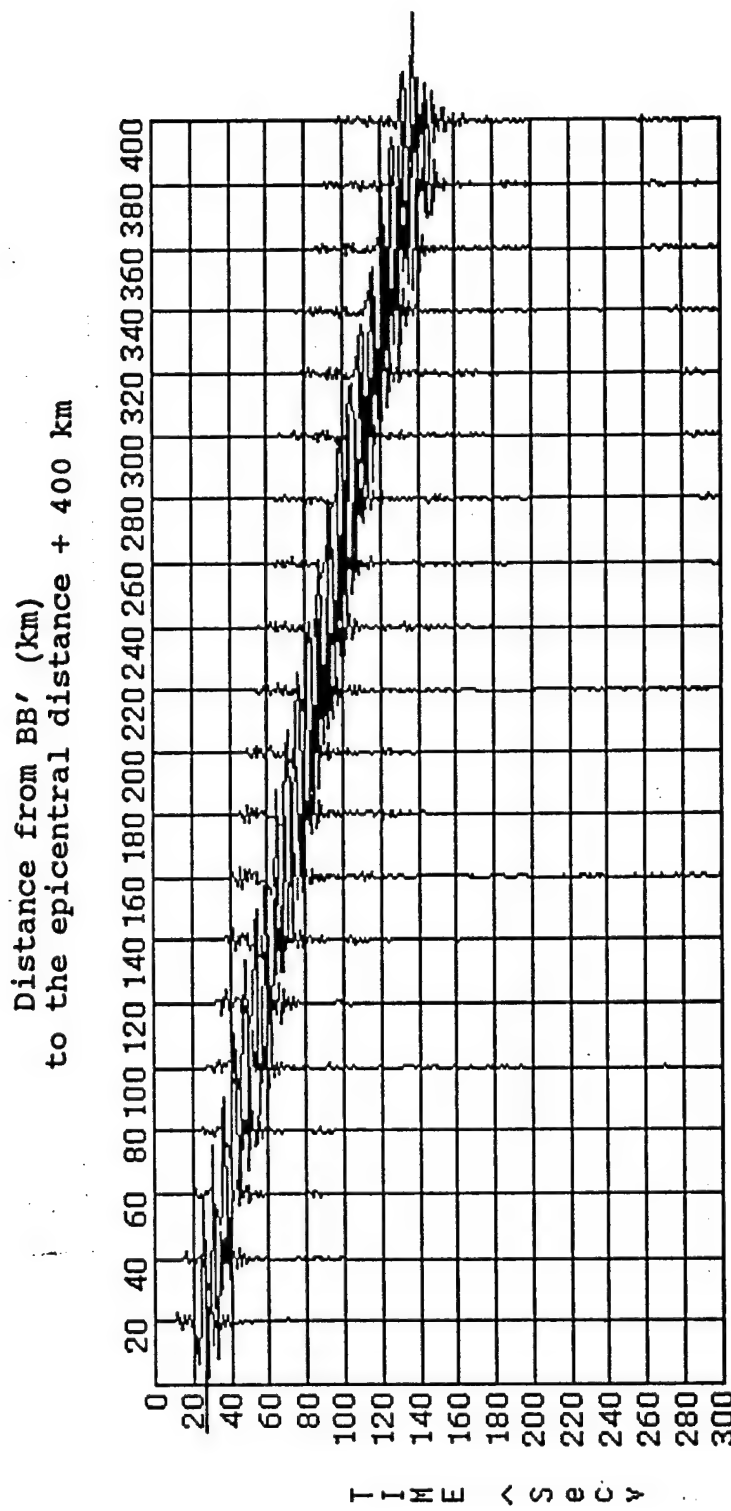


Figure 7-(b): The finite-element synthetic seismogram for the Basin Model of Figure 4-(b), (basin width = 250 km, basin depth = 15 km), with the basin velocity of 3.51 km/sec, as observed at distances of 20 km to 400 km by a source with a center frequency 0.334 Hz. (the basin is replaced by averaged granitic/basaltic material, i.e., no basin.)

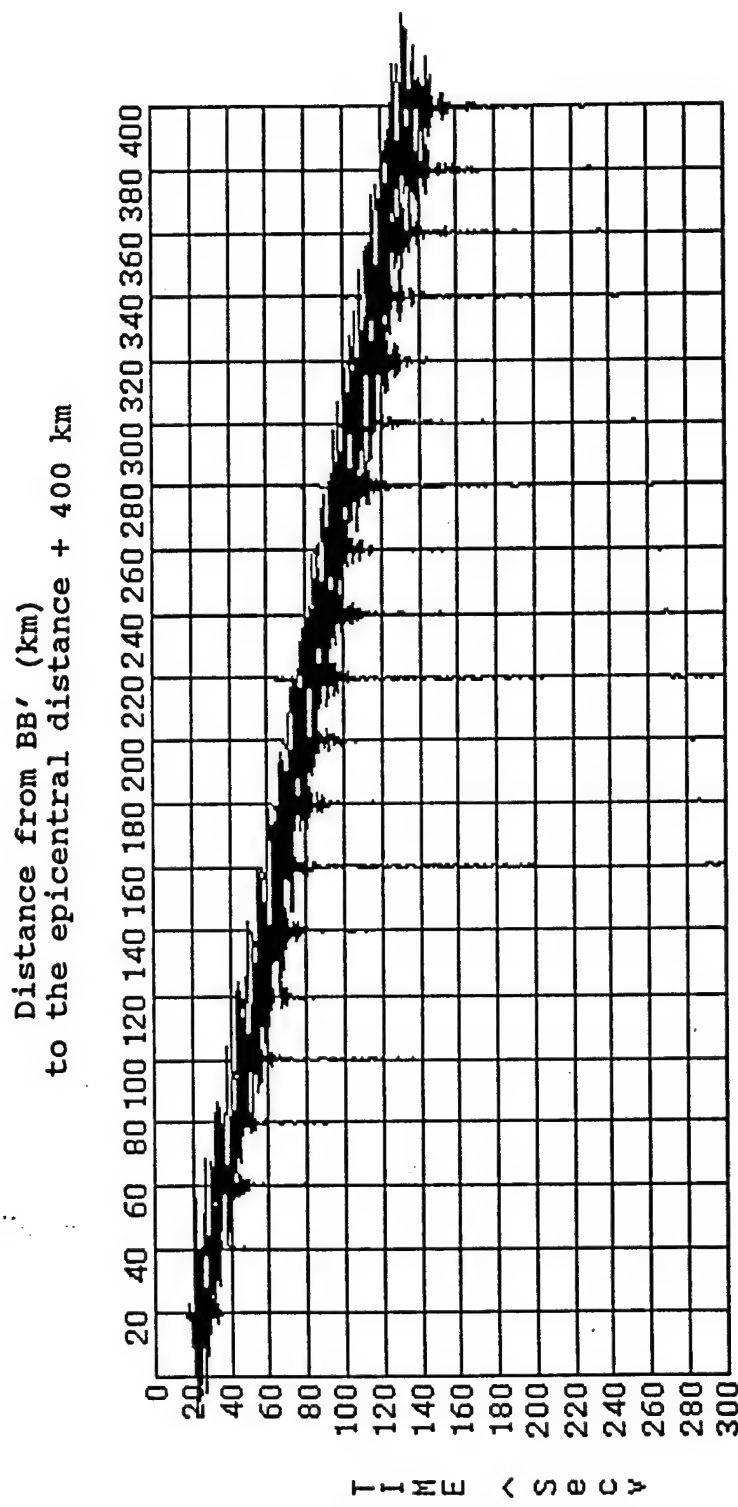


Figure 7-(c). The finite-element synthetic seismogram for the Basin Model of Figure 4-(b), (basin width = 250 km, basin depth = 15 km), with the basin velocity of 3.51 km/sec, as observed at distances of 20 km to 400 km by a source with a center frequency 0.667 Hz.

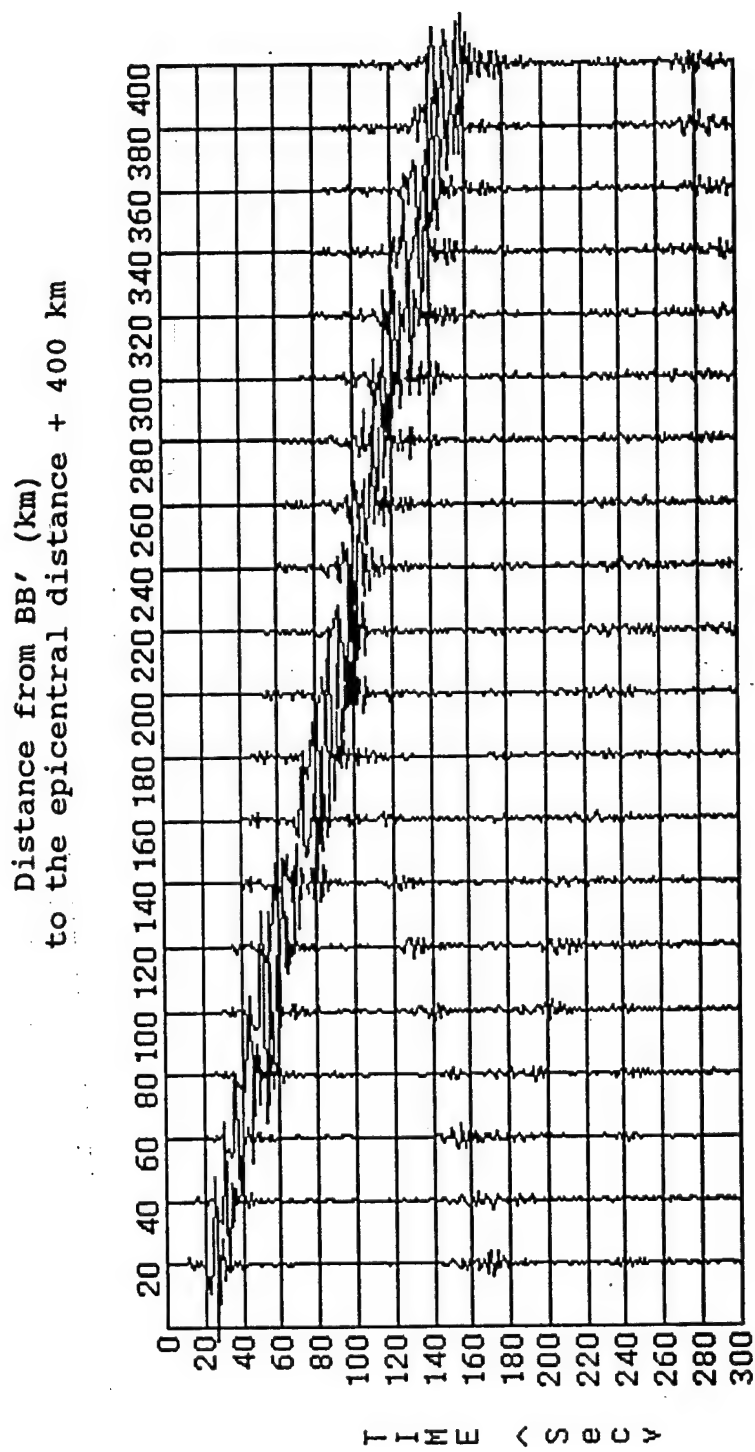


Figure 8-(a). The finite-element synthetic seismogram for the Basin Model of Figure 4-(b), (basin width = 150 km, basin depth = 15 km), with the basin velocity of 2.70 km/sec, as observed at distances of 20 km to 400 km by a source with a center frequency 0.334 Hz.

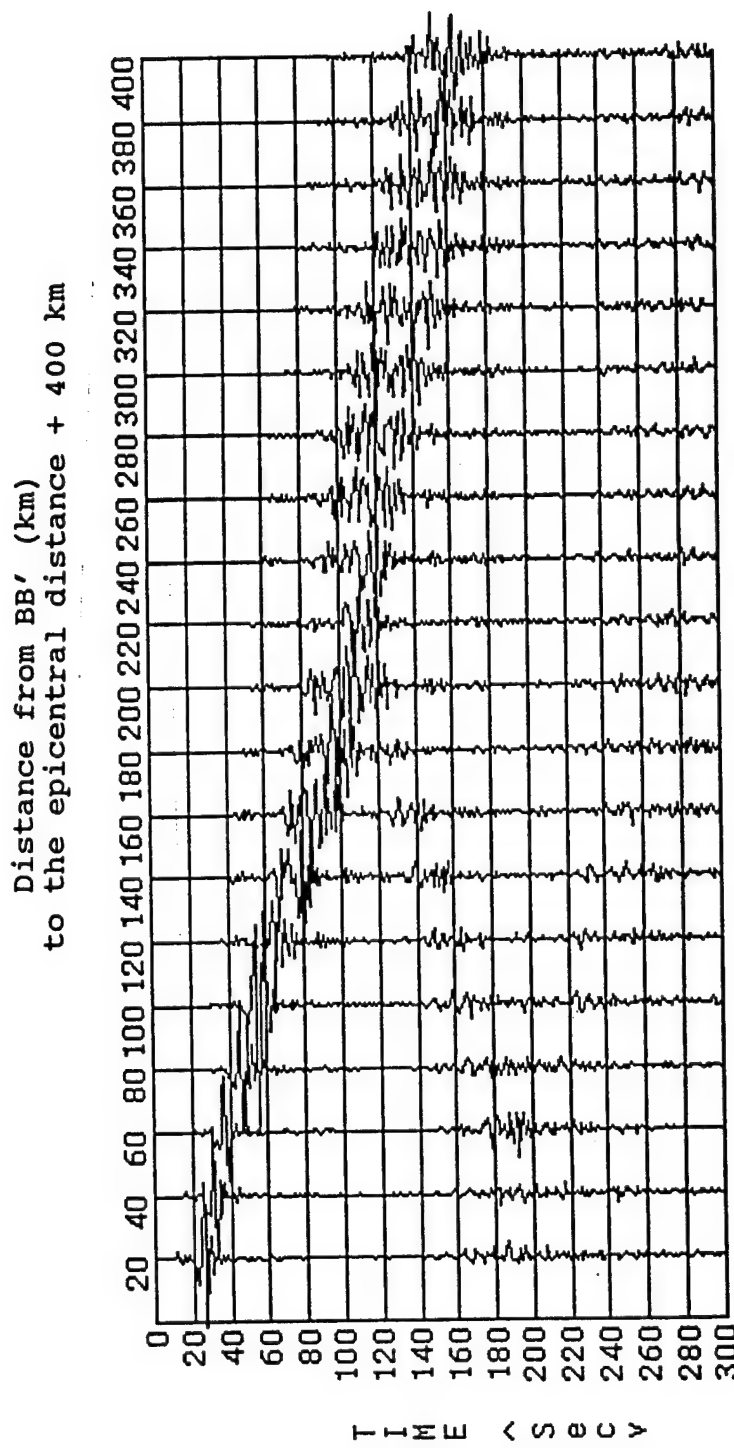


Figure 8-(b). The finite-element synthetic seismogram for the Basin Model of Figure 4-(b), (basin width = 150 km, basin depth = 15 km), with the basin velocity of 2.20 km/sec, as observed at distances of 20 km to 400 km by a source with a center frequency 0.334 Hz.

and 2.2 km/sec. The model was excited by the input waves given at the cross section BB' as the result of an impulsive source with a center-frequency of 0.334 Hz exploded in Island Margin Model as shown in Figure 6-(b) as the input to the Barents Sea portion of the Novaya Zemlya to ARCESS path.

In both cases, in addition to the arrivals of Sn and Lg observed from 20 to 400 km from BB', there are scattered events from the two limbs of the basin clearly shown at the locations between the input source and the left limb of the basin as marked by the dashed lines. The reflections arriving later but stronger for the basin velocity of 2.2 km/sec case (Figure 8-(a)) are due to a higher contrast of velocity between the crust and the basin sediments in comparison with that of the sediment velocity 2.7 km/sec case (Figure 8-(b)). For a basin width of 150 km, these scattered events arrive at the distance about 200 km from BB'; for that of 250 km, they arrive at the distance about 320 km.

In the locations closer to the input source at BB', the main features as shown in Figure 8-(a) and 8-(b) are the emergent arrivals of Sn, which are followed by the distinct Lg arrivals. While at the locations adjacent to or beyond the left limb of the basin, the Lg waves are developed into a complicated long tremor or coda, with their amplitude diminishing with time. With the presence of basin, the the arrivals of Lg waves are delayed.

3.2 Effects of Basin Width:

Figures 9-(a) and 9-(b) are the finite-element synthetic seismograms with the configurations of the model identical to these for Figures 8-(a) and 8-(b), except a basin width of 250 km was used. All the essential wave characteristics as revealed in Figures 8-(a) and 8-(b) are preserved. However, for a basin width of 250 km in comparison

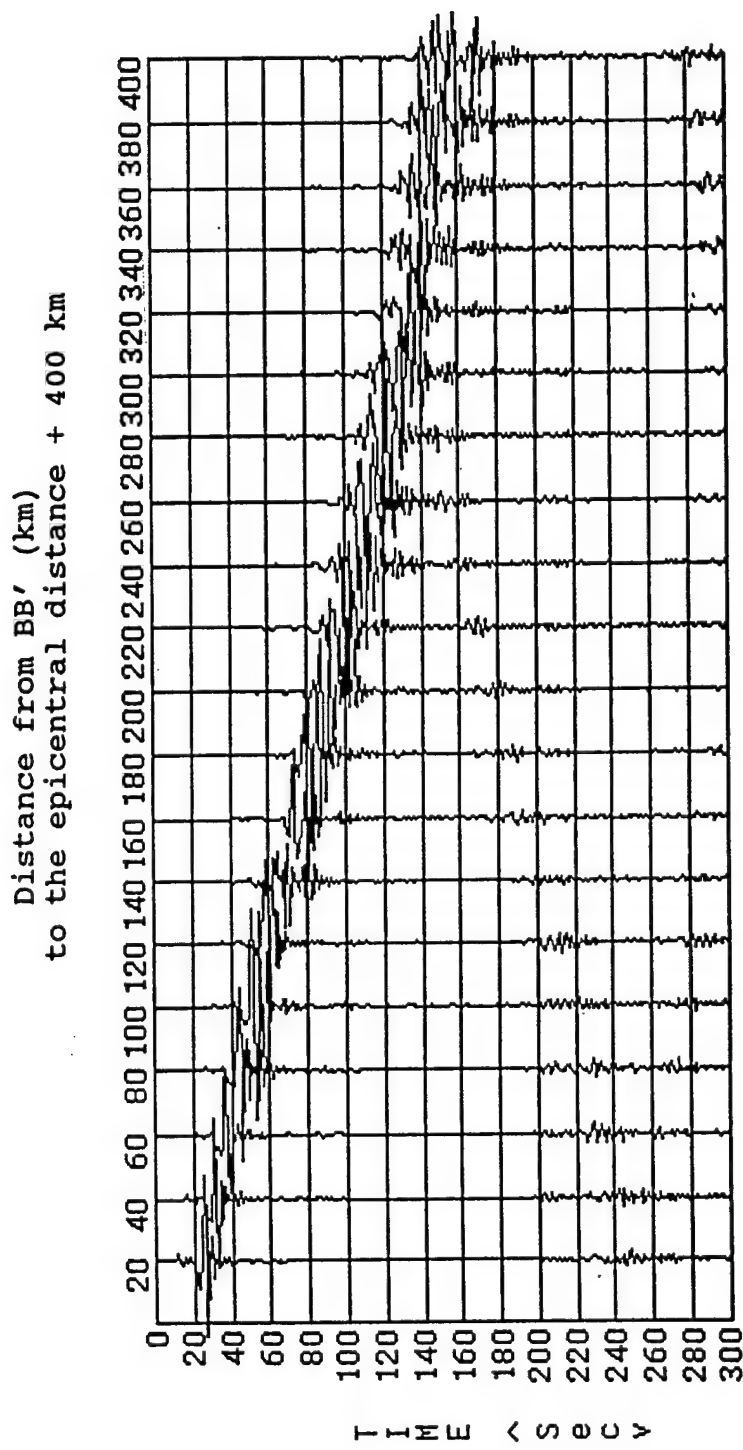


Figure 9-(a). The finite-element synthetic seismogram for the Basin Model of Figure 4-(b), (basin width = 250 km, basin depth = 15 km), with the basin velocity of 2.70 km/sec, as observed at distances of 20 km to 400 km by a source with a center frequency 0.334 Hz.

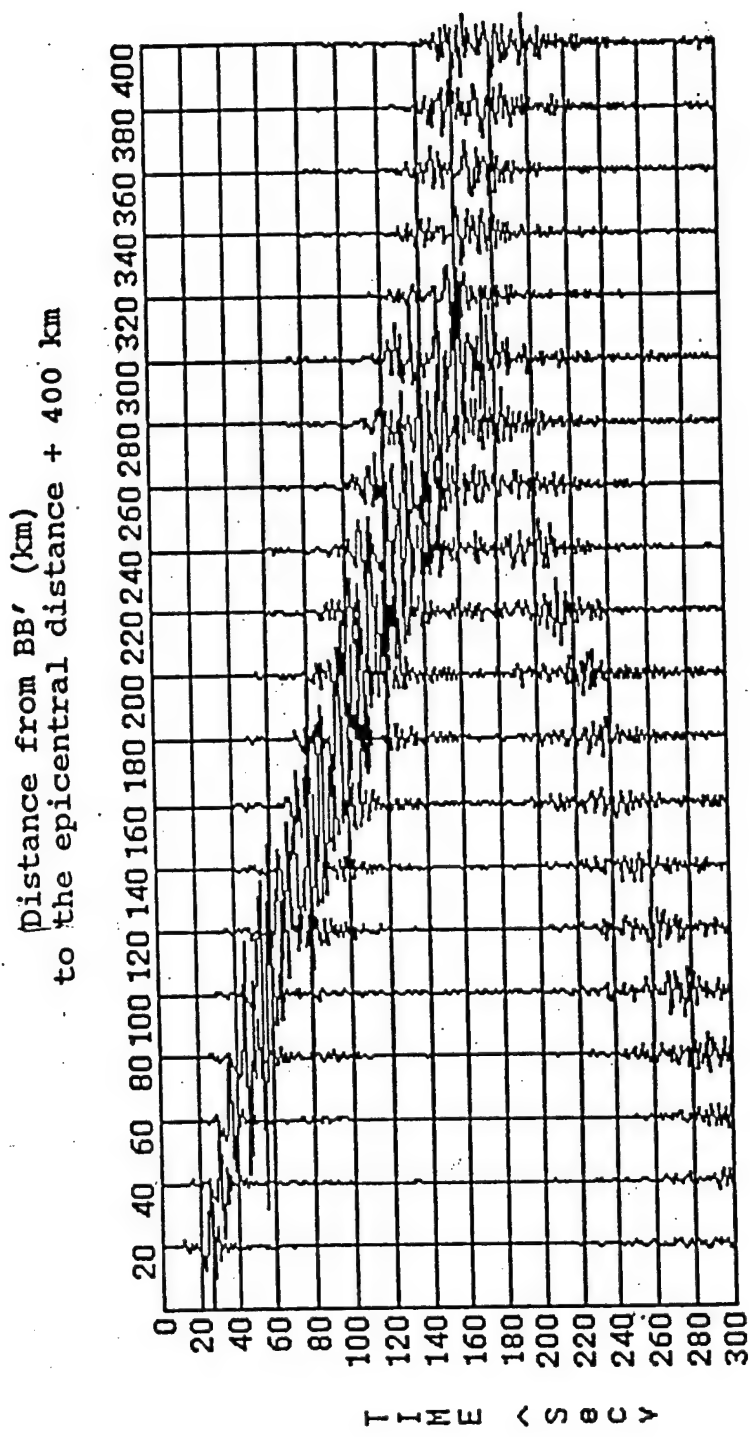


Figure 9-(b). The finite-element synthetic seismogram for the Basin Model of Figure 4-(b), (basin width = 250 km, basin depth = 15 km), with the basin velocity of 2.20 km/sec, as observed at distances of 20 km to 400 km by a source with a center frequency 0.334 Hz.

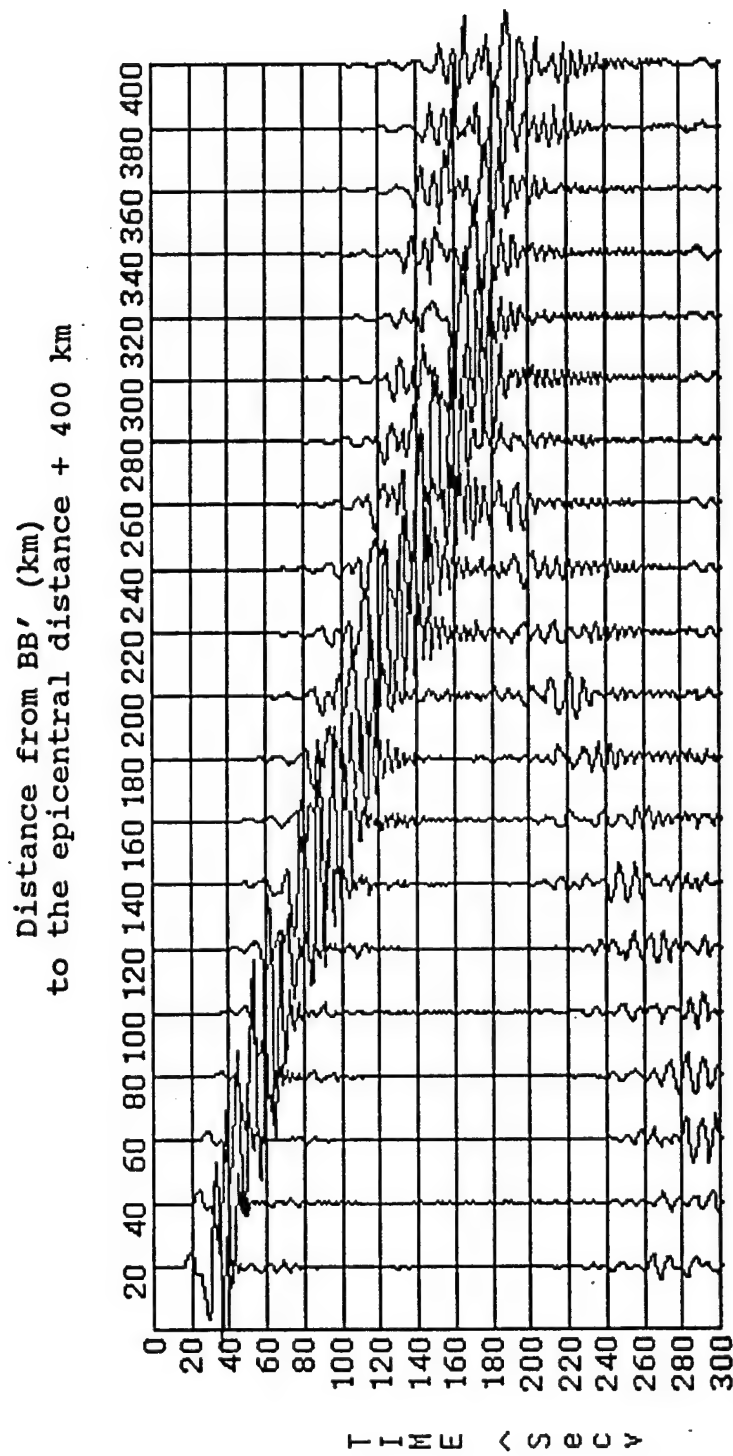


Figure 10-(a). The finite-element synthetic seismogram for the Basin Model of Figure 4-(b), (basin width = 250 km, basin depth = 15 km), with the basin velocity of 2.20 km/sec, as observed at distances of 20 km to 400 km by a source with a center frequency 0.167 Hz.

with that of 150 km, there are laterally scattered waves from the limbs of the basin. The scattered waves are delayed by traveling an additional width of 100 km in the basin. These scattered waves contain both the Sn and Lg arrivals and have nearly the same characteristics as those of Sn and Lg waves.

3.3 Effects of Frequency Content:

With the sediment velocity of 2.20 km/sec and the basin width of 250 km as constant, Figures 10-(a), 10-(b), and 10-(c) are the finite-element synthetic seismograms to demonstrate the effects of the center-frequencies of the source 0.167, 0.334, and 0.667 Hz on the Lg wave propagation.

The essential features of the arrivals of Sn and Lg as well as the scattered events due to the presence of the basin are very similar for three different center-frequencies of the source. The arrivals of Sn are more emergent for the center-frequency 0.167 Hz than those for that 0.334 and 0.667 Hz. The amplitudes of both the arrivals of Sn and Lg as well as the scattered events are comparable for the center-frequency of 0.167 Hz, and those of the Sn and Lg are higher than the scattered for the center-frequency of either 0.334 Hz or 0.667 Hz.

The model parameters used for generating Figures 11-(a), 11-(b) and 11-(c) are the same as those for Figures 10-(a), 10-(b), and 10-(c) except the sediment velocity is now changed to 2.7 km/sec. While the other wave characteristics of Sn and the scattered events due to the presence of the basin remain similar, the amplitudes of Sn, Lg, and the scattered events are sharply decreased due to the differences of the sediment velocity.

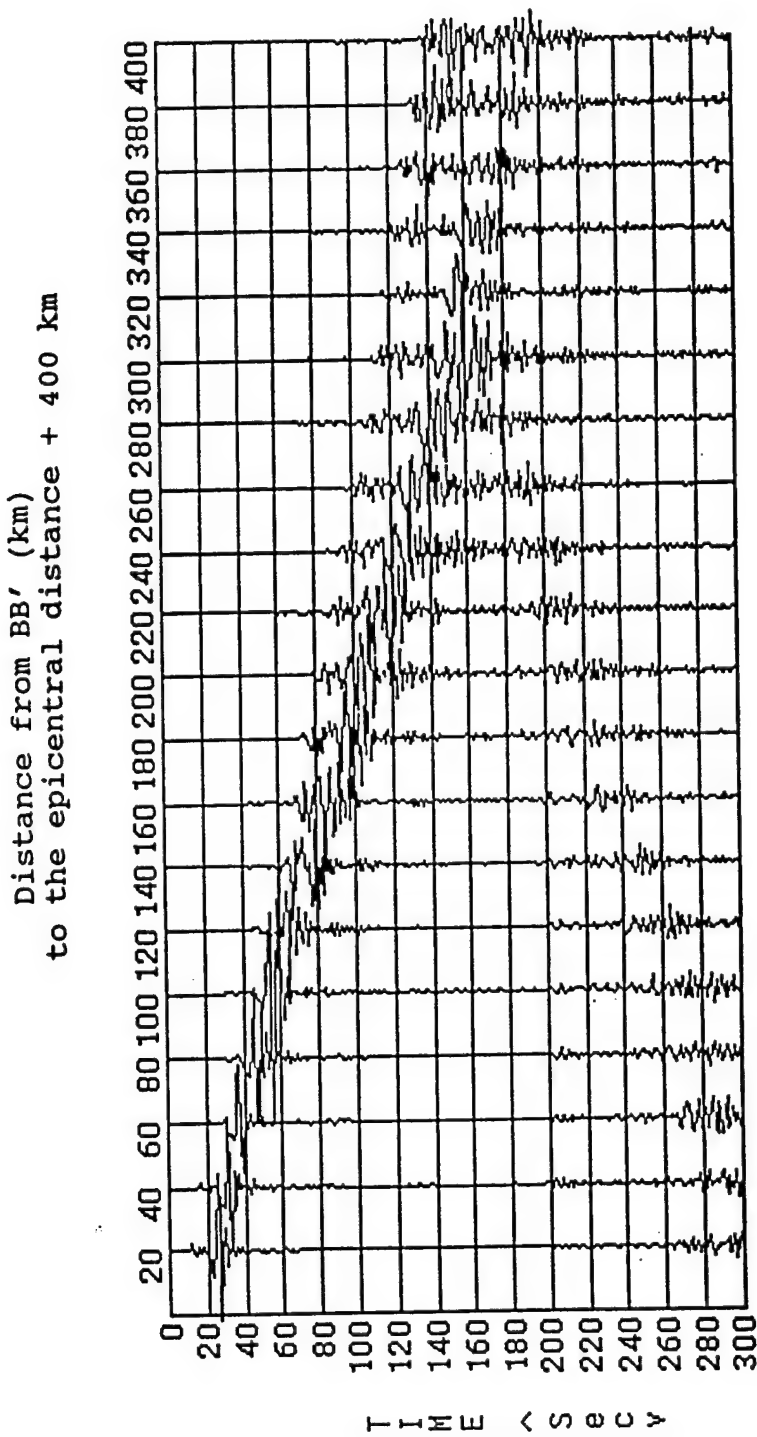


Figure 10-(b). The finite-element synthetic seismogram for the Basin Model of Figure 4-(b), (basin width = 250 km, basin depth = 15 km), with the basin velocity of 2.20 km/sec, as observed at distances of 20 km to 400 km by a source with a center frequency 0.334 Hz.

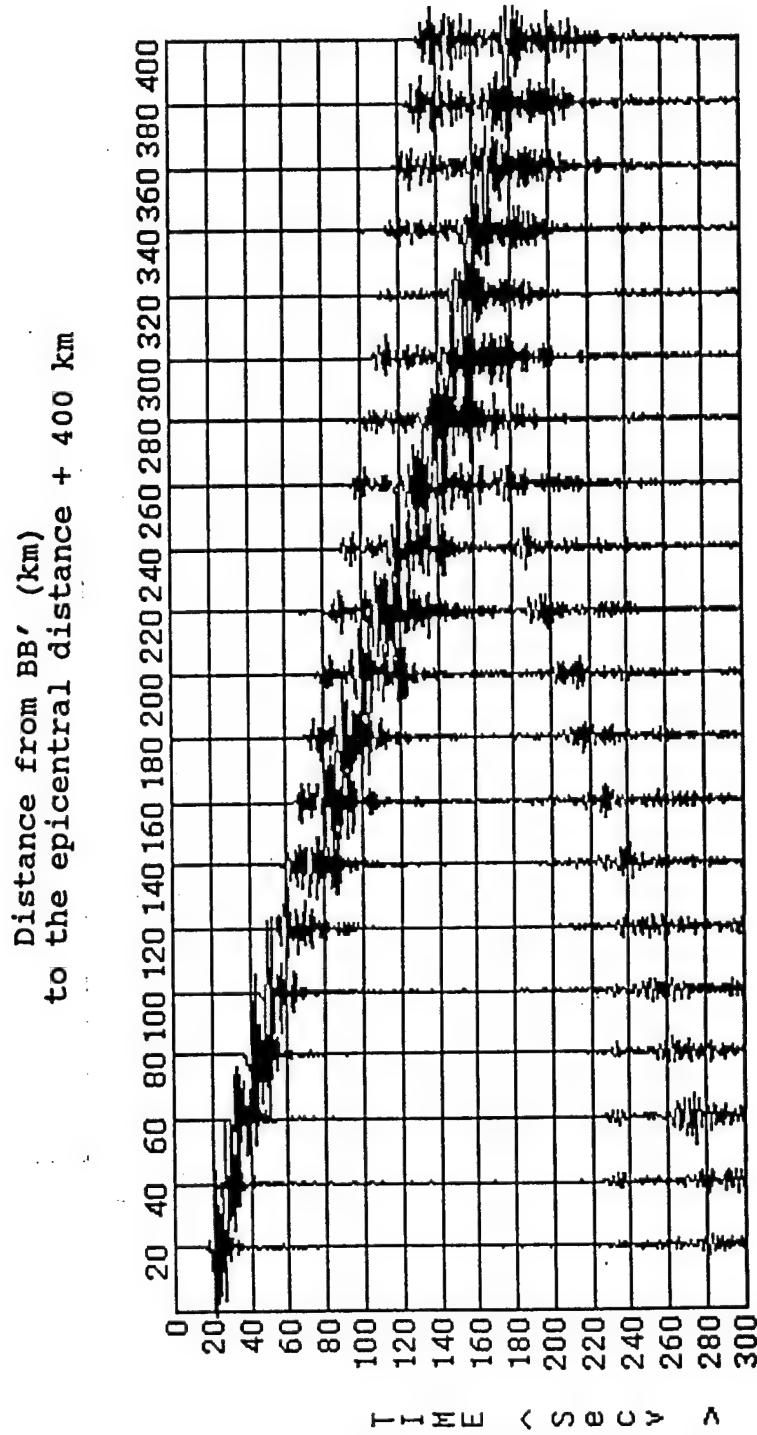


Figure 10-(c). The finite-element synthetic seismogram for the Basin Model of Figure 4-(b), (basin width = 250 km, basin depth = 15 km), with the basin velocity of 2.20 km/sec, as observed at distances of 20 km to 400 km by a source with a center frequency 0.667 Hz.

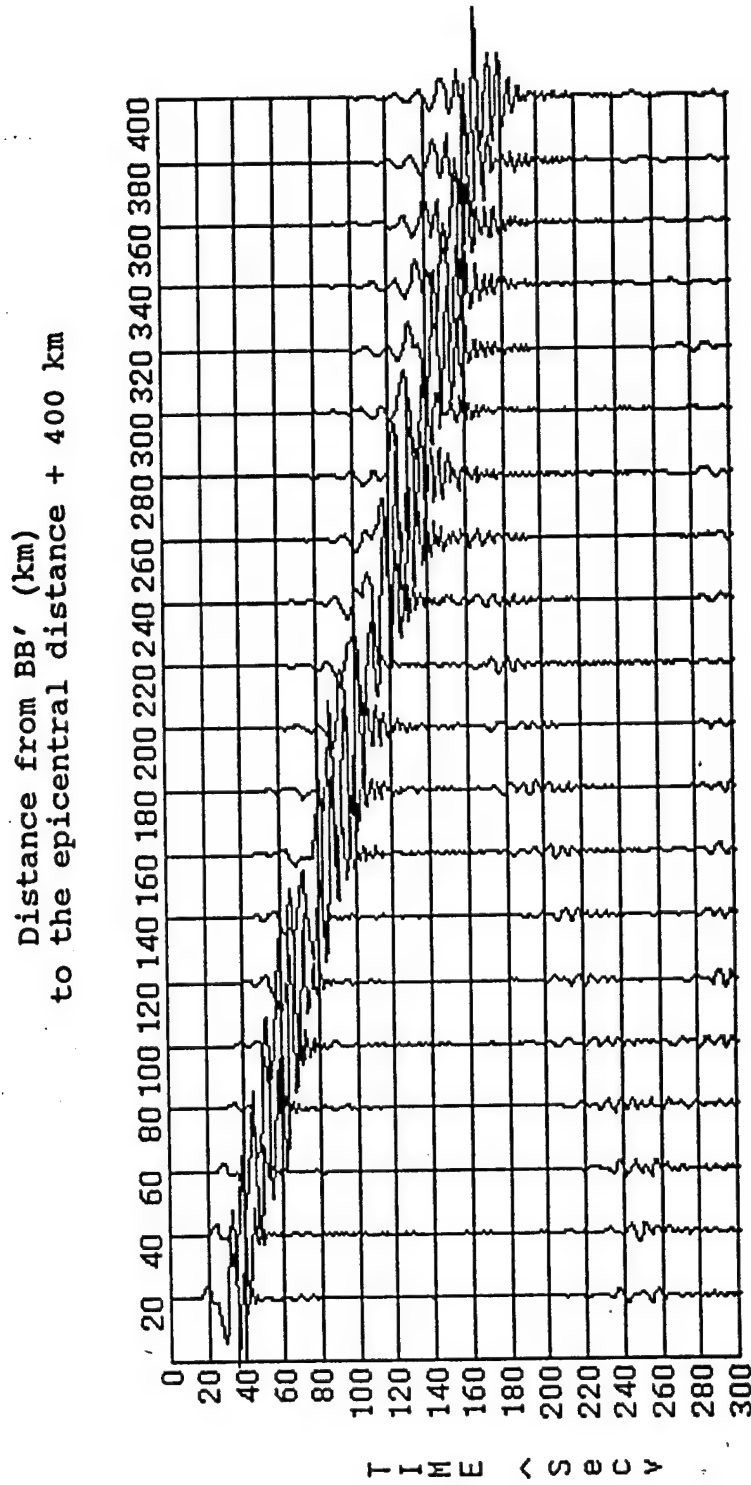


Figure 11-(a). The finite-element synthetic seismogram for the Basin Model of Figure 4-(b), (basin width = 250 km, basin depth = 15 km), with the basin velocity of 2.70 km/sec, as observed at distances of 20 km to 400 km by a source with a center frequency 0.167 Hz.

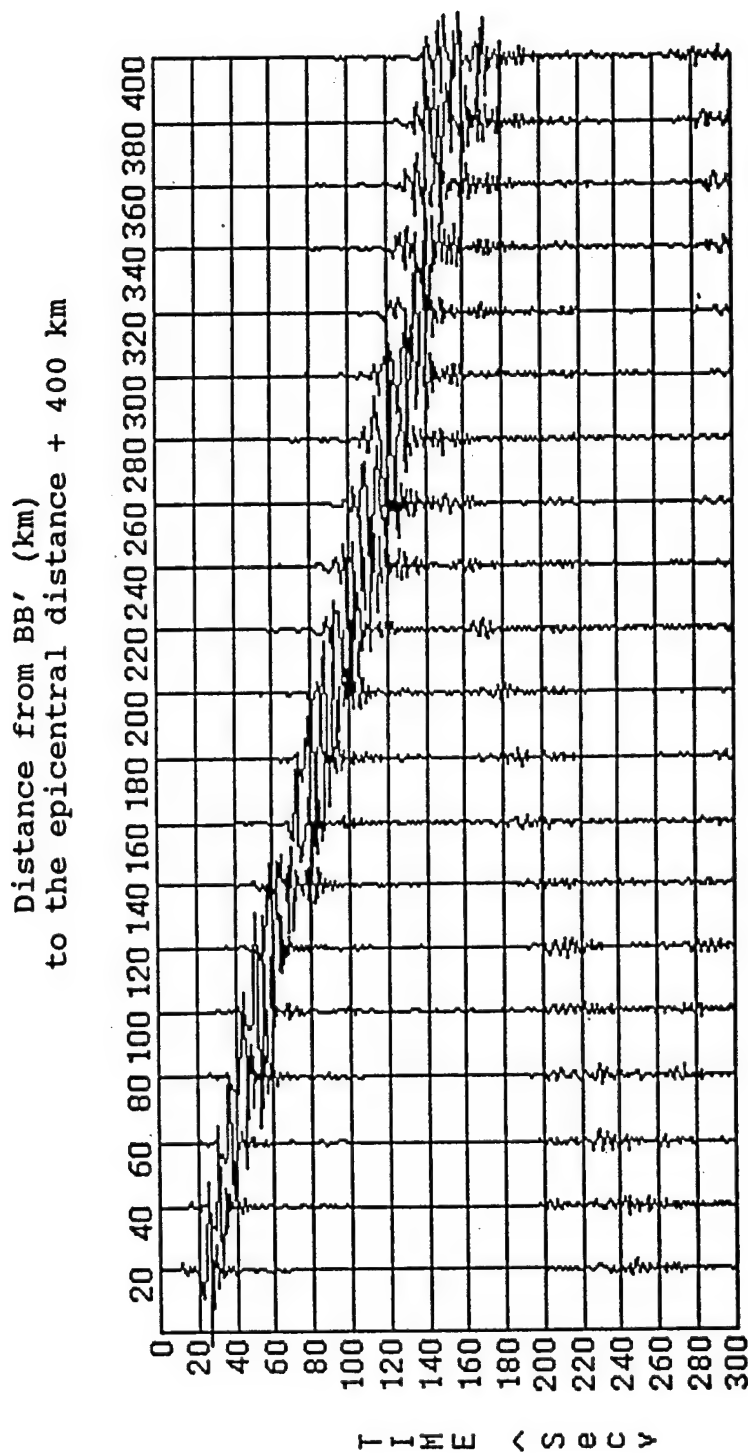


Figure 11-(b). The finite-element synthetic seismogram for the Basin Model of Figure 4-(b), (basin width = 250 km, basin depth = 15 km), with the basin velocity of 2.70 km/sec, as observed at distances of 20 km to 400 km by a source with a center frequency 0.334 Hz.

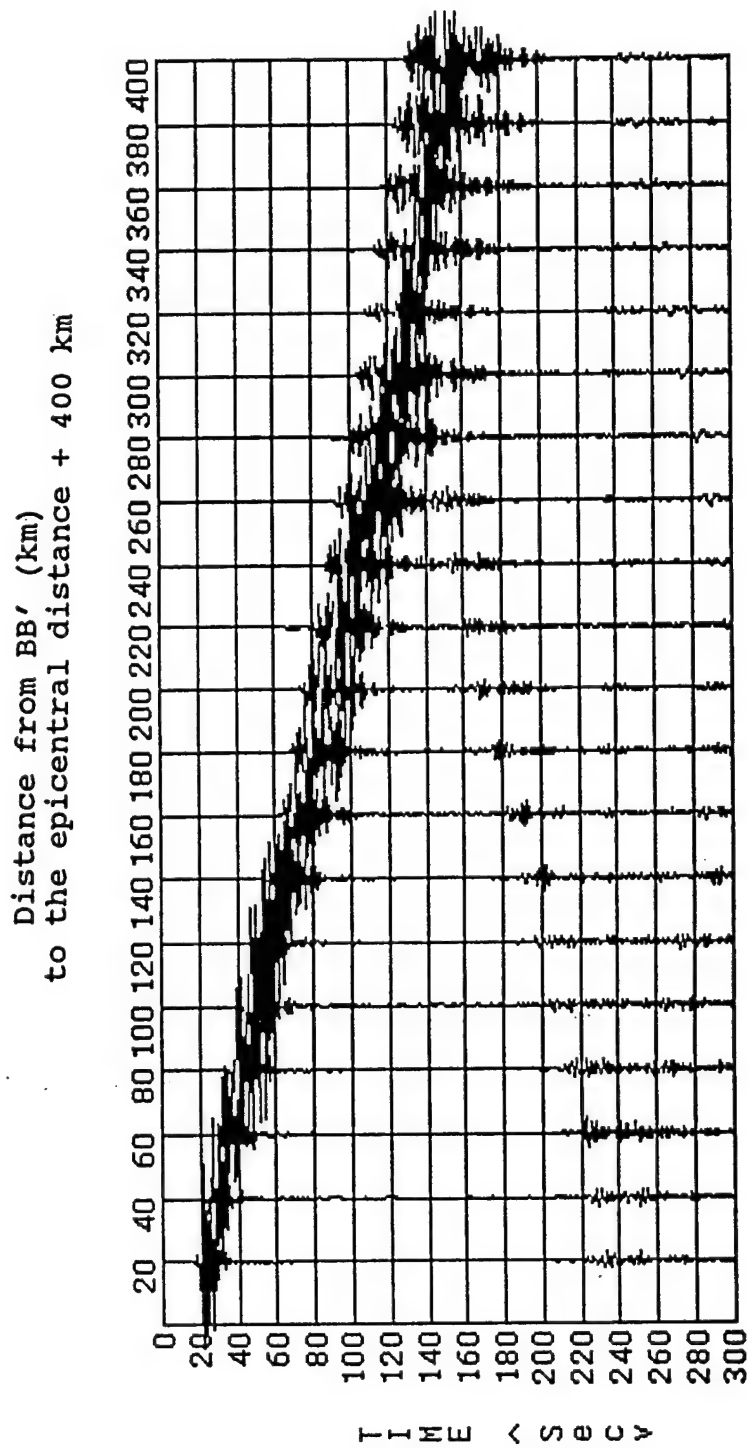


Figure 11-(c). The finite-element synthetic seismogram for the Basin Model of Figure 4-(b), (basin width = 250 km, basin depth = 15 km), with the basin velocity of 2.70 km/sec, as observed at distances of 20 km to 400 km by a source with a center frequency 0.667 Hz.

4 Model II:

4.1 Effects of Basin Width:

Figures 12-(a) and 12-(b) show the finite-element synthetic seismograms for Model II with a center-frequency of the source 0.334 Hz, a sediment velocity of 2.7 km/sec and two basin widths of 150 km and 250 km. Both the Sn and Lg waves are well developed in the distances from 20 to 400 km from the cross section BB'. However, in the case of the basin width 250 km, the amplitude of the Lg decays more rapidly than that in the case of the basin width 150 km. The scattered waves due to the limbs of the basin are clearly observed in both the basin widths.

Figures 13-(a) and 13-(b) give the finite-element synthetic seismograms for Model II with a sediment velocity 2.2 km/sec; otherwise the model is identical to that used in Figures 12-(a) and 12-(b). In Figures 13-(a) and 13-(b), the scattered waves due to the limbs of the basin arrive later but stronger because of a higher velocity contrast between the crust and the sediments in the basin in comparison with a sediment velocity 2.70 km/sec as shown in Figures 12-(a) and 12-(b).

4.2 Effect of Basin on the Blockage of Lg

The Lg amplitudes as observed on the left limb of the basin beyond the distance of 300 km from the cross section BB' for the basin width 250 km are drastically decreased in comparison with those on the right-side of the basin facing the source and in the basin proper. Figure 12-(b) shows clearly that the Lg waves have been blocked by the presence of the basin.

In the case of the basin width 150km, the blockage of Lg as shown in Figure 12-(a) is not as obvious as in the case for the basis width 250 km. The amplitudes of Lg for

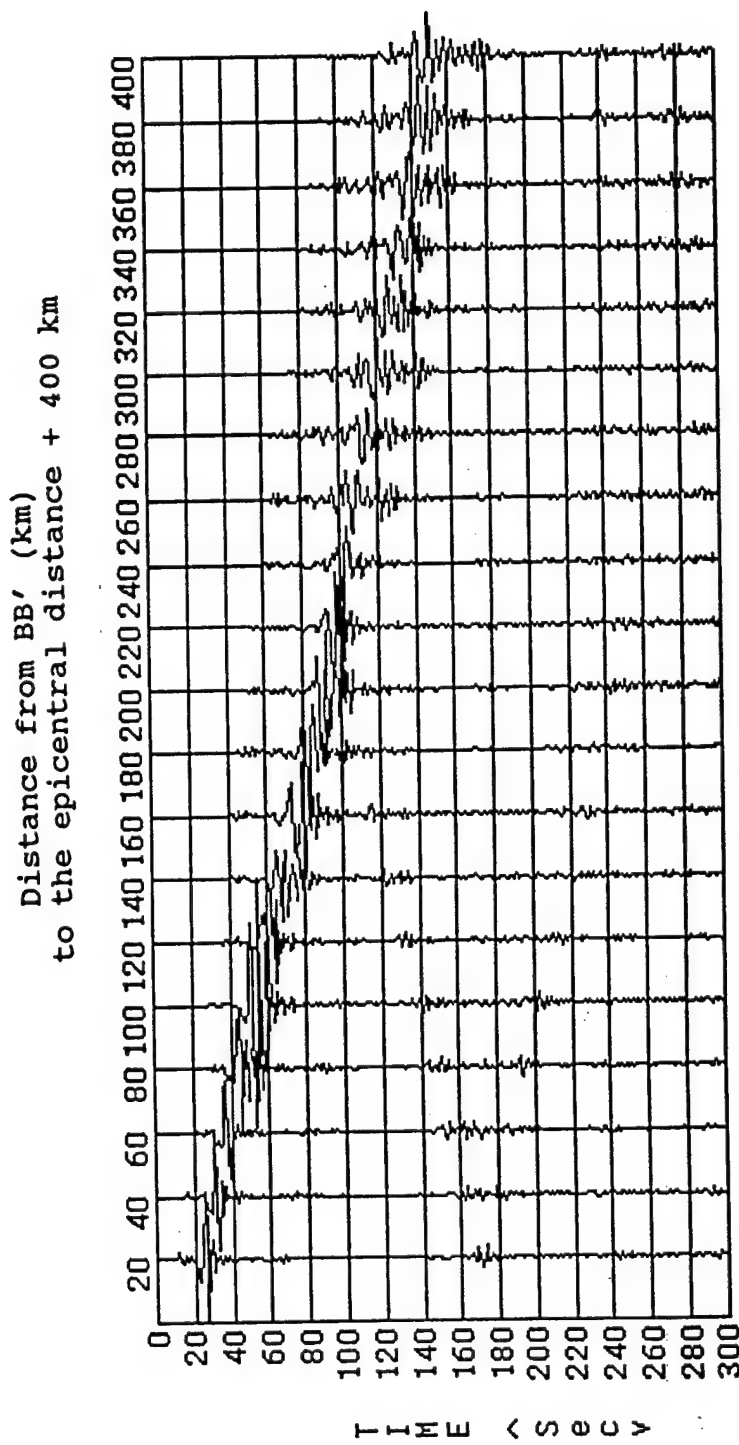


Figure 12-(a). The finite-element synthetic seismogram for the Basin Model and Crust-Pinch Model of Figure 4-(c), (basin width = 150 km, basin depth = 15 km, height of Moho-uplift = 10 km), with the basin velocity of 2.70 km/sec, as observed at distances of 20 km to 400 km by a source with a center frequency 0.334 Hz.

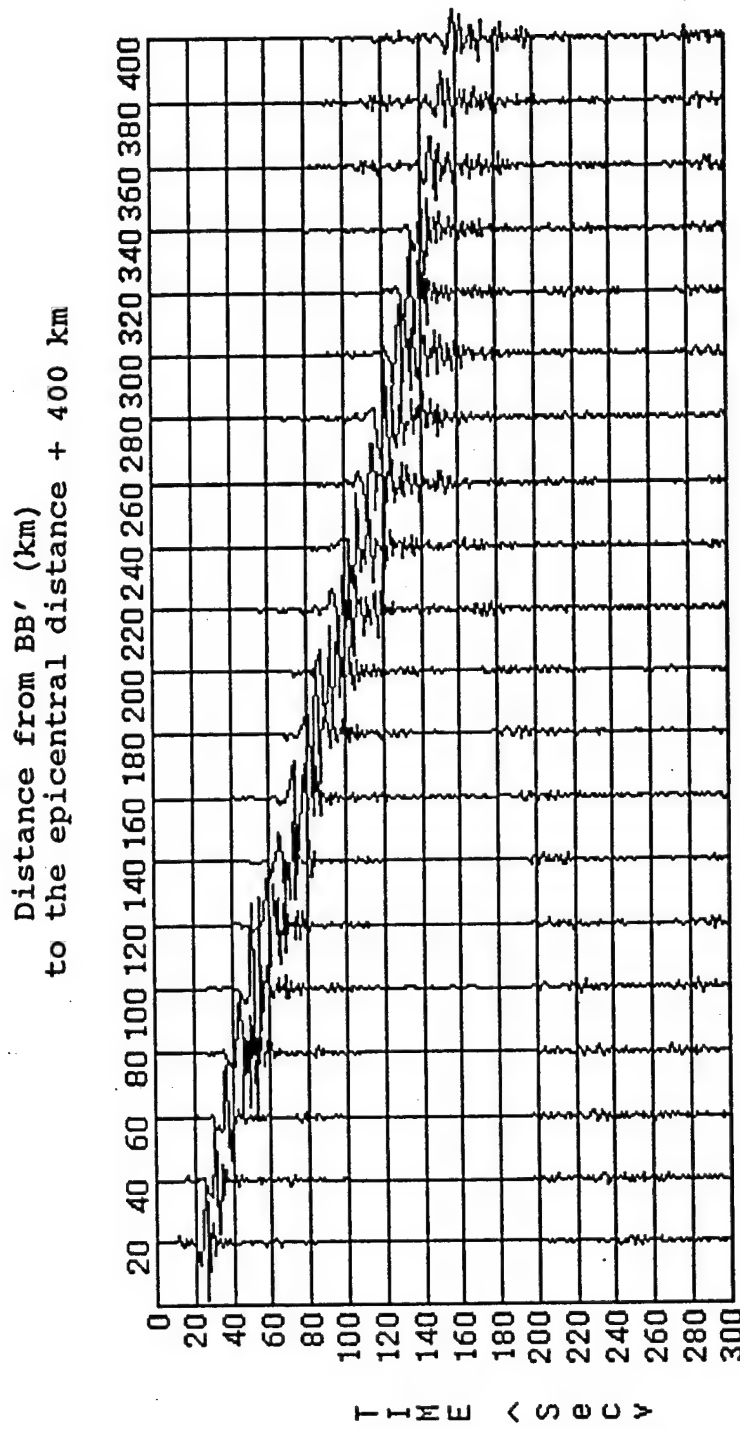


Figure 12-(b). The finite-element synthetic seismogram for the Basin Model and Crust-Pinch Model of Figure 4-(c), (basin width = 250 km, basin depth = 15 km, height of Moho-uplift = 10 km), with the basin velocity of 2.70 km/sec, as observed at distances of 20 km to 400 km by a source with a center frequency 0.334 Hz.

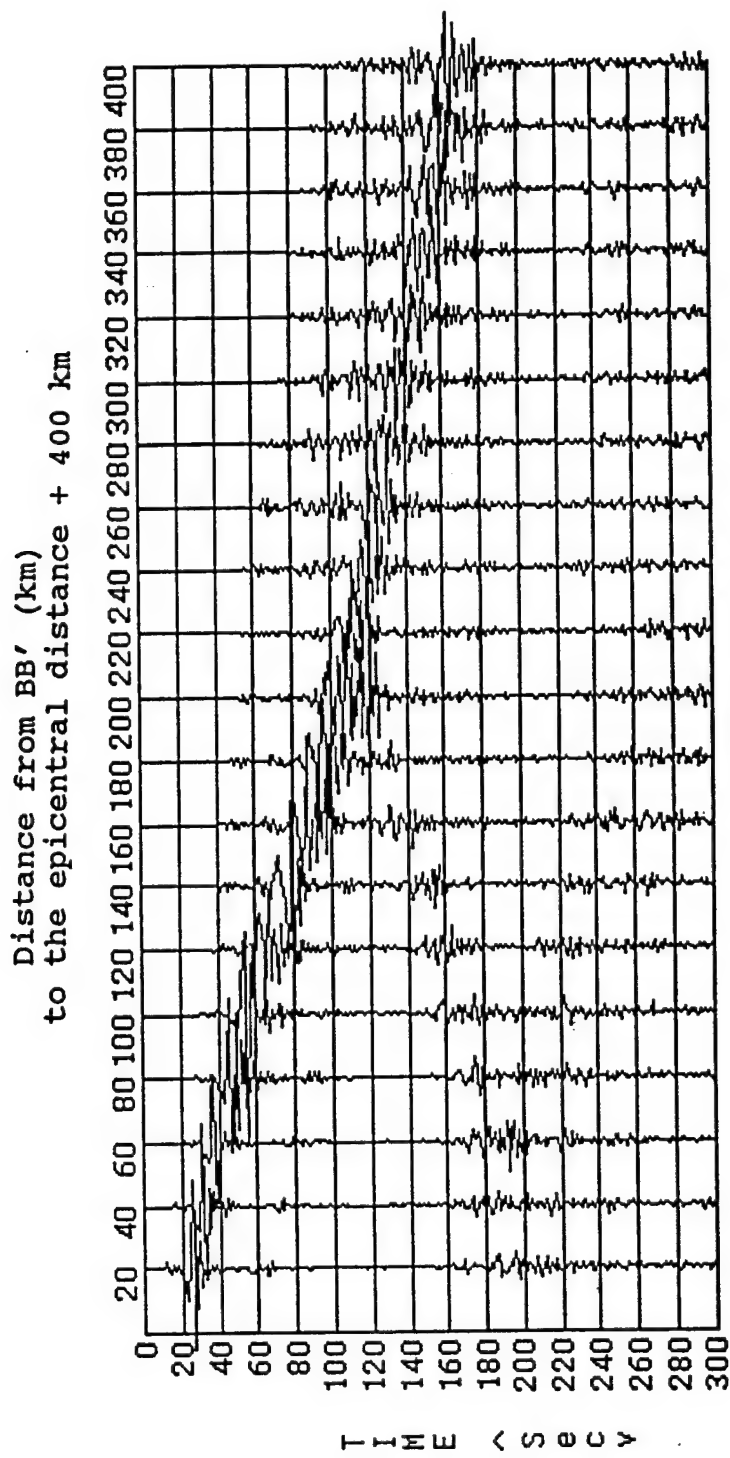


Figure 13-(a). The finite-element synthetic seismogram for the Basin Model and Crust-Pinch Model of Figure 4-(c), (basin width = 150 km, basin depth = 15 km, height of Moho-uplift = 10 km), with the basin velocity of 2.20 km/sec, as observed at distances of 20 km to 400 km by a source with a center frequency 0.334 Hz.

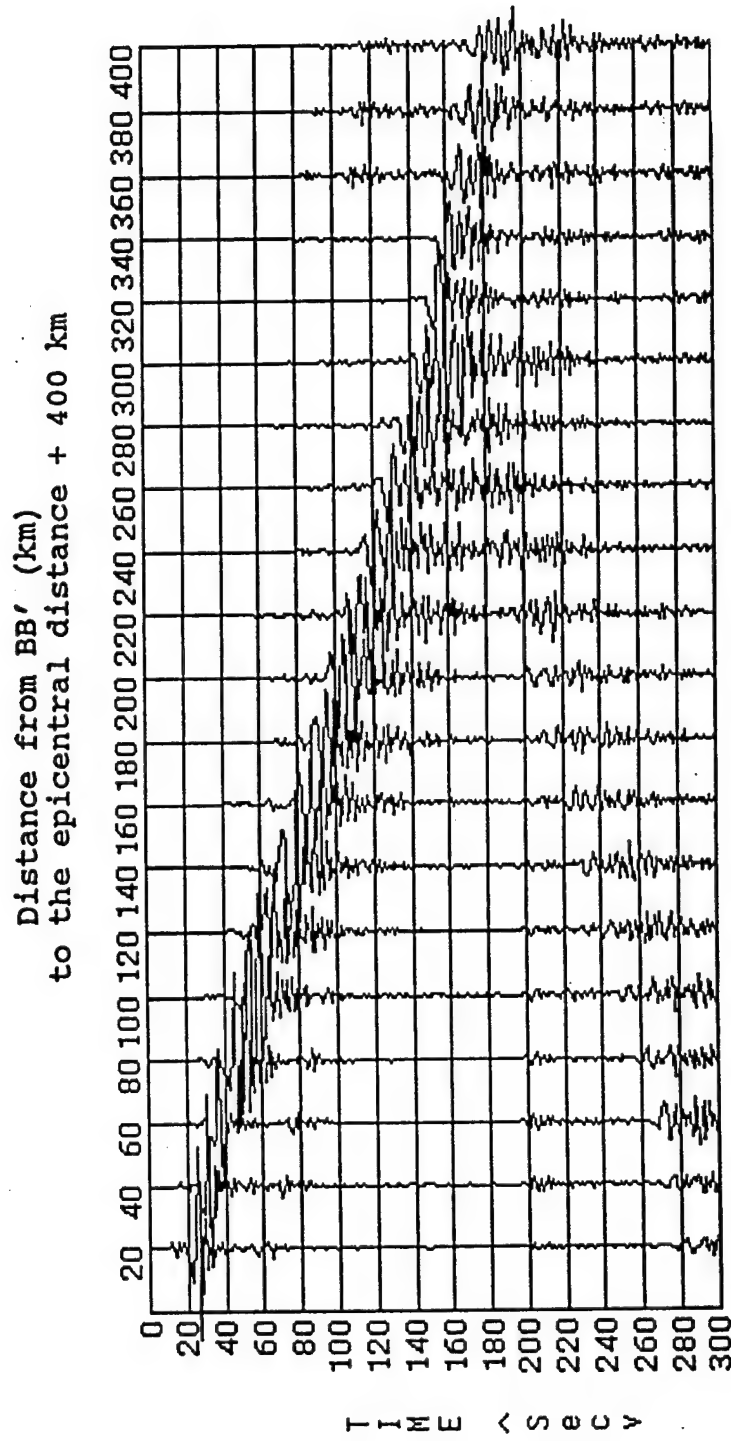


Figure 13-(b): The finite-element synthetic seismogram for the Basin Model and Crust-Pinch Model of Figure 4-(c), (basin width = 250 km, basin depth = 15 km, height of Moho-uplift = 10 km), with the basin velocity of 2.20 km/sec, as observed at distances of 20 km to 400 km by a source with a center frequency 0.334 Hz.

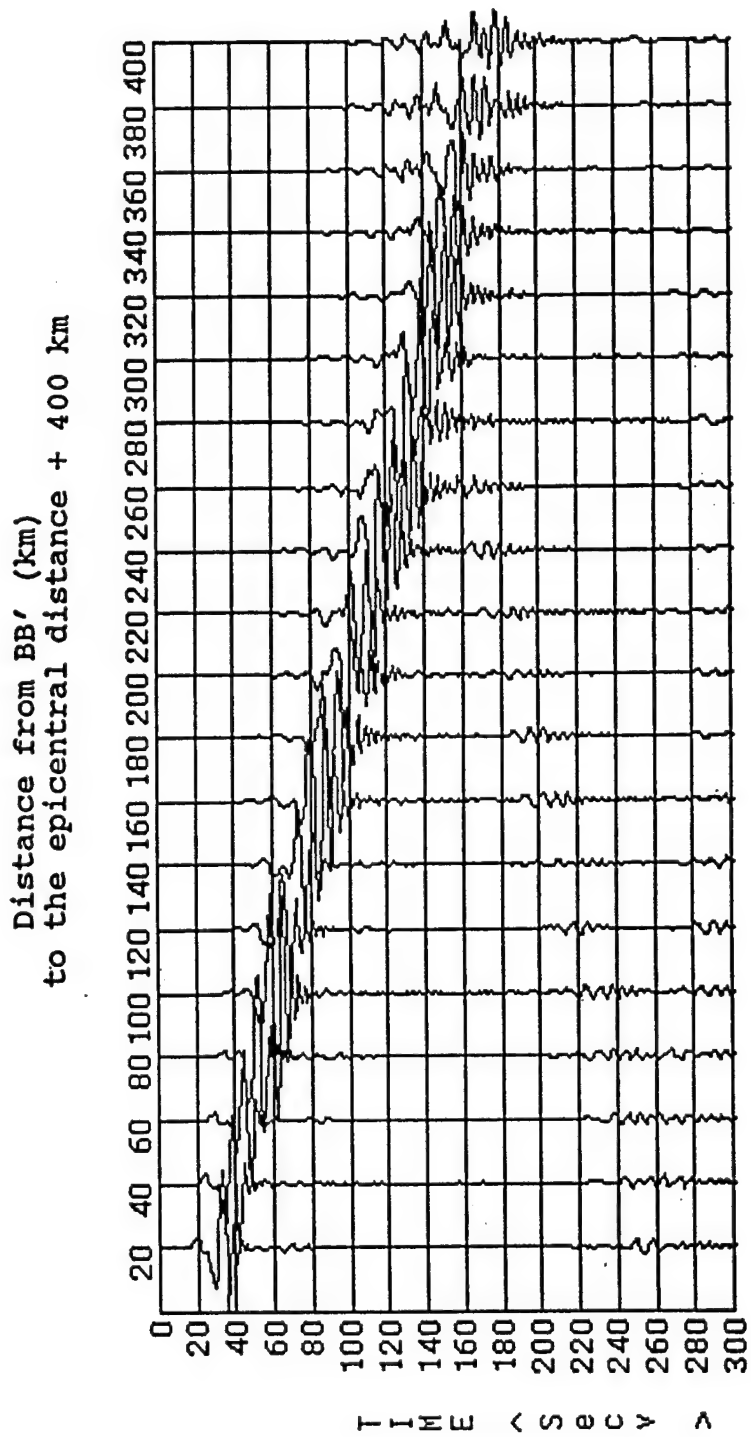


Figure 14-(a). The finite-element synthetic seismogram for the Basin Model and Crust-Pinch Model of Figure 4-(c), (basin width = 250 km, basin depth = 15 km, height of Moho-uplift = 10 km), with the basin velocity of 2.70 km/sec, as observed at distances of 20 km to 400 km by a source with a center frequency 0.167 Hz.

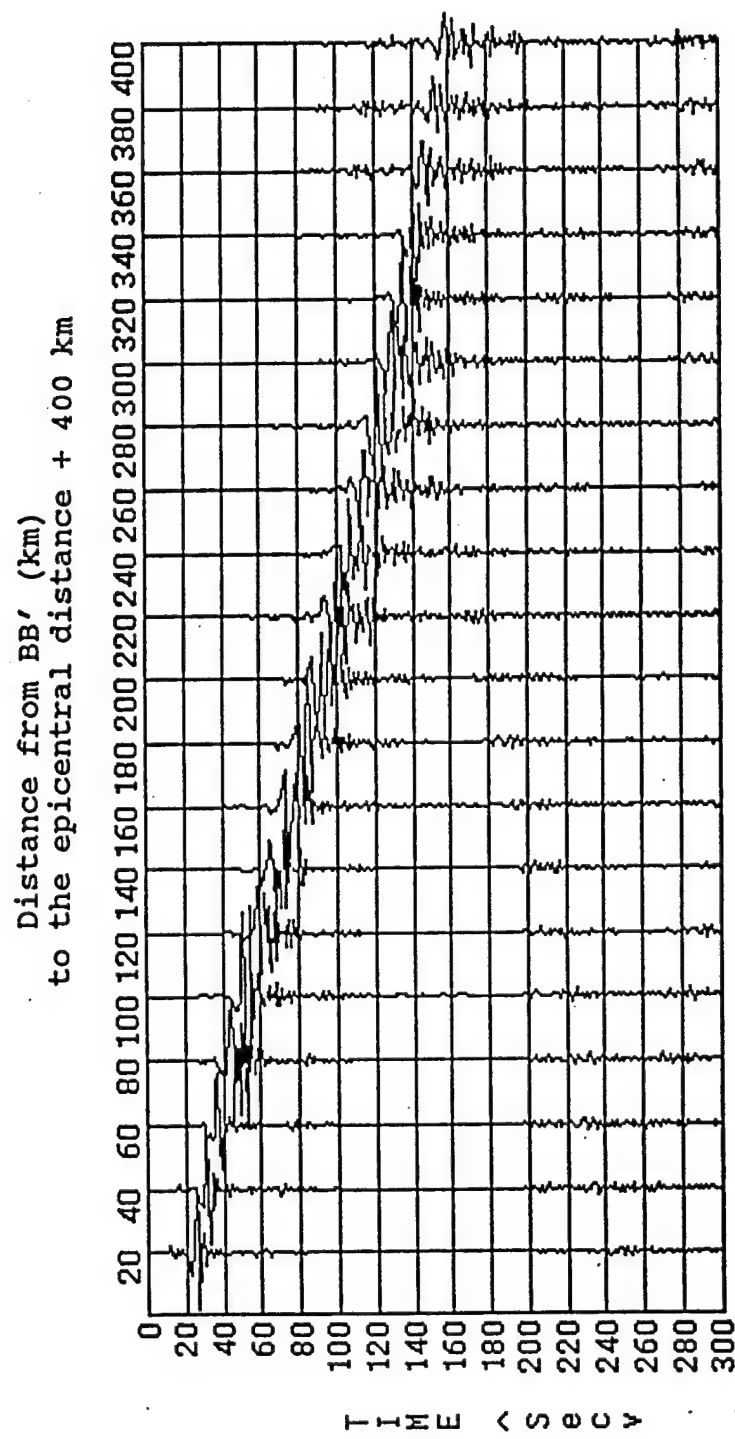


Figure 14-(b). The finite-element synthetic seismogram for the Basin Model and Crust-Pinch Model of Figure 4-(c), (basin width = 250 km, basin depth = 15 km, height of Moho-uplift = 10 km), with the basin velocity of 2.70 km/sec, as observed at distances of 20 km to 400 km by a source with a center frequency 0.334 Hz.

the basic width of 150 km after the epicentral distance of 620 km, that is beyond the left limb of the basin, are only slightly different from that of less than 620 km. The Lg amplitudes in this case remain nearly constant beyond the epicentral distance of 620 km.

The blockage of Lg propagation across a sedimentary basin, therefore, is not as simple as one may expect. The phenomenon of the blockage of the Lg waves very much depends primarily on the dimension of the basin, and the contrast between the sediment velocity and the surrounding crust velocity. However, one of the most important factors of Lg blockage is due to attenuation by the presence of low Q sediments in the basin. We will address the Lg attenuation and its blockage in the sequel.

4.3 Effects of Center-Frequency:

Figures 14-(a), 14-(b) and 14-(c) are the finite-element synthetic seismograms for Model II with a basin width 250 km, and a sediment velocity 2.7 km/sec held constant but varying the center-frequency of the source, 0.167, 0.334, and 0.667 Hz. Figures 15-(a), 15-(b) and 15-(c) are the same as Figures 14-(a), 14-(b), and 14-(c) except the sediment velocity is now 2.2 km/sec. While a pronounced appearance of emergence of both the Sn and Lg waves as well as the scattered waves is observed for a lower center-frequency of the source 0.167 Hz. As the center-frequency of the source becomes higher, both the Sn and Lg as well as the scattered waves have richer high frequency contents. It is clear that the higher the center-frequency of the source becomes, the more the waves are attenuated.

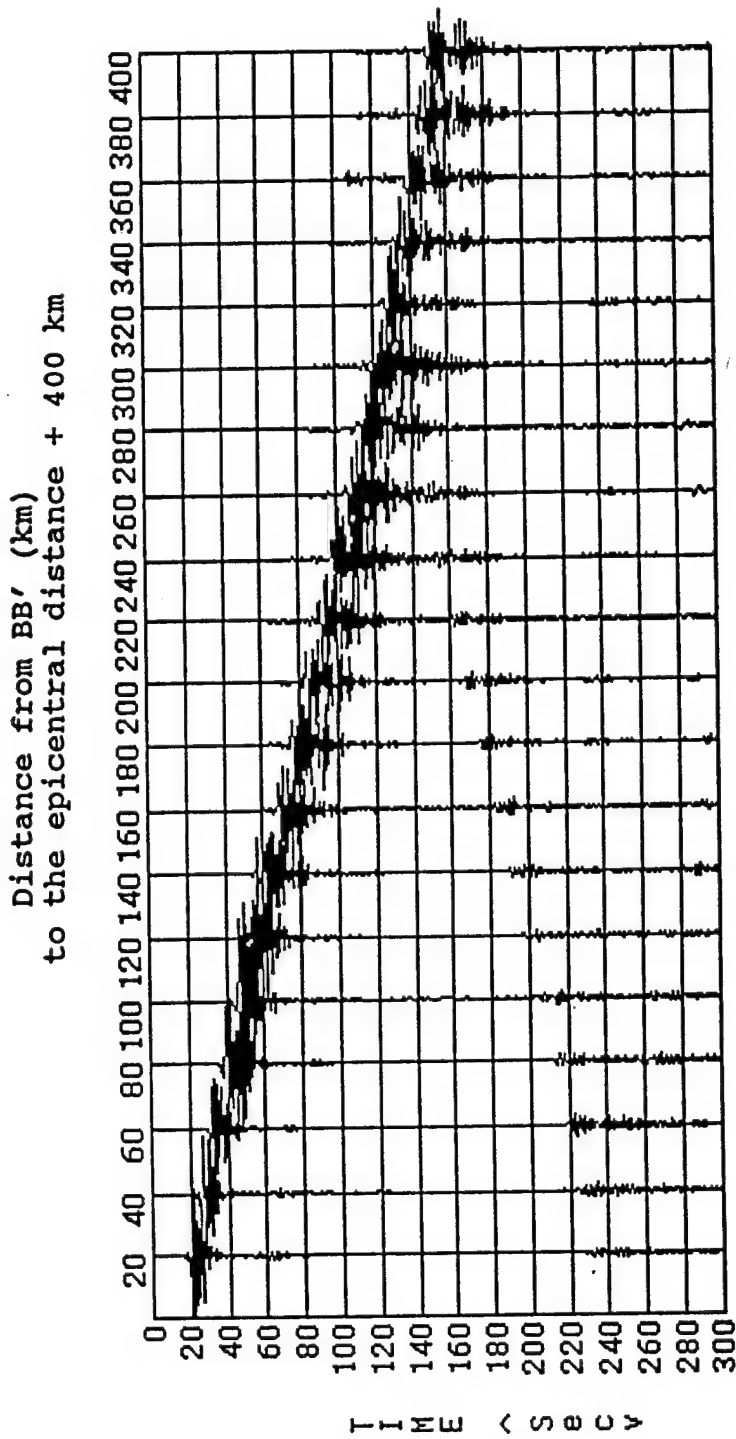


Figure 14-(c). The finite-element synthetic seismogram for the Basin Model and Crust-Pinch Model of Figure 4-(c), (basin width = 15 km, basin depth = 250 km, height of Moho-uplift = 10 km), with the basin velocity of 2.70 km/sec, as observed at distances of 20 km to 400 km by a source with a center frequency 0.667 Hz.

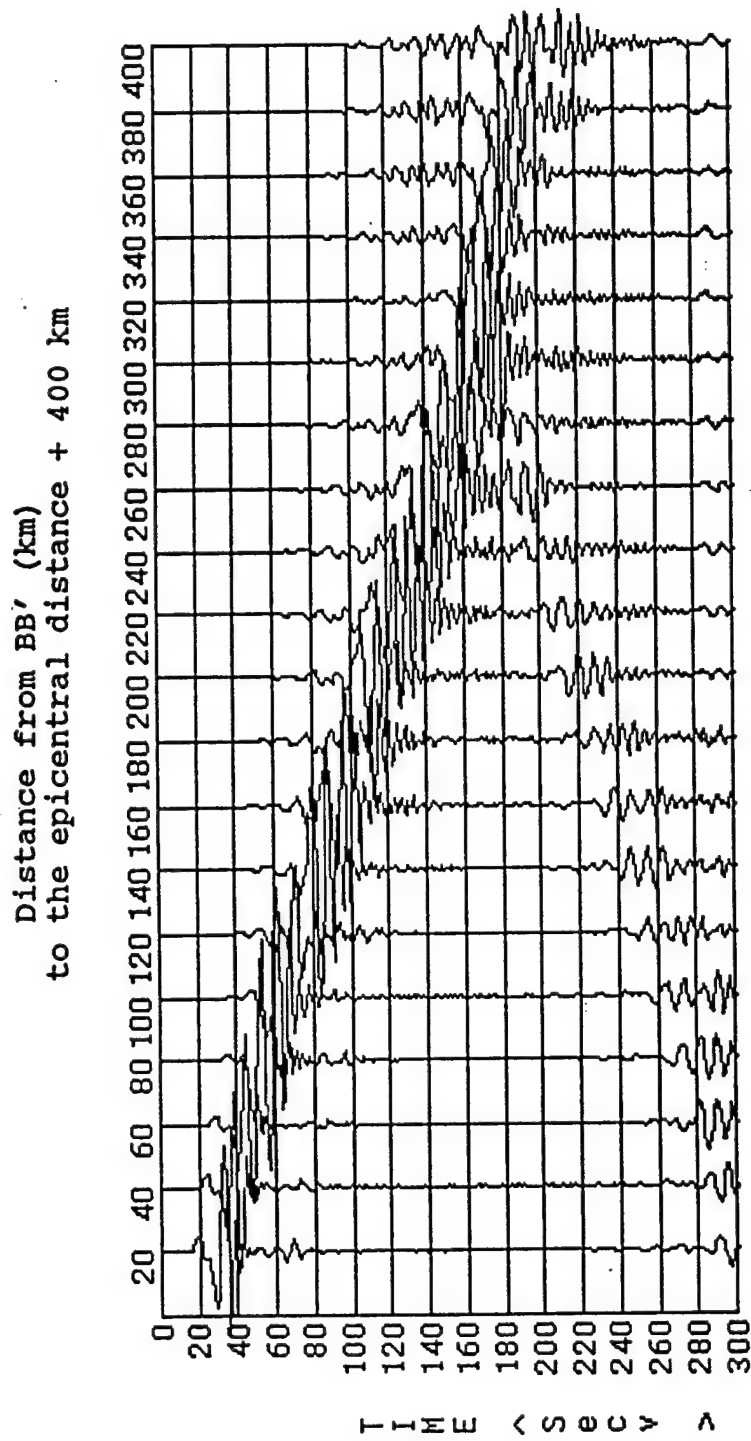


Figure 15-(a). The finite-element synthetic seismogram for the Basin Model and Crust-Pinch Model of Figure 4-(c), (basin width = 250 km, basin depth = 15 km, height of Moho-uplift = 10 km), with the basin velocity of 2.20 km/sec, as observed at distances of 20 km to 400 km by a source with a center frequency 0.167 Hz.

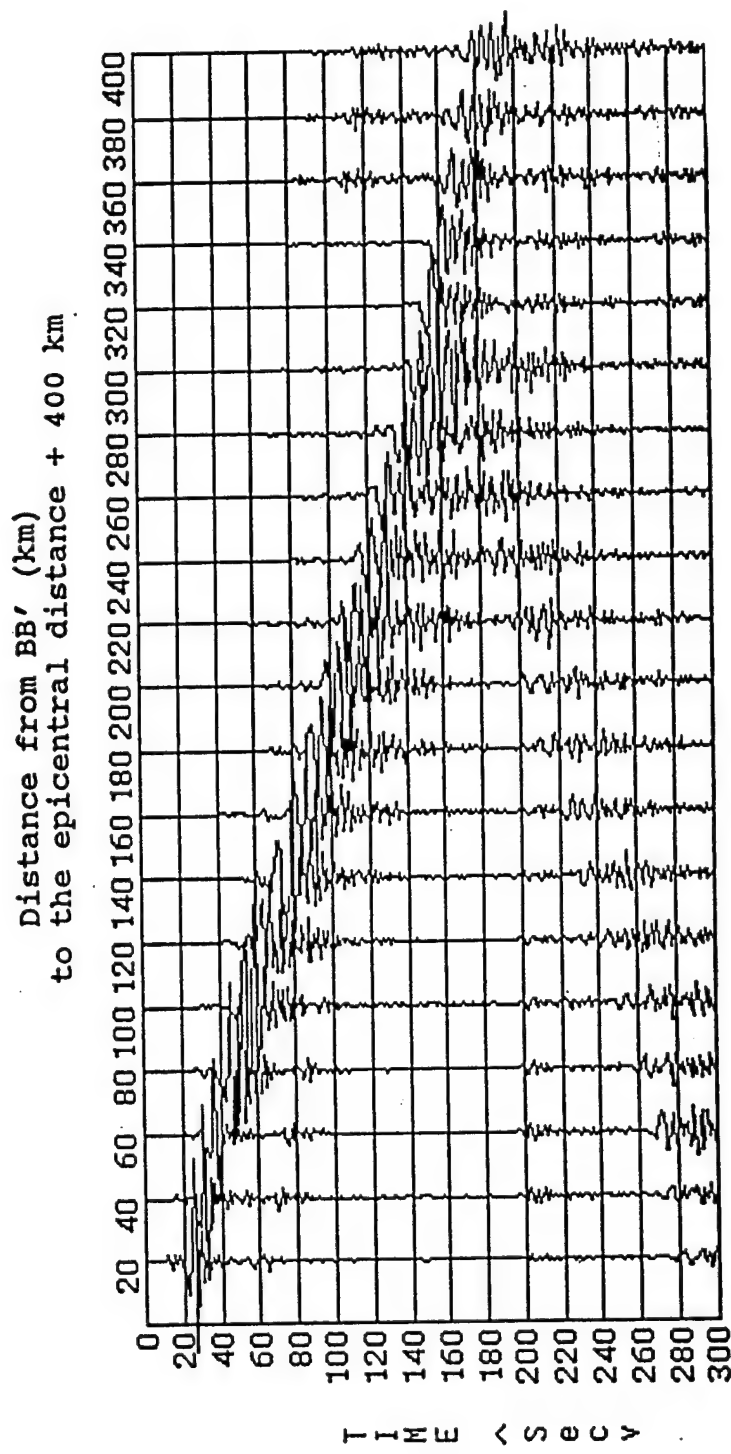


Figure 15-(b). The finite-element synthetic seismogram for the Basin Model and Crust-Pinch Model of Figure 4-(c), (basin width = 250 km, basin depth = 15 km, height of Moho-uplift = 10 km), with the basin velocity of 2.20 km/sec, as observed at distances of 20 km to 400 km by a source with a center frequency 0.334 Hz.

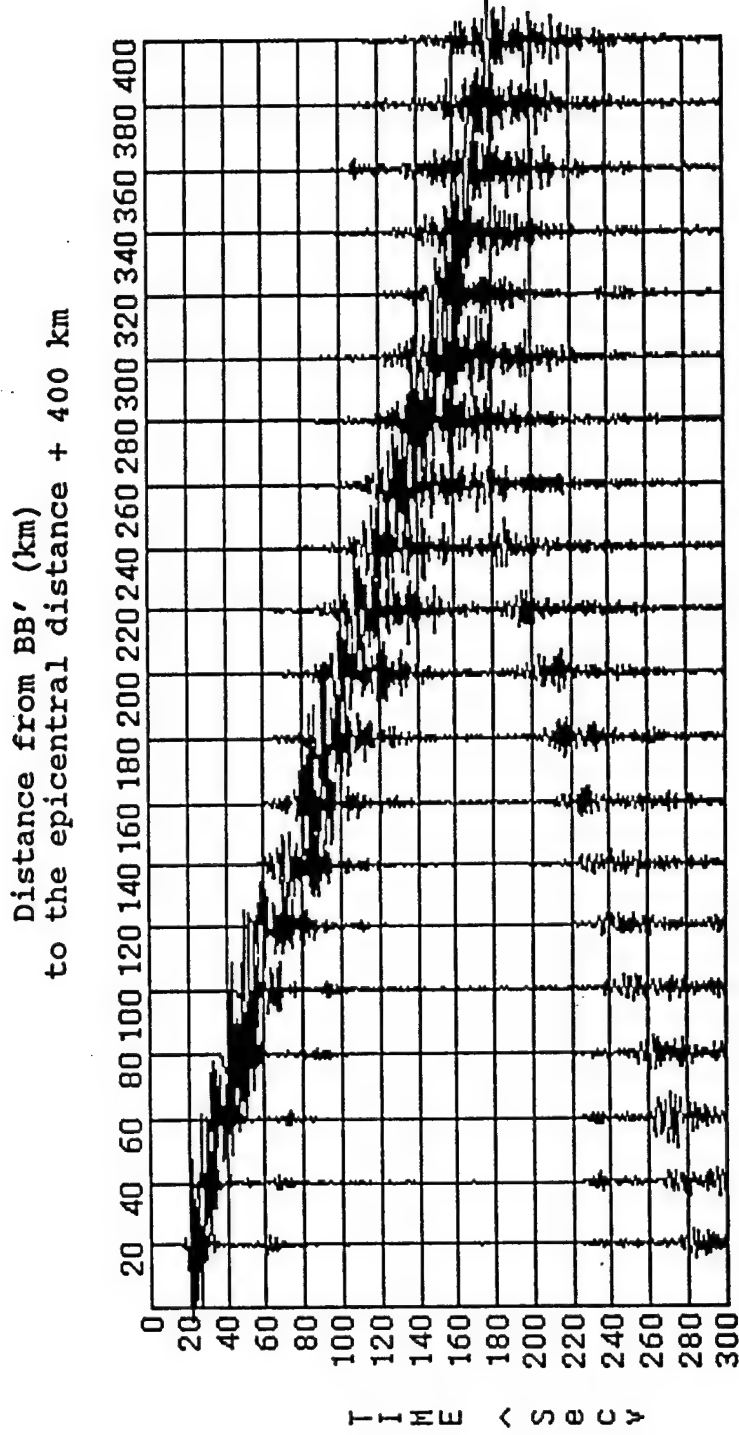


Figure 15-(c). The finite-element synthetic seismogram for the Basin Model and Crust-Pinch Model of Figure 4-(c), (basin width = 250 km, basin depth = 15 km, height of Mono-uplift = 10 km), with the basin velocity of 2.20 km/sec, as observed at distances of 20 km to 400 km by a source with a center frequency 0.667 Hz.

4.4 Effects of Sediment Velocity in the Basin

The effects of the velocity of sedimentary basin on both the development and appearance of Sn, and Lg are substantive. When the contrast of the velocities between the basin and the surrounding granitic/basaltic crust increases, the wave train of the Lg is lengthened drastically.

4.5 Effects of Uplifted Moho of Model II on Lg:

Although an uplifted Moho appears to have only a minor effect on the Lg propagation (See, for example, Figures 13-(a) and 13-(b)), an uplifted Moho associated with a low-velocity sediment basin does have some effects on Lg propagation.

(1) The larger the velocity contrast between the basin sediments and the surrounding crust is, the stronger is scattering, and the longer are the delay and attenuation of the Lg waves.

(2) The wider the basin width is, the longer is the delay of the Lg waves.

Whether it is Model I or Model II without or with the presence of an uplifted Moho. There are several wave-packet-like arrivals observed beyond the distance of the left limb of the basin. The ones followed Sn may be interpreted as a conversion of the Sn-to-Lg wave from the interface.

5 Attenuation and Blockage of the Lg wave Propagation:

So far we have not considered the effect of sediments on attenuation of the Lg waves. Chan and Mitchell (1985), and Mitchell and Hwang (1987) pointed out that the reduction of Lg amplitude might be caused by the attenuation of the thick low-Q sediments as the Lg waves travel crossing the Barents Sea.

Now we introduce attenuation in the sediments of the basin with quality factors Q_s in finite-element modeling. Consider a series of basin models with different attenuation values of quality factors, $Q_s = \infty, 150, 100, 50$, with a fixed basin velocity of 2.2 km/sec and a fixed basin width of 250 km.

Figures 16-(a), 16-(b), 16-(c), and 16-(d) are the finite-element synthetic seismograms observed at the epicentral distances from 620 to 800 km for Model I with a basin width 250 km, sediment velocity 2.20 km/sec, a center-frequency of the impulsive source 0.334 Hz, and $Q_s = \infty, 150, 100$, and 50, respectively. Figure 16-(a) with an attenuation quality factor $Q_s = \infty$ is identical to Figure 9-(b), i.e., without attenuation. Figures 9-(b) and 16-(a) have shown that the blockage of Lg by the presence of the basin. However, Figures 16-(b), 16-(c), and 16-(d) show the blockage of Lg even more clearly when the attenuation of the Lg waves is considered. The Lg waves are noticeably attenuated at the epicentral distances beyond the left limb of the basin, i.e., greater than 700 km.

Figures 17 gives a comparison of seismic waves, including Sn , Lg and all other waves, at the same locations of observation for the cases with different Q_s values. The four traces in the figures correspond to the cases of $Q_s = \infty, Q_s = 150, 100$, and 50, respectively. Comparisons of the seismic waves observed at the distances of 250 km, 350 km and 400 km from the source are given in 17-(a), 17-(b), and 17-(c), respectively. These figures show that the Lg amplitude is highly attenuated as Q_s decreases in value, from Trace 1 ($Q_s = \infty$) to Trace 4 ($Q_s = 50$).

On the other hand, the presence of a low- Q sedimentary basin affects very little on the amplitude of Sn , as the Sn waves are refracted mostly through the upper mantle.

For the present models studied, we found that thick low- Q sediments cause serious attenuation and reduction of the Lg amplitudes, but do not cause any time delay of

the Lg wave propagation.

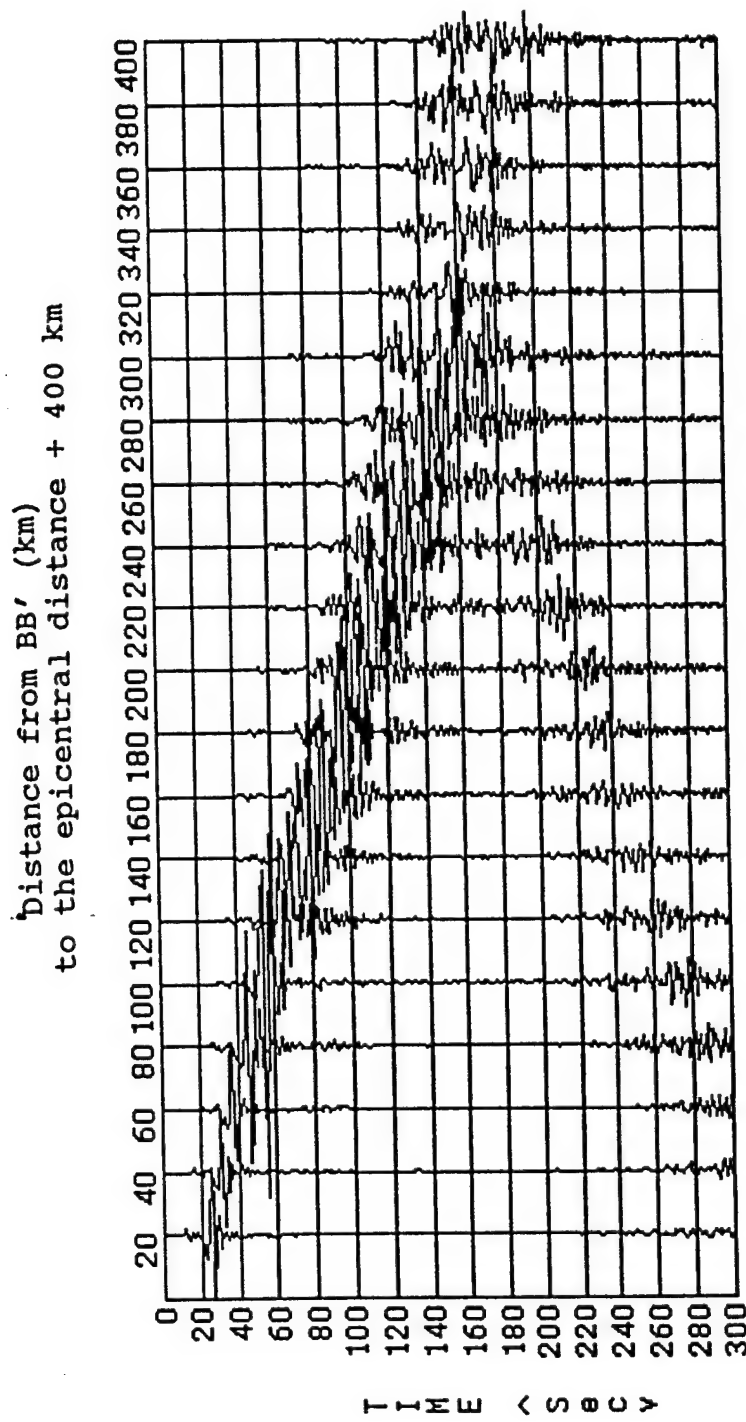


Figure 16-(a). The finite-element synthetic seismograms for the basin models of Figure 4-(b), with the basin velocity of 2.2 km/sec and with $Q_s = \infty$, as observed at distances of 20 km to 400 km from BB'.

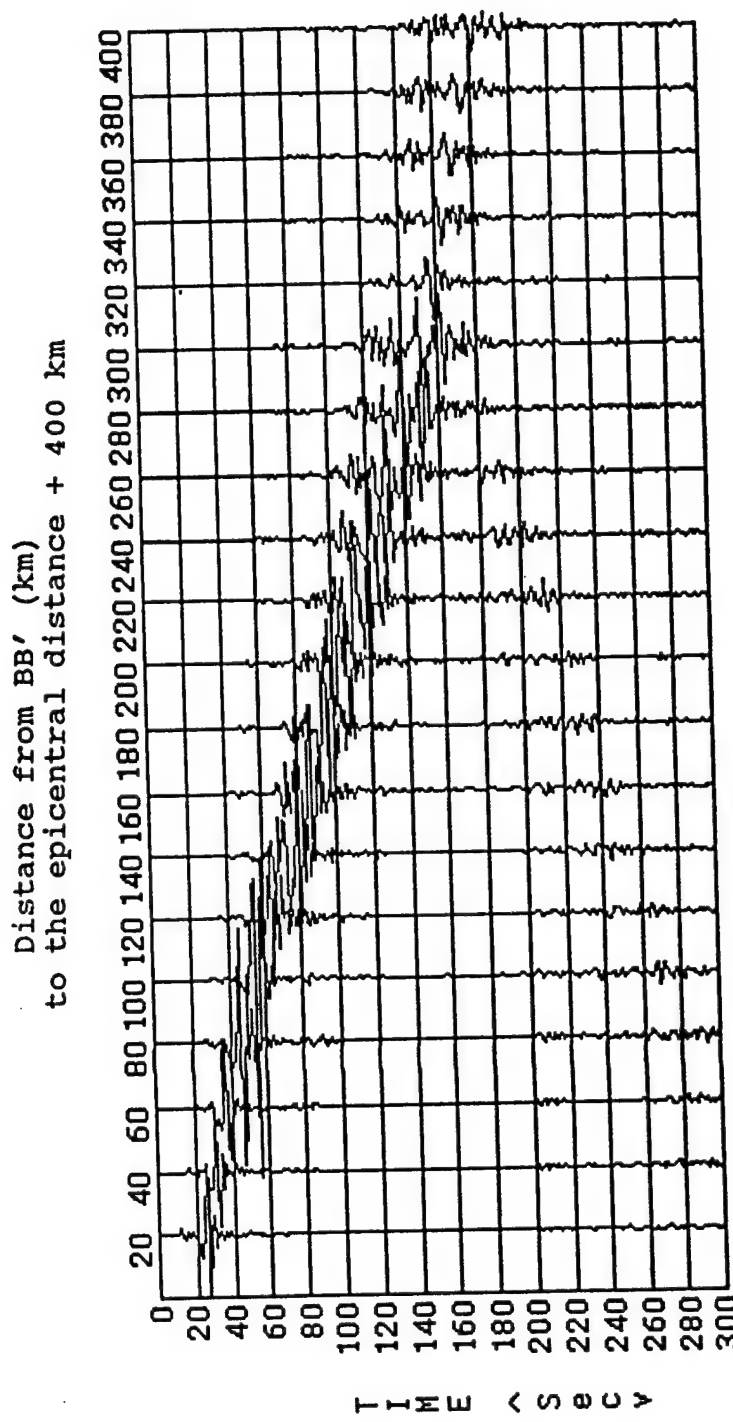


Figure 16-(b). The finite-element synthetic seismograms for the basin models of Figure 4-(b), with the basin velocity of 2.2 km/sec and with $Q_s = 150$, as observed at distances of 20 km to 400 km from BB'

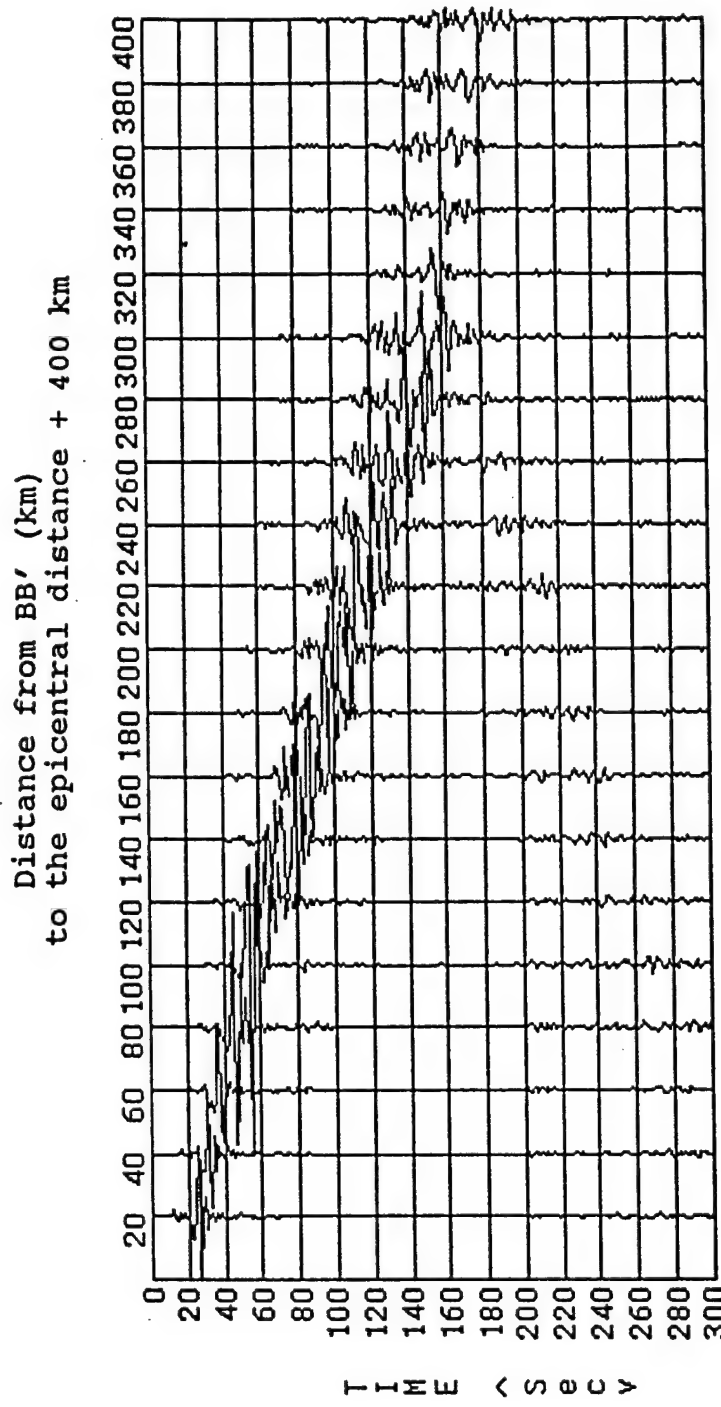


Figure 16-(c). The finite-element synthetic seismograms for the basin models of Figure 4-(b), with the basin velocity of 2.2 km/sec and with $Q_s = 100$, as observed at distances of 20 km to 400 km from BB',

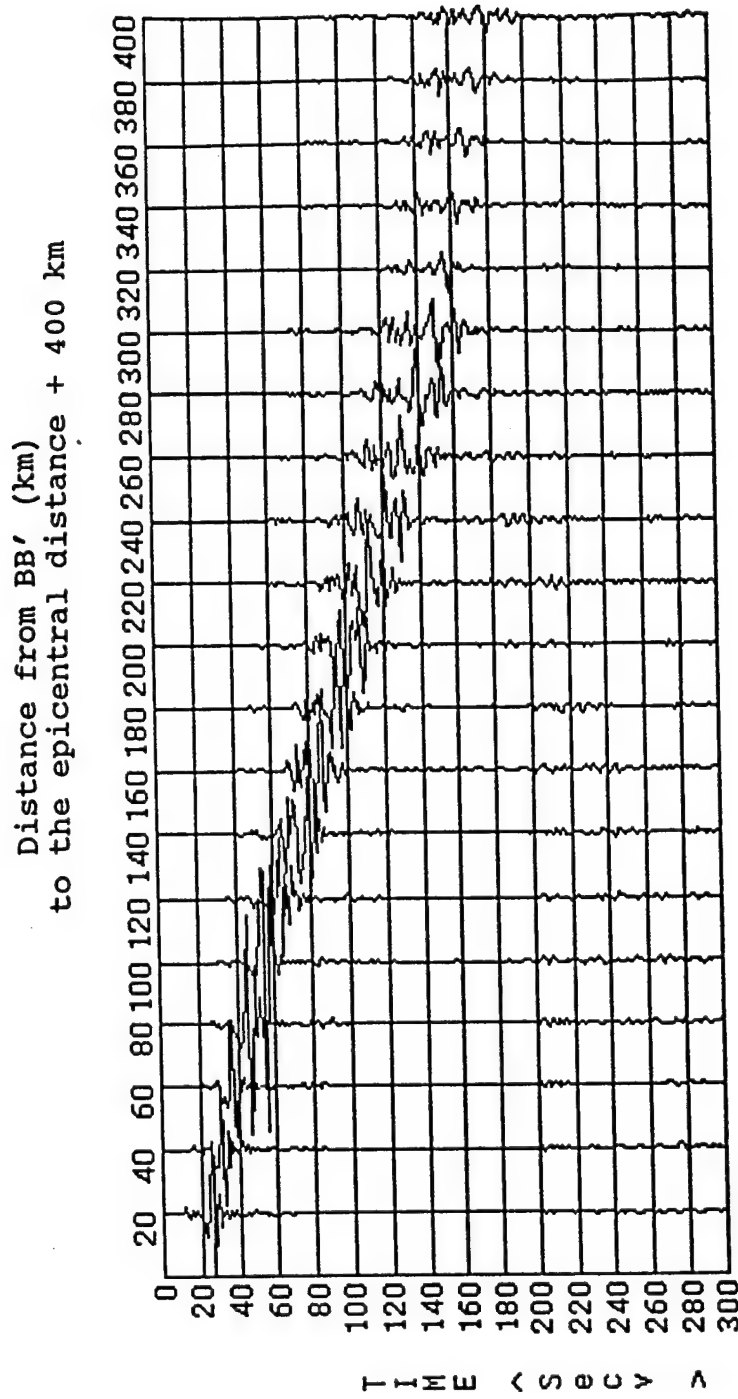


Figure 16-(d). The finite-element synthetic seismograms for the basin models of Figure 4-(b), with the basin velocity of 2.2 km/sec and with $Q_s = 50$, as observed at distances of 20 km to 400 km from BB'

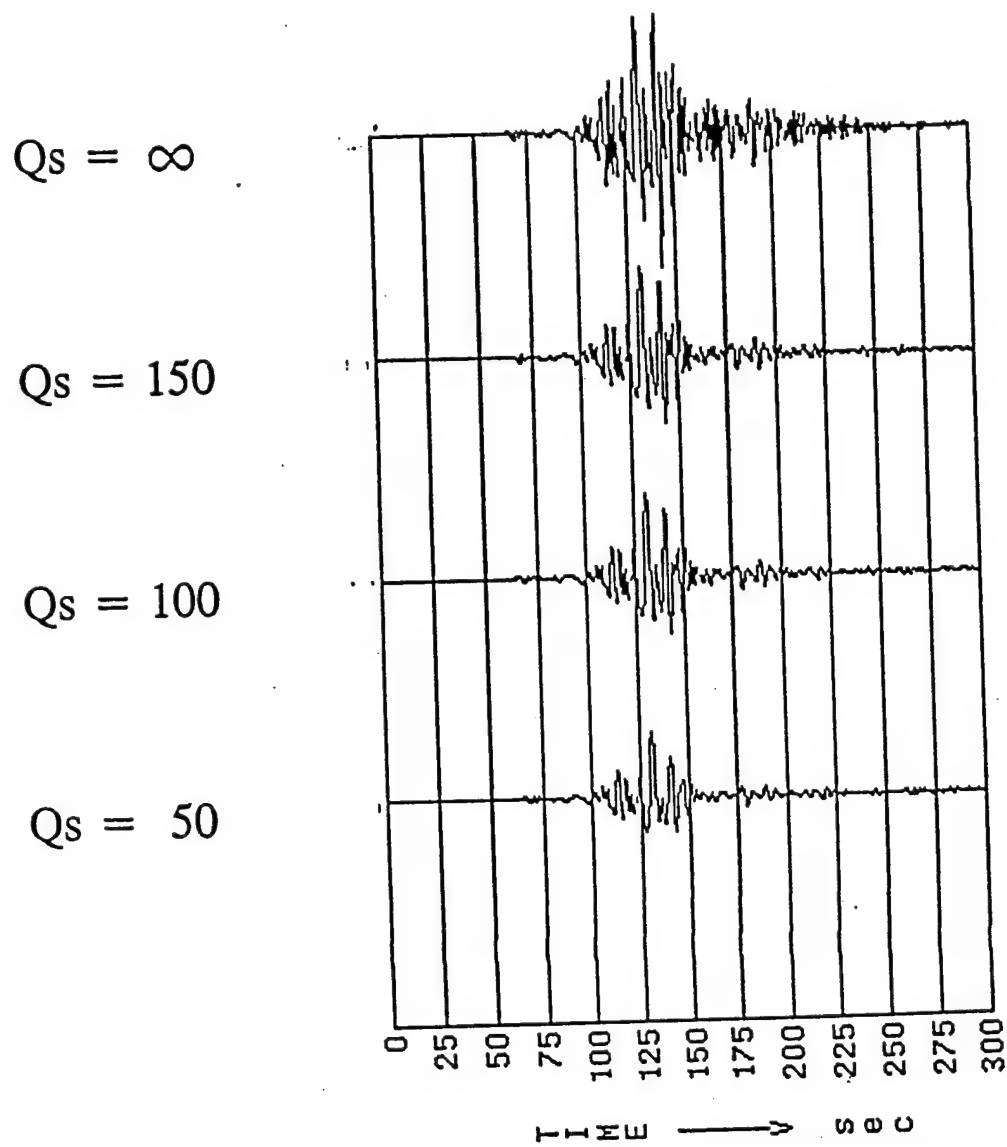


Figure 17-(a). The comparison of seismic waves at the same locations of observation at distance of 250 km from BB' for cases with different Q_s values.

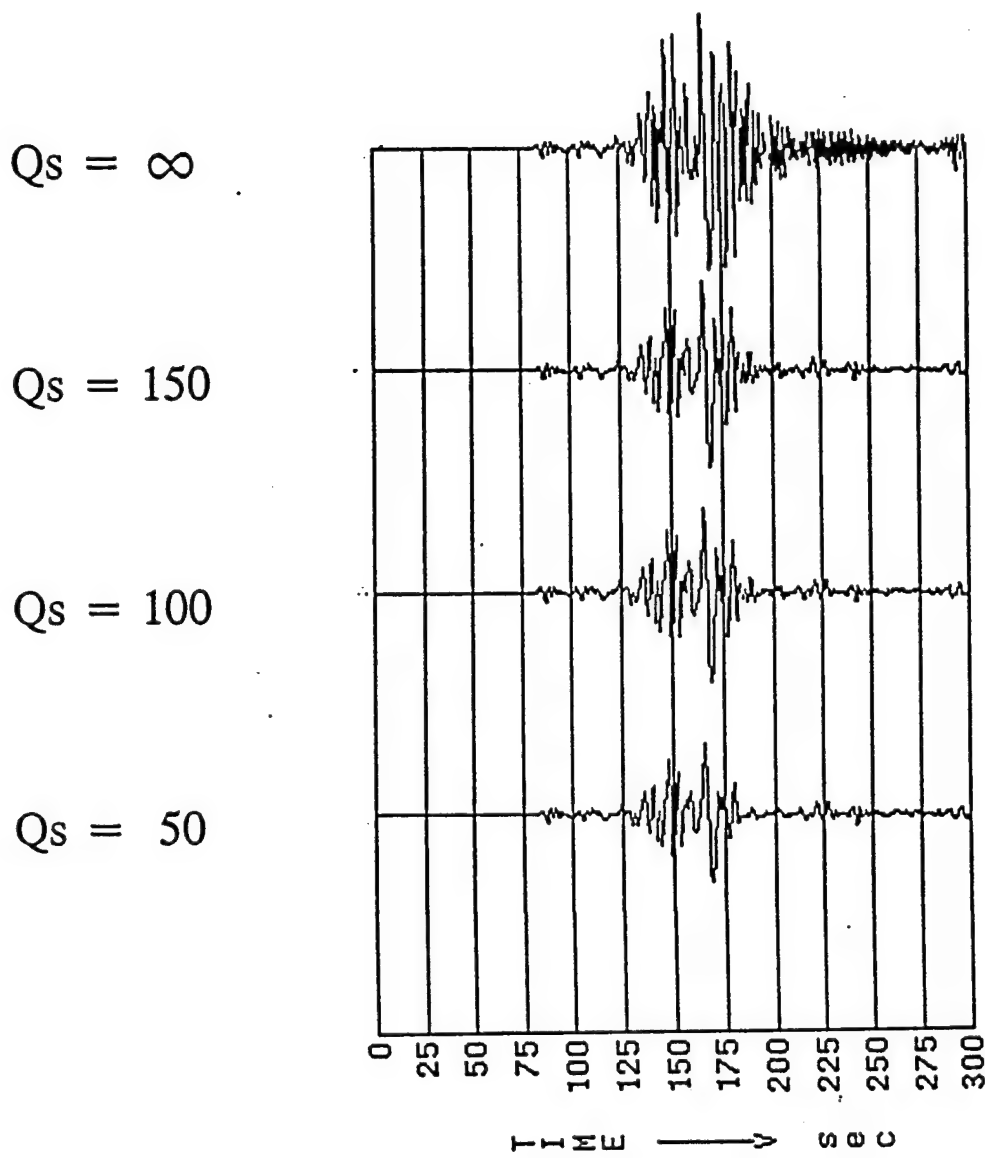


Figure 17-(b). The comparison of seismic waves at the same locations of observation at distance of 350 km from BB' for cases with different Q_s values.

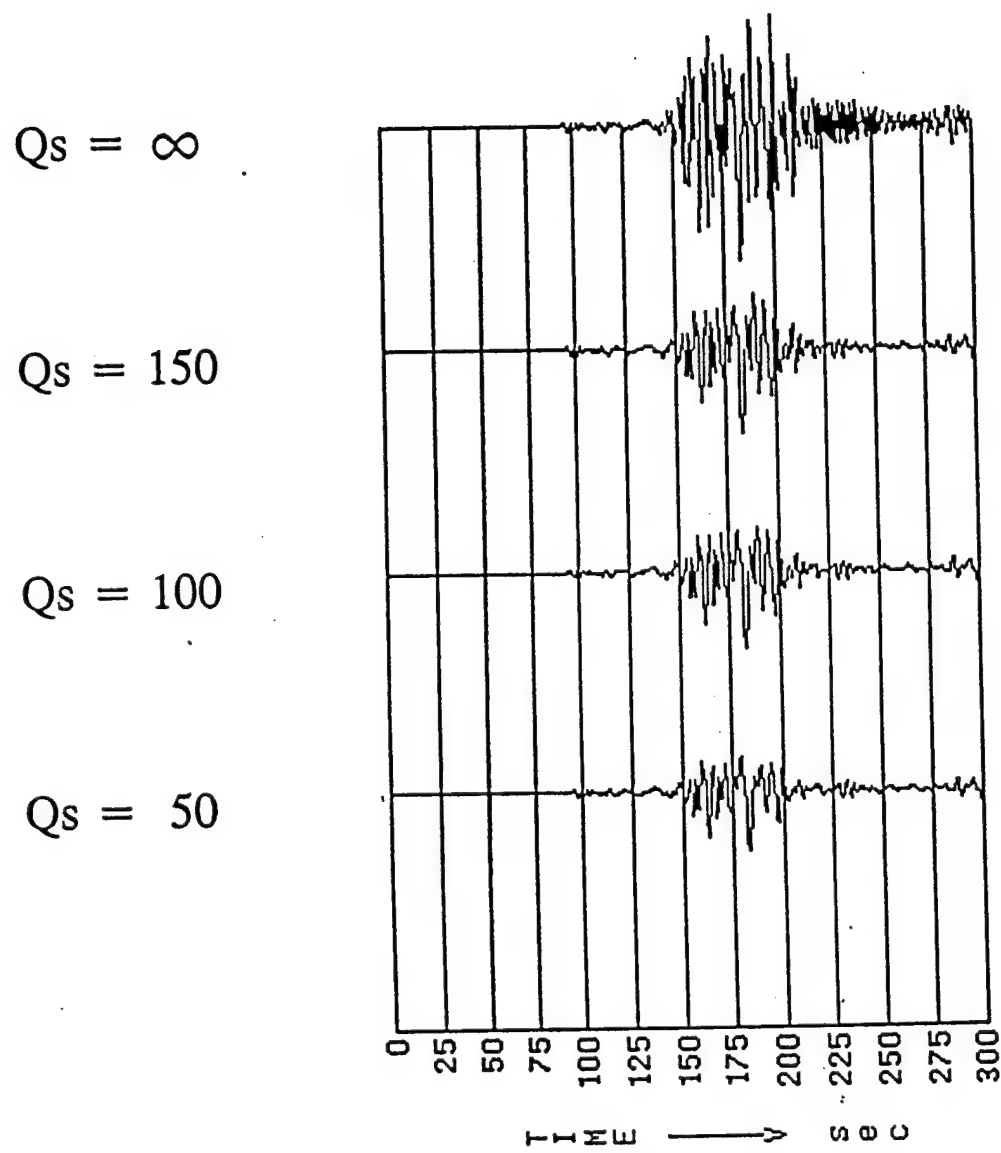


Figure 17-(c). The comparison of seismic waves at the same locations of observation at distance of 400 km from BB' for cases with different Q_s values.

Comparisons Of Finite-Element Modeling Results With Real (Observational) Data

We have learned through finite-element modeling as much about the effects of island margin, basin, and shield in terms of basin width, center-frequency of an impulsive source, and wave velocity of sediments in a basin, as well as attenuation in terms of quality factor on the Lg wave propagation.

An ultimate test of the goodness of finite-element modeling is to compare finite-element synthetic seismograms based on geologically realistic structure models with real data.

Among the available data, it seems that three Lg propagation paths used by Baumgardt (1991) in his study of the blockage of the Lg waves most appropriate to make comparisons of finite-element modeling with observational data.

- (1) The ARCESS FRAO trace of the December 4, 1988 Novaya Zemlya explosion, representing an oceanic path. The epicentral distance from the former USSR test sites of Novaya Zemlya to ARCESS is about 1,100 km. The December 4, 1988 Novaya Zemlya explosion had a magnitude of 5.7.
- (2) The NORSAR NO1AO(a) trace of the September 4, 1972 Kola Peninsula explosion (PNE), representing nearly a continental path. The epicentral distance from Kola Peninsula to NORSAR is about 1,310 km slightly greater than that for the above Novaya Zemlya explosion to ARCESS. The Kola Peninsula explosion had a magnitude

of 4.6.

(3) The NORSAR N01A0(b) trace of the October 25, 1984 Novaya Zemlya explosion, representing a mixed path from the island margin, through the Barents Sea across the Baltic shield to NORSAR. The epicentral distance of this event of a magnitude of 5.9 is 2,300 km.

The great-circle paths of the above three events are shown in Figure 18. The playback traces of these three events are displayed in Figure 19, showing the arrivals of Pn, Sn, and Lg. These traces as pointed out by Baumgardt (1991) have been filtered in the 0.6 to 3.0 Hz frequency band. Although the traces of these events have been recorded with different short-period instrument responses, these differences should not affect the relative amplitude information in a major way. Because of the difference in magnitude and instrument response, Baumgardt scaled the amplitudes of the second trace of NORSAR by a factor of three to the first trace of ARCESS so that the Pn amplitudes for both traces are equalized. The third trace of the Novaya Zemlya to NORSAR event of October 25, 1984 is as playbacked.

So far as Sn and Lg are concerned, comparison of the NORSAR trace for the Kola Peninsula explosion with the trace of ARCESS for the Novaya Zemlya event shows noticeably that the wave train of the Lg waves is well developed for the ARCESS trace, while it is virtually missing for the NORSAR trace. The Sn waves are nearly the same for both the traces. The great-circle path for Sn and Lg traveling from Novaya Zemlya to ARCESS could be considered as Model I or Model II in the previous finite-element modeling, while that from Kola Peninsula to NORSAR could be considered as Model III, a continental paths from the Baltic shield margin through the Baltic shield. Again, we have used the method of segment by segment finite-element calculation. The island margin portion of the model is identical to that used before, as shown in

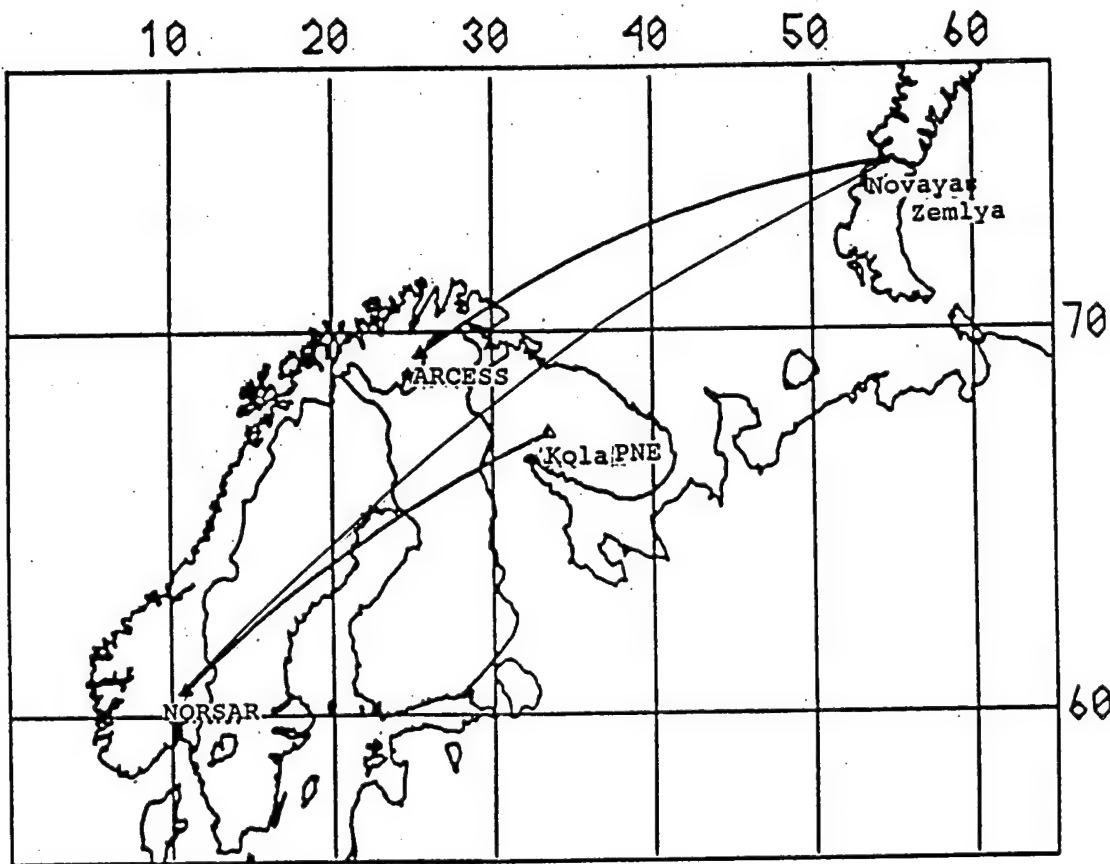
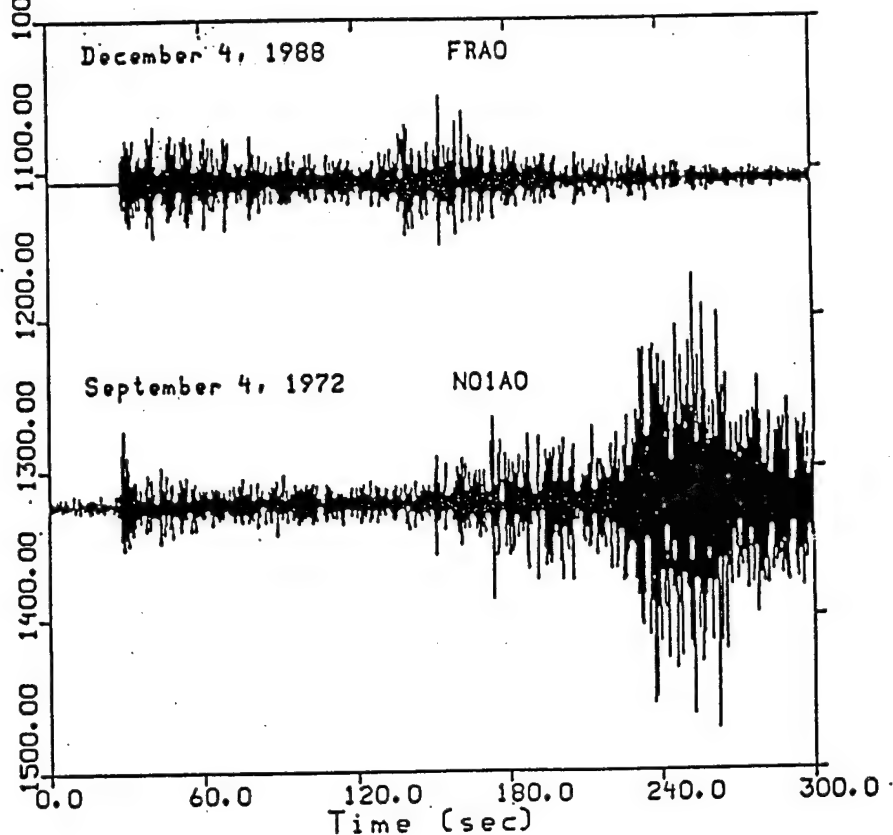


Figure 18. Map showing comparisons of the propagation path from the Kola Peninsula to NORSAR, the Novaya Zemlya to ARCESS and from Novaya Zemlya to NORSAR. The two paths from Novaya Zemlya to ARCESS and from the Kola PNE to NORSAR are nearly parallel great-circle paths and have almost identical epicentral distance.

Novaya Zemlya - ARCESS
 Kola Peninsula PNE - NORSAR
 Filter 0.6 - 3.0 Hz

(a)



NORSAR Data
 Filter 0.6 - 3.0 Hz

(b)

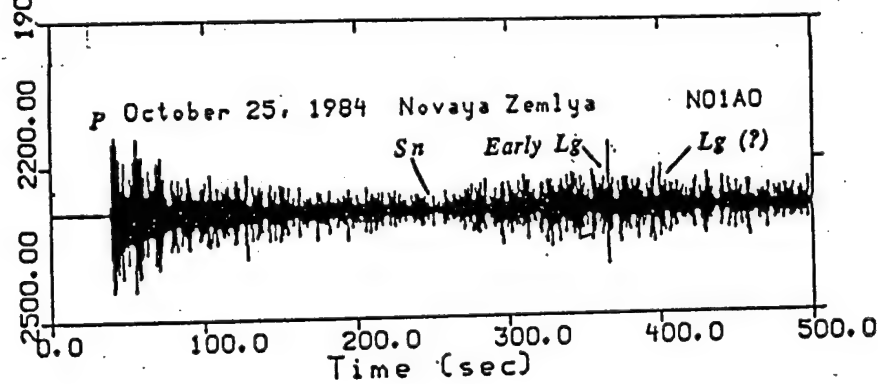


Figure 19-(a). Comparison of the ARCESS FRA0 trace of the December 4, 1988 explosion with the NORSAR NO1AO recording of the September 4, 1972 Kola Peninsula explosion.
 (b) The NORSAR NO1AO trace of the October 25, 1984 explosion.

Figure 4-(a), except that now the epicentral distance to the cross section BB' is 500 km. The explosion source in Island Margin Model is an impulsive, transient source of the fourth derivative of Gaussian type forcing functions with a center-frequency of 0.334 Hz.

Finite-element Modeling of the December 4, 1988 Novaya Zemlya Explosion and Compared with the ARCESS Data:

On the basis of Model I, synthetic seismograms for the Novaya Zemlya December 4, 1988 explosion are generated by means of finite-element modeling for an epicentral distance from 800 to 1,300 km from the explosion as shown in Figure 4-(a). The Barnes Sea is modeled as a sedimentary basin. The geophysical parameters of the model are that:

1. the configuration of the basin is shown in Figure 4-(b), with a basin width of 700 km.; the density of the sediments was taken to be 2.45 gm/cm³; the shear-wave velocity was taken to be 2.3 km/sec, and Q_s was 100.
2. for the granitic/basaltic crust, the shear-wave velocity was assumed to be 3.58 km/sec at the top and gradually increased to 3.75 km/sec at the bottom of the crust; its density ranged from 2.67 gm/cm³ to 2.90 gm/cm³, and an averaged Q_s 200.
3. for the upper mantle, the S velocity was taken to be 4.70 km/sec and the density 3.3 gm/cm³.

Figure 20-(a) gives the finite-element synthetic seismograms for the December 4, 1988 Novaya Zemlya explosion at an epicentral distance of 800 to 1,300 km. The arrivals of S_n is distinct and the signal of S_n attenuates with distance. The wave train of Lg, although it also suffers attenuation, disappeared beyond the epicentral

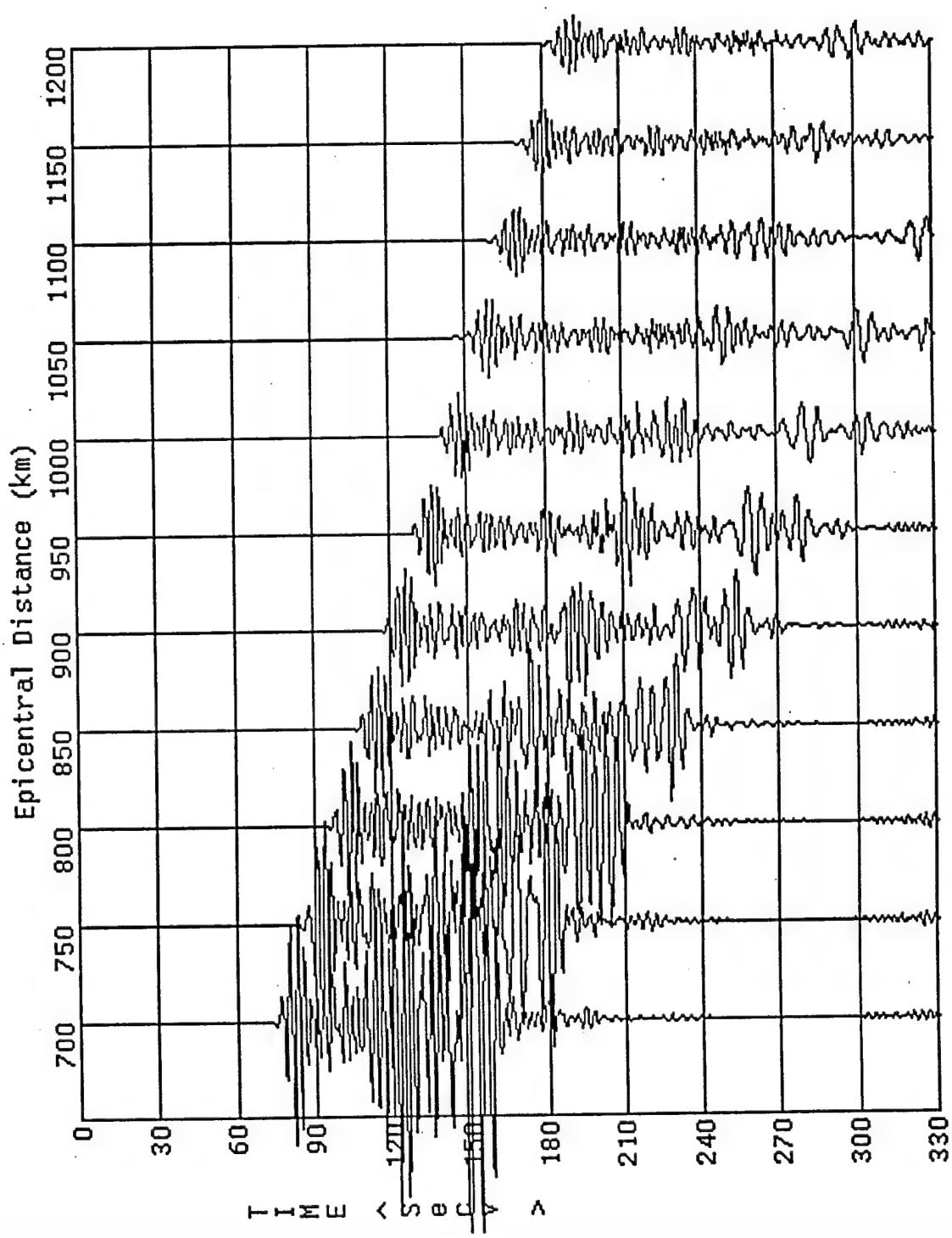


Figure 20-(a). The finite-element synthetic seismogram of Lg waves of the simulated model for the ARCESS trace of the December 4, 1988 explosion.

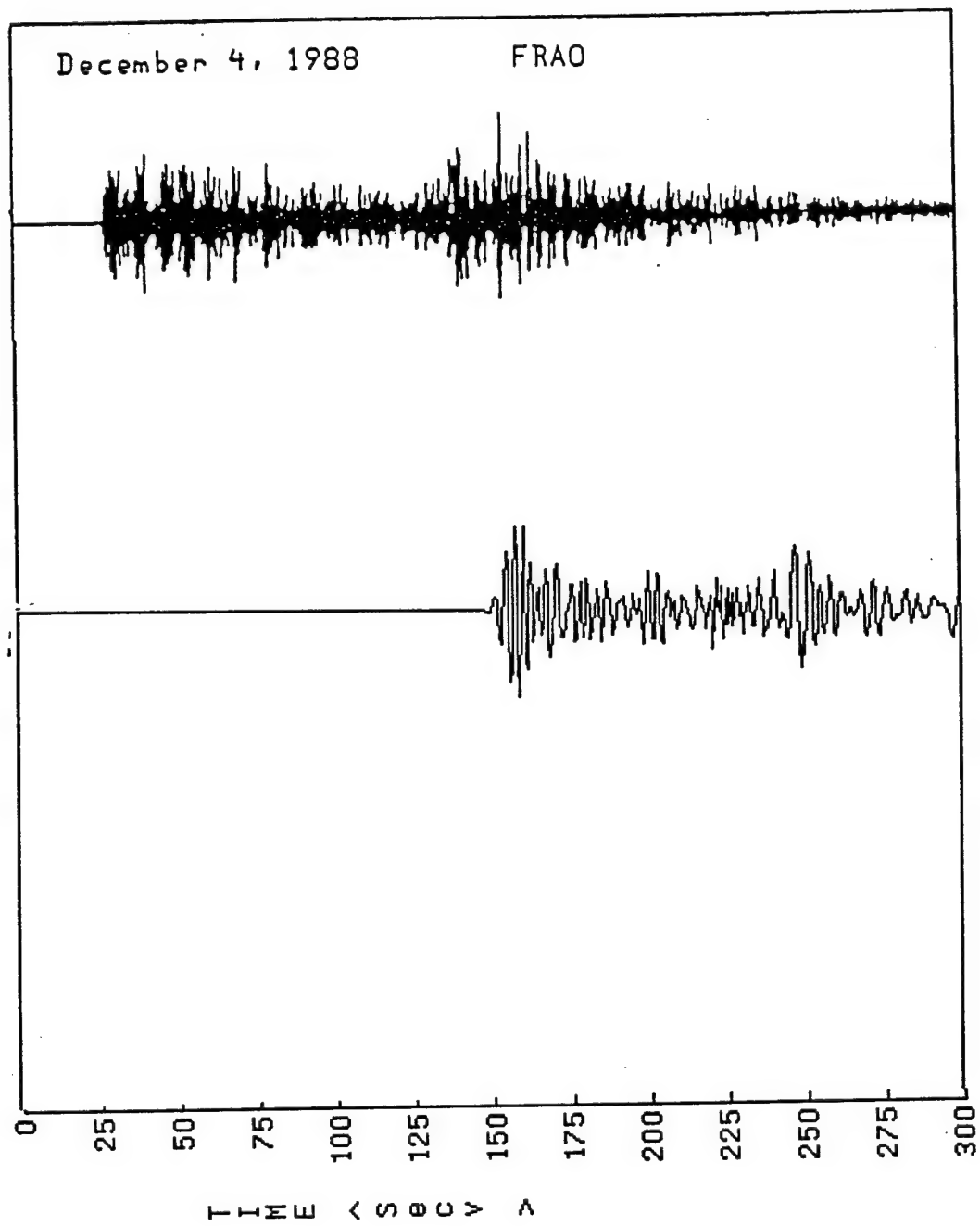


Figure 20-(b). Comparison of the numerical result and the real data for the ARCESS FRA0 trace of the December 4, 1988 explosion.

distance of about 1,100 km on the other side of the Barents Sea.

Figure 20-(b) plots both the ARCESS trace and the finite-element modeled trace for comparison, showing the onset of Sn and the absence of the Lg wave altogether. Agreement between the finite-element modeling results and the real data is very encouraging.

Finite-element Modeling of the September 4, 1972 Kola Peninsula Explosion and Compared with the NORSAR Data:

On the basis of Model III, the Baltic shield model, a series of seismograms have been generated at an epicentral distance of 800 to 1,300 km.

The structural model of the Baltic shield as shown in Figure 4-(d) includes a two-km thick low velocity layer, which has a shear-wave velocity of 2.6 km/sec and density of 2.3 gm/cm³, and a Q_s value of 100. The geophysical parameters of the granitic/ basaltic crust and the upper mantle are the same as those used in modeling the above Novaya Zemlya event.

Figure 21-(a) shows the finite-element synthetic seismograms for the Kola Peninsula event. The distinct features of these seismograms are the prominent Lg wave onset across all the epicentral distances. There is no question about it that the Lg waves are propagated without any blockage. The Sn wave propagation for the Kola Peninsula explosion has nearly the same characteristics of those for the Novaya Zemlya explosion, as they should be because the propagation paths in both the explosions are refracted through the upper mantle.

Figure 21-(b) shows the comparison of the finite-element trace with the NORSAR N01A0(a) trace, giving the arrivals of the Sn and Lg clearly. As the center-frequency

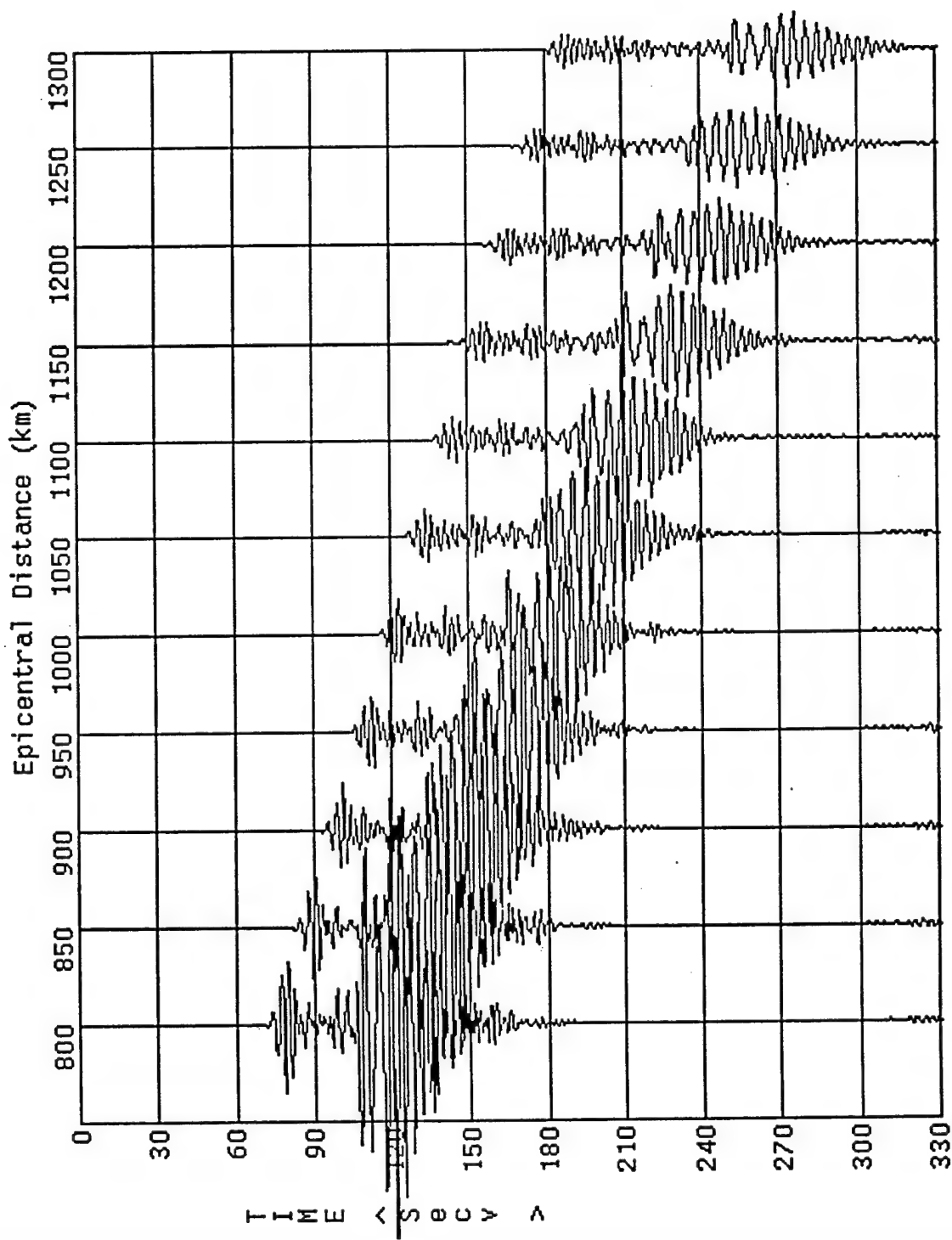


Figure 21-(a). The finite-element synthetic seismogram of Lg waves for the structural model of the simulated model for the NORSAR NO1AO of the September 4, 1972 Kola Peninsula explosion.

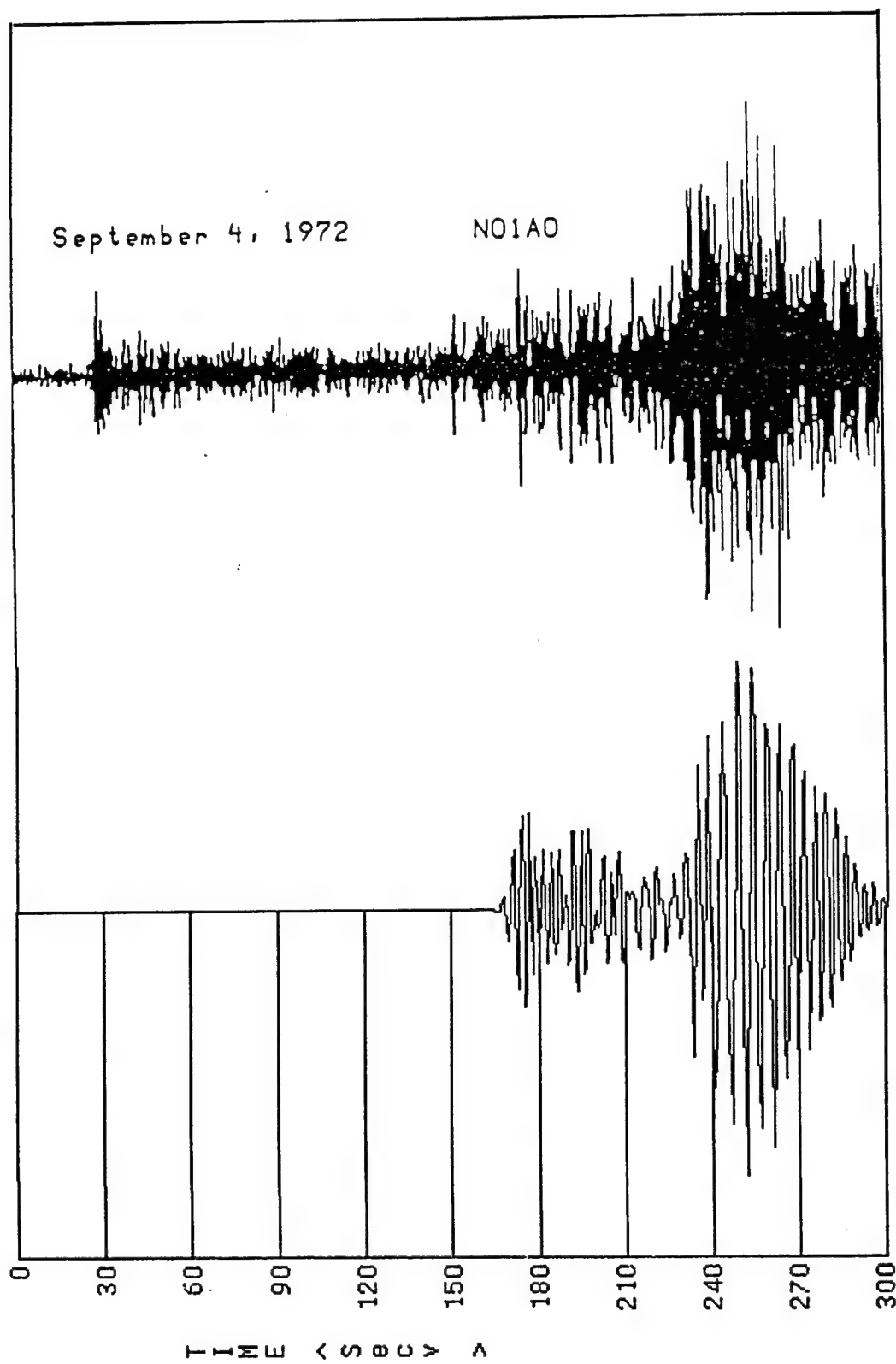


Figure 21-(b). Comparison of the numerical result and the real data for the NORSAR N01A0 of the September 4, 1972 Kola Peninsula explosion.

of the impulsive source in finite-element modeling is not high enough in comparison with the trace of the real data, the frequency contents of both the Sn and Lg in finite-element modeling results appear to be lower. However, all the characteristics of the Sn and Lg waves through finite-element modeling are very similar to the observed trace NO1AO(a).

Finite-element modeling of the October 25, 1984 Novaya Zemlya Explosion and Compared with the NORSAR Data:

The above two comparisons of the finite-element modeling results with the observed data are for the Lg propagation for a purely continental path and for an oceanic path.

From the above two explosions, we have gained considerable physical insight to the problem of the blockage and scattering of the Lg wave as the wave is propagated through the island margin, and then its continuation of across the Barents Sea through the segment by segment finite-element calculation. We have assessed the influence of the Barents Sea on the Lg waves in term of frequency, basin width, sediment velocity, and the geometry of the crust and the upper mantle contact.

Our interest in this section is naturally to investigate the influence of the island margin, the Barents Sea, and the Baltic shield altogether on the Lg wave propagation. For this purpose we have constructed a complete model, named Model IV. Model IV thus includes three segments, namely, the island margin, the Barents Sea, the Baltic shield margin, and the Baltic Shield as shown in Figure 4-(d). Baltic Shield Margin Model is now connected to Model I at the cross section of CC' to form Model IV. Adopting Model II with an uplifted Moho in Model IV would not make any significant changes on the arrival time or amplitude of the Lg waves, but it would only have a

very minor difference in amplitude and arrival time of the Sn onset. Therefore, in the present analysis, Model IV adopts Model I with a horizontal Moho.

All the physical parameters of Model IV are exactly identical to Model I used for the comparison of the finite-element modeling results with the ARCESS trace of the December 4, 1988 Novaya Zemlya explosion except the dimensions of three segments are changed to that:

1. The termination cross section BB' of the island margin portion of Model IV is placed at an epicentral distance of 400 km.
2. The termination cross section CC' of the Barents Sea portion of Model IV is placed at an epicentral distance of 1,300 km.
3. The continuation portion of the cross section CC', i.e., Model III of the Baltic shield, which connects to the above two segments to complete Model IV.

Figures 22-(a) and 22-(b) show the finite-element synthetic seismograms for the continuation portion of Model IV which clearly show that the Sn onsets are prominent, and the energies for both early and Lg are very weak. Apparently the Lg waves have already been blocked as they are propagated across the Barents Sea Basin.

Figure 22-(c) shows the comparison of the NORSAR N01A0(b) of the October 25, 1984 Novaya Zemlya explosion with the finite-element simulated trace at the same epicentral distance 2,300 km. The time of the arrival of Sn at the NORSAR station agrees with the finite-element modeling calculation perfectly. The arrival of early Lg with small amplitude, which was interpreted by Baumgardt as a converted Lg at the continental margin of the Baltic shield, also agrees the finite-element simulated trace. The arrival of Lg, which was predicted, had nearly the same amplitude as that of Sn. Apparently, the Lg waves as propagated across the Barents Sea have been blocked by the low-velocity sediments in the basin. Although a Lg to Sn conversion might also

have taken place at the continental margin of the Baltic shield.

The above three direct comparisons between the finite-element modeling results and the real observational data substantiate that the blockage of Lg for the propagation paths from Novaya Zemlya to ARCESS and to NORSAR is certainly caused by the presence of the low-velocity sediments in the Barents Sea.

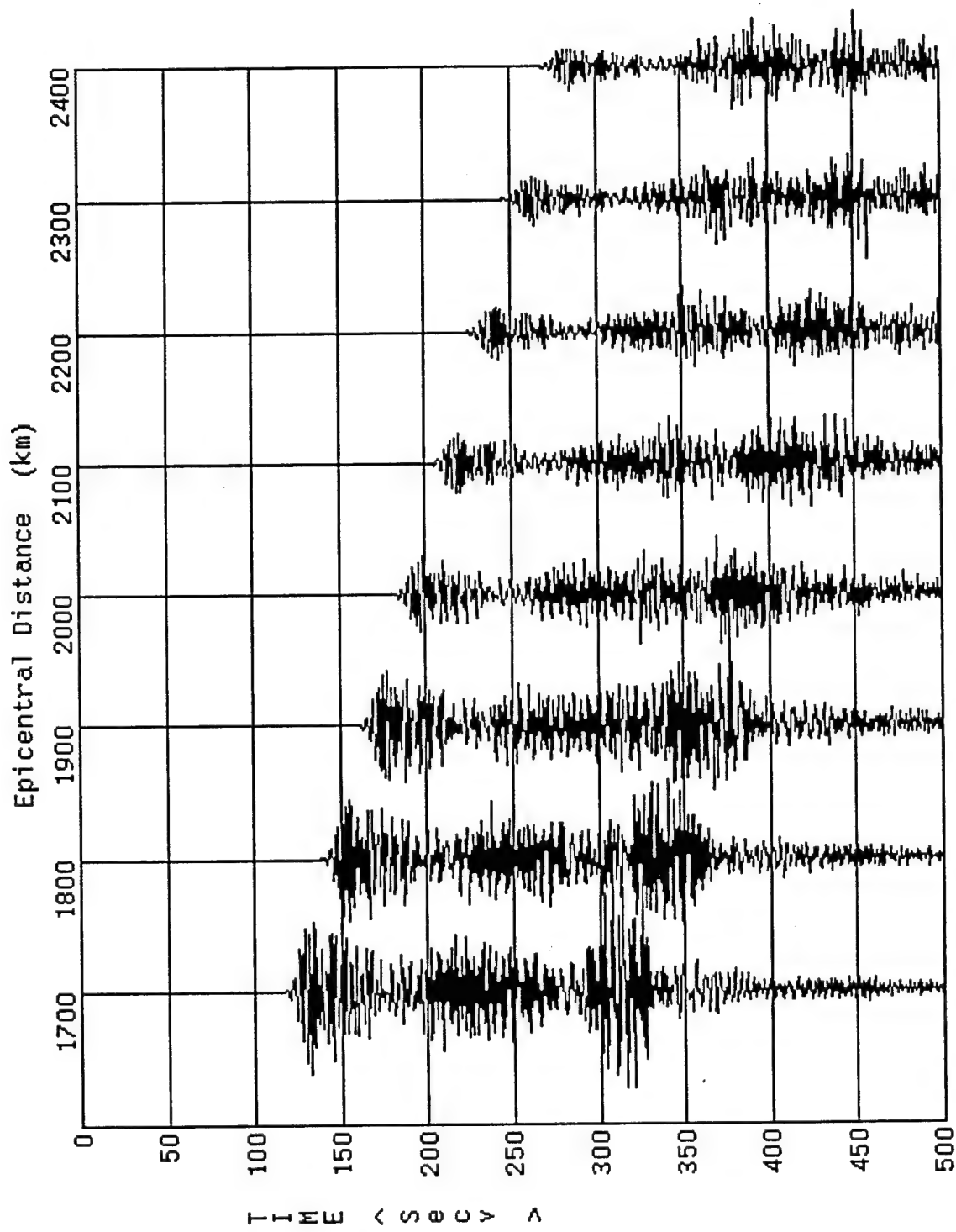


Figure 22-(a). The finite-element synthetic seismogram of Lg waves of the simulated model for the October 25, 1984 Novaya Zemlya explosion, recorded at NORSAR for epicentral distances 1,700 to 2,400 km.

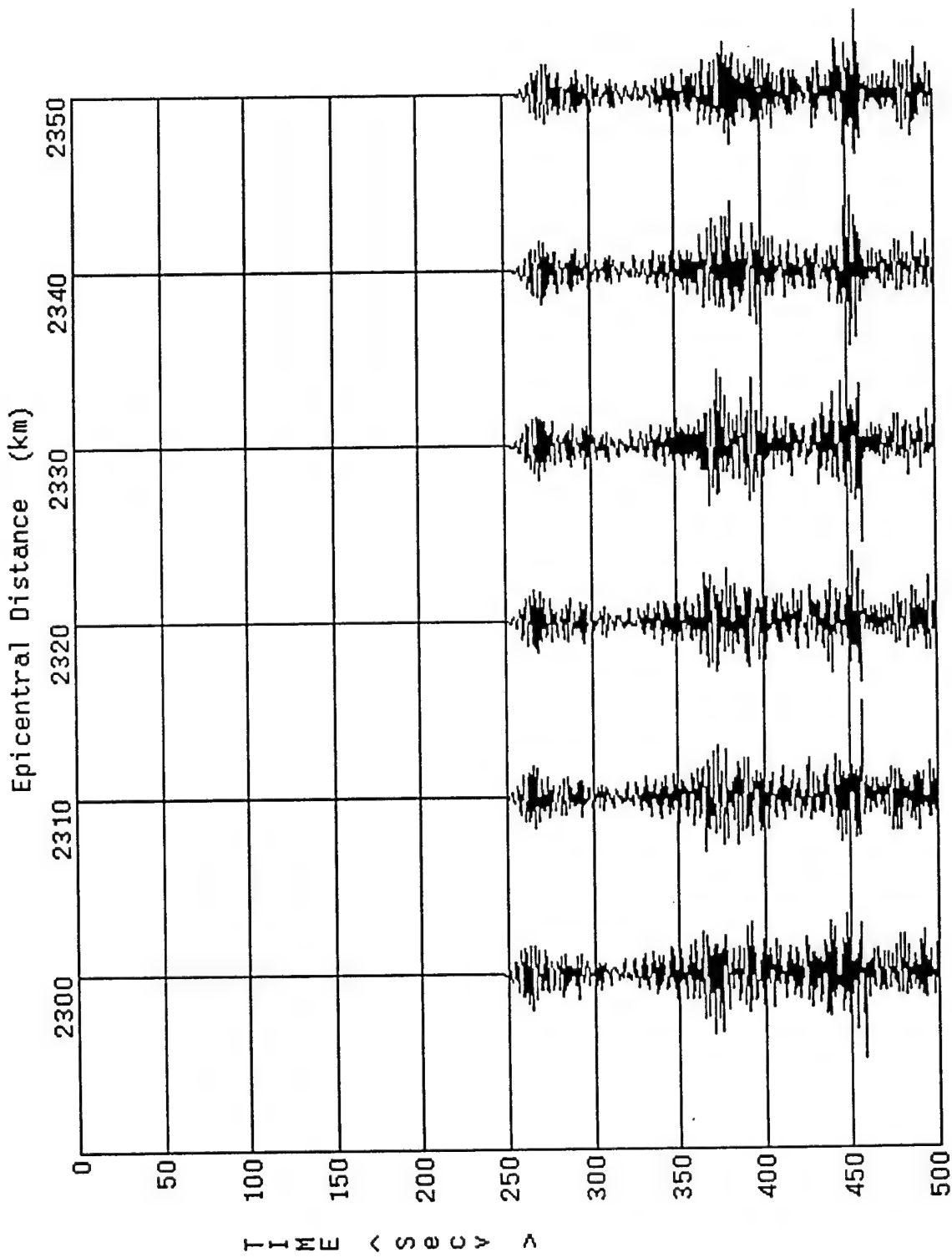


Figure 22-(b). The finite-element synthetic seismogram of Lg waves of the simulated model for the October 25, 1984 Novaya Zemlya explosion, recorded at NORSTAR for epicentral distances 2,300 to 2,350 km.

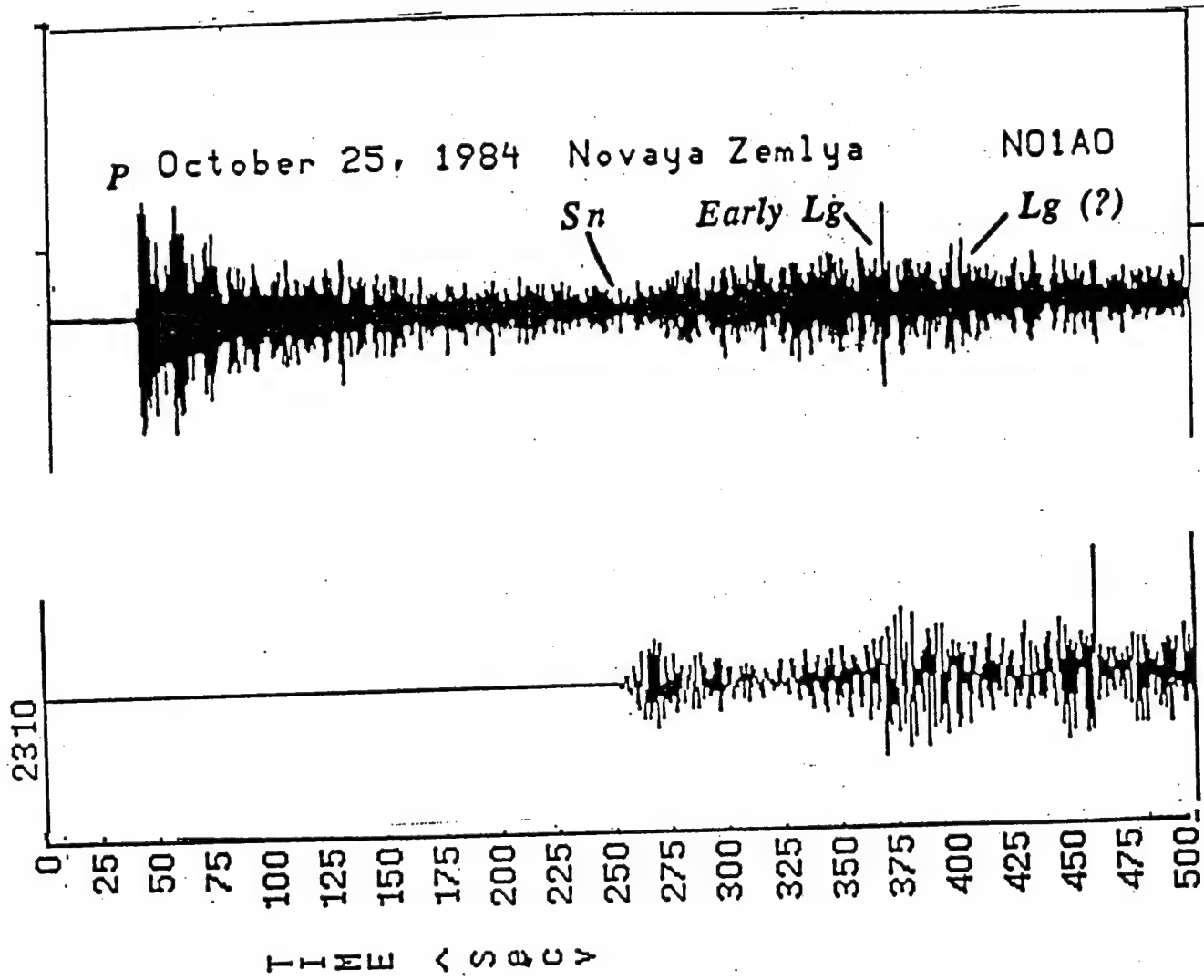


Figure 22-(c). Comparison of the numerical result and the real data for the NORSAR N01AO of the October 25, 1984 Novaya Zemlya explosion.

Conclusions

1. Through extended finite-element modeling, it is now proven that large-dimension geologically realistic anti-plane strain problems of SH waves can be efficiently and accurately modeled by means of the method of segment by segment calculation.
2. Finite-element modeling of the Lg wave propagation along the great-circle paths from Novaya Zemlya to ARCESS designated as Model I and Model II, and from Kola Peninsula to NARSAR designated as Model III indicates that
 - a. For the center-frequencies 0.167, 0.334 and 0.667 Hz of the source, the effect of frequency content on Lg is only minor. The arrivals of both Sn and Lg are on time except the arrivals of Sn are more emergent for the center-frequency of 0.167 Hz. The amplitudes of Sn, Lg and scattered waves for those three frequencies are nearly independent of frequency. The Lg waves are well developed in the absence of the large-dimension of sedimentary basin of the Barents Sea.
 - b. For a given center frequency of the source, the Lg wave propagation is dependent on the dimension of basin width. The amplitude of the Lg wave decays more rapidly for a large basin width than for a small basin width. The presence of a basin causes the time delay of the Lg wave. As the transmission path of Sn is principally through the upper mantle, the Sn arrival is virtually transparent of the presence of the basin.
 - c. The velocity of sediments in the basin plays a significant role in the propagation and blockage of the Lg waves. The velocity contrast between the sediments in the basin and the surrounding crust influences the development and appearance of the

Lg waves. A higher value of this velocity contrast lengthens the Lg wavetrain.

d. Among all the effects, one of the most important factors is the effect of wave attenuation. With reasonable Qs for the sediments in the basin, the blockage of the Lg wave by the presence of the Barents Sea Basin is very much accentuated. Therefore, estimation of the quality factors not only for the sediments in the basin but also for the surrounding crust is of considerable importance.

3. Comparisons of the finite-element modeling results of the former USSR test sites of Novaya Zemlya to ARCESS and to NORSAR, and of the Kola Peninsula to NORSAR with the real data of the seismic traces N01A0(a,b) and FRAO, respectively show that

a. The characteristics of an emergence of Sn and the expected time of the arrival of Sn are virtually unchanged for all the above events investigated.

b. The Lg waves are very well developed for the September 4, 1972 Kola Peninsula explosion as the Lg waves are propagated across the continental path of the Baltic shield only.

c. The wavetrain of Lg is completely absent for the December 4, 1988 Novaya Zemlya event to ARCESS and has extremely low amplitude for the October 25, 1984 Novaya Zemlya event.

4. Comparison of the finite-element simulated results of the October 25, 1984 Novaya Zemlya explosion with the NORSAR trace NO1AO(b) shows that the time of the arrival of Sn at NORSAR agrees with the finite-modeling calculation perfectly. The arrival of early Lg with small amplitude, which was interpreted by Baumgardt as a converted Lg at the continental margin of the Baltic shield, also agrees the finite-element simulated trace. Although Lg to Sn conversion and Lg scattering might also have taken place at the Baltic shield continental margin, such conversion and

scattering did not cause any major changes in the already small amplitude Lg waves, which was revealed by finite-element modeling and observations.

On the basis of finite-element modeling and the above three direct comparisons between the finite-element modeling results and the observational data, the blockage of Lg for the propagation paths from Novaya Zemlya to ARCESS and to NORSAR is caused by the presence of the low-velocity sediments in the Barents Sea.

References

Alford, R.M., K.R. Kelly, and D.M. Boore (1974). Accuracy of finite difference modelling of the acoustic wave equation, *Geophysics*, **39**, 834-842.

Bath, M., (1954). The elastic waves Lg and Rg along Euro-asiatic paths, *Ark. Geofys.*, **2**, 295-324.

Bath, M., and S. Crampin (1965). Higher modes of seismic surface waves – Relations to channel waves, *Geophys. J.R. Astr. Soc.*, **9** 309-321. Baumgardt, D.R., (1985). Comparative analysis of teleseismic P coda and Lg waves from underground nuclear explosions in Eurasia, *Bull. Seism. Soc. Am.*, **75**, 1413-1433.

Baumgardt, D.R., (1987). Spectral determination of regional and teleseismic Lg attenuation and source multiplicity in explosions, DARPA/AFGL Seismic Research Symposium, 15 - 18 June 1987, Harbor House, Nantucket, MA.

Baumgardt, D.R., (1990a). Investigation of teleseismic Lg blockage and scattering using regional arrays, *Bull. Seism. Soc. Am.*, **80**, 2261-2281.

Baumgardt, D.R., (1990b). Causes of Lg amplitude variations and scattering in the Eurasian continental craton, Proceedings of the 12th Annual DARPA/AFGL Seismic Research Symposium, 18 - 20 Sept., 1990, 224-233.

Baumgardt, D.R., (1991). High frequency array studies of long range Lg propagation and the causes of Lg blockage and attenuation in the Eurasian continental craton, Final Report PL-TR-91-2059 (II).

Bouchon, M., (1982). The complete synthesis of seismic crustal phases at regional distances, *J. Geophys. Res.*, **87**, 1735-1741.

Cara M. and J.B. Minster, (1981). Multi-mode analysis of Rayleigh-type Lg, Part 1. Theory and applicability of the method, Bull. Seism. Soc. Am., **71**, 973-984.

Cao S. and K.J. Muirhead, (1993). Finite difference modelling of Lg blockage, Geophys. J. Int., **115**, 85-96.

Cara, M. J.B. Minster, and R. LeBras, (1981). Multi-mode analysis of Rayleigh-type Lg, Part 2. Application to southern California and the northwestern Sierra Nevada, Bull. Seism. Soc. Am., **71**, 985-1002.

Chan, W.W. and B. J. Mitchell (1985). Surface wave dispersion, crustal structure, and sediment thickness variations across the Barents shelf, Geophys. J. R. Astron. Soc., **80**, 329-344.

Clarke, J.W. and J. Rachlin (1990). Geology of the Barents Sea Structural Basin. U.S. Geological Survey, Military Geology Project, Open-File Report, July, 1990.

Crampin S., E.M. Chesnokov, and R.A. Hipkin (1984). Seismic anisotropy – The state of the art: II, Geophys. J.R. Astr. Soc., **76**, 1-16.

Fan, Z.X. and Y.C. Teng (1989). The application of simulation modeling of seismic wave in the transversely isotropic and viscoelastic media, Bull. of Chinese Geophys. Soc., Applied Geophys., **1**, 37-56.

Gregersen, S. (1984), Lg-wave propagation and crustal structure differences near Denmark and the North Sea, Geophys. J.R. Astr. Soc., bf 79, 217-314.

Gramberg,I.S.,(1988). The Barents Shelf Plate (in Russian), Volume 196, Nedra, Leningrad.

Hughes, T.J.R. (1987). The Finite-Element Method, Prentice-Hall, Englewood Cliffs, N.J..

Kadinsky-Cade, K., M. Barazangi, J. Oliver, and B. Isacks (1981). Lateral variations of high-frequency seismic wave propagation at regional distances across the

Turkish and Iranian Plateaus. *J. Geophys. Res.*, **86**, 9377-9396.

Kanasewich, E.R., T. (1973). Seismic waves in laterally inhomogeneous media, *Bull. seism. Soc.*, *bf 63*, 2167-2176.

Kennett, B.L.N. (1984), Lg-wave propagation and crustal structure differences near Denmark and the North Sea, *Geophys. J.R. Astr. Soc.*, *bf 79*, 217-314.

Kennett, B.L.N. (1986). Lg waves and structural boundaries, *Bull. seism. Soc.*, **76**, 1133-1141.

Kennett, B.L.N., S. Gregersen, S. Mykkeltveit, and S. Newmark (1985). Mapping of crustal heterogeneity in the North Sea basin via the propagation of Lg-waves, *Geophys. J. R. Astron. Soc.*, **83**, 299-306.

Knopoff, L., F. Schwab, K. Nakanishi, and F. Chang (1975). Evaluation of Lg as a Discriminant among Different Continental Crustal Structures, *Geophys. J. R. Astron. Soc.*, **39**, 41-70.

Marfurt, K.J. (1984). Accuracy of finite-difference and finite-element modeling of the scalar and elastic wave equations, *Geophysics*, **49**, 533-549.

Nuttli, O.W. (1973). Seismic wave attenuation and magnitude relations for eastern North America, *J. Geophys. Res.* **78**, 876-885.

Mitchell, B.J. and H.J. Hwang (1987). Effect of low-Q sediments and crustal Q on Lg attenuation in the United States. *Bull. Seism. Soc. Am.*, **77**, 1197.

Molnar, P. and J. Oliver (1969). Lateral variations of attenuation in the upper mantle and discontinuities in the lithosphere, *J. geophys. Res.* *bf 74*, 2648-2682.

Ni, J. and M. Barazangi (1983). High-frequency seismic wave propagation beneath the Indian Shield, Himalayan Arc, Tibetan Plateau and surrounding regions: high uppermost mantle velocities and efficient Sn propagation beneath Tibet. *Geophys. J. R. Astron. Soc.*, **72**, 665-689.

Oliver, J. and M. Ewing, (1957). Higher modes of continental Rayleigh waves, Bull. Seism. Soc. Am., **47**, 187-204.

Oliver, J. and M. Ewing, (1958a). Normal modes of continental surface waves, Bull. Seism. Soc. Am., **48**, 33-49.

Oliver, J. and M. Ewing, (1958b). The effect of surficial sedimentary layers on continental surface waves, Bull. Seism. Soc. Am., **47**, 339-354.

Panza, G.F., and G. Calcagnile (1975). Lg, Li and Rg from Rayleigh modes, Geophys. J. R. Astron. Soc., **40**, 475-487.

Piwinckii, A.J. (1981). Deep structure of the earth's crust and upper mantle in the USSR according to geological, geophysical, and seismological data: Dneiper-Donetsk and Pri-Caspian depressions, UCID-19203, Lawrence Livermore Laboratory, Livermore, California.

Press, F. and M. Ewing, (1952). Two slow surface waves across North America, Bull. Seism. Soc. Am., **42**, 219-228.

Regan, J., and D.G. Harkrider, (1989). Numerical modelling of SH Lg waves in and around continental margins, Geophys. J. Int., bf 98, 107-130.

Ruzaikin, A., I. Nersesov, V. Khalturin, and P. Molnar (1977). Propagation of Lg and lateral variations in crustal structure in Asia. J. Geophys. Res., **82**, 307-316.

Teng, Y.C. (1989). Three-dimensional finite-element analysis of waves in acoustic media with inclusion, J. Acoust. Soc. Am., **86**, 414-422.

Teng, Y.C. (1990). Finite-element results of the slow compressional wave in a porous medium at ultrasonic frequencies, J. Appl. Phys. **68**, 4335-4337.

Teng, Y.C. (1993). Scattering of transient waves by finite cracks in an anti-plane strain elastic solid, J. of Compu. Acou., bf 1, No.1, 101-116.

Teng, Y.C. and T.F. Dai (1989). Finite-element prestack reverse-time migration

for elastic waves, *Geophysics*, **54**, 1204-1208.

Teng, Y.C. and J.T. Kuo (1988a). finite-element source simulation for elastodynamics, *Model Optimization in Exploration Geophysics*, Vol. 3, Vieweg Braunschweig-Wiesbaden, 277-298.

Teng, Y.C. and J.T. Kuo (1988b). A finite-element algorithm for solving the transient problem in a fluid-solid coupled medium, *IMACS, COMPU. ACOU.: Wave Propagation*, 239-257.

Teng, Y.C. and Z.L. Zhang (1990). Three-dimensional modelling of elastic waves, *Acta Geophysica Sinica*, **33**, n.1, 44-53.

Teng, Y.C., T.F. Dai, and J.T. Kuo (1986). Finite-element reverse-time migration for elastic waves, 56th Ann. Internal. Mtg., Soc. Explor. Geophys., Expanded Abstract, 611-614.

Teng, Y.C., T.F. Dai, and J.T. Kuo (1988). Pre-stack finite-element reverse-time migration for elastic waves, *Geophysical Prospecting for Petroleum (PRC)*, **27**, n.2, 10-26.

Zienkiewicz, O.C. (1977). *The Finite Element Method*, McGraw-Hill Book Co., New York, London.